Spring 1-1-2012

# A Multicomponent Bioactive Tissue-Engineered Blood Vessel: Fabrication, Mechanical Evaluation and Biological Evaluation with Physiological-Relevant Conditions

Walter Bonani
*University of Colorado at Boulder*, walter.bonani@colorado.edu

# *A MULTICOMPONENT BIOACTIVE TISSUE-ENGINEERED BLOOD VESSEL: FABRICATION, MECHANICAL EVALUATION AND BIOLOGICAL EVALUATION WITH PHYSIOLOGICAL-RELEVANT CONDITIONS*

*by*

*WALTER BONANI*

*M.A., University of Trento, Italy, 2006*

*A thesis submitted to the*

*Faculty of the Graduate School of the*

*University of Colorado in partial fulfillment*

*of the requirement for the degree of*

*Doctor of Philosophy*

*Department of Mechanical Engineering*

*2012*

This thesis entitled:
A multicomponent bioactive tissue-engineered blood vessel:
fabrication, mechanical evaluation and biological evaluation with
physiological-relevant conditions
written by Walter Bonani
has been approved for the Department of Mechanical Engineering

WEI TAN

ANTONELLA MOTTA

Boulder, April 4th, 2012.

The final copy of this thesis has been examined by the signatories, and we
Find that both the content and the form meet acceptable presentation
standards
Of scholarly work in the above mentioned discipline.

**Bonani, Walter** (Ph.D., Mechanical Engineering)

**A Multicomponent Bioactive Tissue-engineered Blood Vessel:**

**Fabrication, Mechanical Evaluation and Biological Evaluation with Physiological-Relevant Conditions**

Thesis directed by Assistant Professor Wei Tan (University of Colorado), Full Professor Claudio Migliaresi and Assistant Professor Antonella Motta (University of Trento)

## ABSTRACT

The high long-term failure rate of synthetic vascular grafts in the replacement of small vessels is known to be associated with the lack of physiological signals to vascular cells causing adverse hemodynamic, inflammatory or coagulatory events. Current studies focus on developing engineered vascular devices with ability of directing cell activity in vitro and in vivo for tissue regeneration. It is also known that controlled molecule release from scaffolds can dramatically increase the scaffold ability of directing cell activities in vitro and in vivo for tissue regeneration. To address the mechanical and biological problems associated with graft materials, we demonstrated a degradable polyester-fibroin composite tubular scaffolds which shows well-integrated nanofibrous structure, endothelial-conducive surface and anisotropic mechanical property, suitable as engineered vascular constructs.

Tissue regeneration needs not only functional biomolecules providing signaling cues to cells and guide tissue remodeling, but also an adequate modality of molecule delivery. In fact, healthy tissue formation requires specific signals at well-defined place and time. To develop scaffolds with multi-modal presentation of biomolecules, we patterned electrospun nanofibers over the thickness of the 3-dimensional scaffolds by programming the deposition of interpenetrating networks of degradable polymers poly(ε-caprolactone) and poly(lactide-co-glycolide) acid in tailored proportion. Fluorescent model molecules, drug and growth factors were embedded in the polymeric fibers with different techniques and release profiles were obtained and discussed.

Fabrication process resulted in precise gradient patterns of materials and functional biomolecules throughout the thickness of the scaffold. These graded materials showed programmable spatio-temporal control over the release. Molecule release profiles on each side of the scaffolds were used to determine the separation efficiency of molecule delivery, which achieved >90% for proteins in 200μm scaffolds. Gradient-patterned scaffolds were also used to program simultaneous release of two proteins to the opposite sides of the scaffold and sequential release of proteins to a defined space, which further demonstrate the ability of patterned nanofibers to spatially and temporally confine sustained release. Moreover, results showed that temporal release kinetics could be altered by the structural patterns. Thus, the hierarchically-structured scaffolds presented here may enable development of novel multifunctional scaffolds with defined 3D dynamic microenvironments for tissue regeneration.

## ACKNOWLEDGEMENTS

This doctoral thesis would not have been possible without the constant support of my advisors Professor Wei Tan, Professor Migliaresi and Dr. Antonella Motta, whose encouragement, suggestions and example led me to this important achievement.

I would also like to thank all the amazing colleagues who accompanied me along this doctorate trip, offering me a practical support and a warm friendship.

I thank my parents, my sister and my friends who always supported, encouraged and backed me up, with understanding and love. Finally, I would like to send a sweet thought to Monica, who has someway managed to bear the weight of my swinging mood and has always taken good care of me; lovely, patiently and unconditionally.

# CONTENTS

## LIST OF TABLES

## LIST OF FIGURES

# 1 INTRODUCTION

## 1.1 Cardiovascular system and diseases

The cardiovascular system consists of the heart and blood vessels that distribute blood in to the various parts of the body. The complex system of organs that contributes to the cardiovascular systems has a critical role in the transport of nutrients, biochemical signals and cellular waste product, and in the processes of oxygen/carbon dioxide exchange. Oxygenated blood travels from the left section of the heart to the peripheral capillaries in the peripheral tissues through the arteries, and from the capillaries to the heart through the venous system (systemic circulation). Deoxygenated blood leaves the right section of the heart through the pulmonary arteries and enters the lungs, from where it is carried by the pulmonary veins to the left atrium (pulmonary system). The vascular tree forms a hierarchical system of branched arteries and veins that vary in size, mechanical properties, biochemical and cellular content, and morphological organization, depending on their location and specific function. Largest arteries, such as the aorta, that transport blood away from the heart, branch into smaller diameter muscular arteries and then in smaller arterioles and capillaries, which distribute blood within the tissues and organs. Blood is returned to the heart through venules, which combine

to form small and large veins, which converge in the superior and inferior *vena cavae* [1]. Blood vessels consist of three main layers: the *tunica intima,* the *tunica media,* and the *tunica adventitia.* The *tunica intima* includes the monolayered endothelial lining of the vessel and the underlying layer of connective tissue, the internal elastic lamina. The *tunica media* contains concentric sheets of circumferentially aligned smooth muscle cells embedded in a 3-D structure of loose connective tissue. The largest arteries (called elastic arteries), such as aorta and brachiocephalic have a considerable fraction of elastic tissue, alternated with layers of muscular tissue oriented both in longitudinal and circumferential direction. The tunica adventitia, the outermost layer of the vessel, contains collagen and a limited number of elastic fibers [2].

A number of factors, including, age, genetics, stress, food habits, smoking and alcohol consumption are known to contribute to diseases and disorders associated with this system which are known as cardiovascular diseases. Nowadays, heart, arteries or veins dysfunctions have become the primary cause of death in the USA, the leading causes of mortality in Western society [3]. Atherosclerosis is the major disease of blood vessels, and affects the larger and medium sized elastic and muscular arteries that contain an intima. It consists of artery wall hardening and conduit narrowing (stenosis) through accumulation of fats, cholesterol, calcium and other substances in the inner lumen of the blood vessels. The process is commonly referred as atherosclerotic plaque formation. The lesions of atherosclerosis takes form of coronary artery and peripheral vascular disease, thus leading to ischemia of the heart, brain or peripheral organs. World Health Organizations reports that there were at least 7,200,000 deaths due to stenosis around the world in 2004 [4].

## 1.2 Vascular grafts

Patients with less severe symptoms are treated with numerous non-invasive treatments, such as the use of anti-thrombotic drugs or cholesterol-lowering drugs. Therapies such endovascular procedures, are considered available minimally invasive strategies. In the case of more severe pathologies, surgical bypass and vessel replacement became necessary. Vein replacements have been performed in the largest part with autografts, using healthy sections of patient's own veins.

In the case of highly compromise arteries, bypass surgery and artery stenting are the accepted treatments. Coronary artery bypass grafting or coronary artery stenting are the most common diseases for patients with severe artery blockage. Currently, bypass grafts fall in two general categories: biological and synthetic grafts.

### 1.2.1 Biological grafts

Biological grafts can be natural veins or minor arteries harvested from the patient itself (autograft), from another individual or the same species (allografts or homografts) or from animals (xenografts).

Proposed autologus grafts used in vascular replacement are saphenous veins, internal thoracic arteries, radial artery are used. Although vascular bypass grafting remains the gold standard for revascularization for ischemic heart disease and peripheral vascular disease, many patients do not have healthy suitable vessels, due to previous surgery, vessel diseases or trauma. The vascular substitutes have been proposed and tested are decellularized allografts, decellularized and cross-linked xerografts and artificial synthetic grafts.

### 1.2.2 Synthetic grafts[5]

Nowadays, polytetrafluoroethylene (PTFE), Dacron and polyurethane (PU) are considered standards materials for vascular replacement. Synthetic polymer devices for vascular replacements are the more practical alternative to autografts. Though impressive success of these grafts has been made in aortic and iliac surgery (medium and large arteries), smaller diameter (≤6mm) grafts has been a symbol for the limitations of modern biotechnology because their long-term failure rates are still high [6–8]. Thrombogenicity and graft occlusion represent the major limitations for currently used small diameter vascular grafts. The inability of the body to remodel synthetic materials is related poor long term patency of permanent synthetic grafts.

. Small-diameter vascular grafts are used as medical implants for a number of diseases, such as coronary or periphery artery bypass grafts, pediatric vascular shunts and vascular access grafts. The materials and structures of contemporary grafts provide limited capability of endothelium regeneration and tissue ingrowth. Lack of good tissue ingrowth and regeneration in the grafts makes grafts more prone to ongoing thrombogenity and intima hyperplasia [9–11].

Exposition of a prosthesis surface to blood flow results rapidly in a deposition of blood proteins on the luminal surface and generates the process of platelet activation, leading to thrombus formation via the intrinsic coagulation pathway and ultimately in vessel occlusion. At the same time, activated platelets secrete platelet-derived growth factor (PDGF), which is responsible for the migration of smooth-muscle cells (SMC) from the media into the intima [2].

During the past few decades, many efforts have been made to improve the performance of vascular grafts mainly through the attempts that modify the structure and surface of the contemporary graft materials. These attempts include: (a) increasing structural porosity; (b) increasing mechanical compliance; (c) pre-endothelialization; and (d) incorporating anti-thrombotic molecules on the surface [10,12]. Impressive advancement on these synthetic vascular grafts has been made to improve graft patency. However, as commented by Zilla et al [8], these graft materials have structure-related limitations to regenerating vascular tissue both on the surface and in the transmural space. The non-degradable nature of the materials restricts the remodeling and regeneration capability of media and adventitia.

The most common causes for the poor performance of small-diameter grafts are surface thrombogenicity and intimal hyperplasia (IH), which are mainly mediated by denude of endothelium and lack of sufficient tissue ingrowth [7,13]. Exposition of a bare graft surface to blood flow results rapidly in a deposition of blood proteins on the luminal surface, activating platelets and leading to thrombus formation via the intrinsic coagulation pathway and ultimately to vessel occlusion. Also, activated platelets secrete molecules such as platelet-derived growth factor (PDGF) which is responsible for the proliferation and migration of smooth muscle cells (SMC) from the media into the intima leading to IH. IH narrows the vessel lumen decreasing blood flow to the point that it may in turn promote local thrombosis. Intima hyperplasia can also be induced by flow turbulence at the graft-vessel junction due to the mismatch mechanical compliance of graft and vessel [14]. Graft modification with protein lining, heparin incorporation and polymer resurfacing reduced thrombosis and neo-intimal hyperplasia but did little to improve long-term arterial graft patency [9].

It is generally agreed that efforts to improve the graft should be made on the formation of a physiological vascular tissues including functional endothelium, smooth muscle and connective layers around the vascular graft ensure mimetic biological and mechanical functioning of the graft and allow it better integrated with native blood vessels [6,8,15]. Considering the important role that physiological tissue formation on or around the grafts plays in the long-term patency of small-diameter vascular grafts, a more recent research thrust is to develop various tissue engineering approaches which allow the tissue formation to spontaneously occur *in vitro* or *in vivo* and eventually replace the grafts [16,17].

## 1.3 Vascular Tissue Engineering approach

### 1.3.1 Tissue Engineering

Tissue Engineering is an interdisciplinary field that applies the principles of engineering and life sciences toward the repair and the restoration of damaged tissue functions [18]. The three fundamental tools that Tissue Engineering exploits to achieve successful tissue regeneration are cells, scaffolds and specific signalling factors [19]. An effective interplay and an synergistic cooperation between these three components have been proven to be a critical factors for the process of scaffold-tissue integration and, eventually, for tissue regeneration. Scaffolds have to provide adequate structural and mechanical support and to direct cell activity toward the regeneration of a new physiological tissue by providing chemical, biological and physical cues. For example, active molecules and Growth Factors (GFs), that have the ability to influence cell attachment, migration, proliferation and differentiation, can be encapsulated in the scaffolds and released in situ [20,21].

### 1.3.2 Vascular Tissue Engineering

Tissue engineering has emerged as a promising strategy for vascular tissue regeneration. Tissue engineering approach aims at regenerating damaged tissues or organs, in order to growth an integrated new tissue with the same characteristics of the native one. When in 1986, Weinberg and Bell claimed the construction of new blood vessel in vitro, with bovine aortic endothelial cells, smooth muscle cells and fibroblasts seeded on a collagen matrix [22] [Weinberg and Bell 1986], they signed the road that would address the research strategies for tissue regeneration until the present days. This work has been commonly regarded as the first engineered construct for vascular tissue engineering, though their work had been published seven year in advance to the Tissue Engineering definition [18].Vascular tissue engineering offers a promising alternative approach to address the needs for small-diameter vascular grafts by overcoming the mechanical and/or biological problems associated with the current materials [1]. To avoid adverse hemodynamic conditions, mechanical properties of tissue engineering grafts must closely match those of native arteries, meanwhile the grafts should be sufficiently strong. Many studies have demonstrated the anisotropic mechanical property of natural arteries; higher stiffness in the longitudinal direction can avoid an excessive stimulation of anastomotic regions, while being compliant in the circumferential direction to match the compliance of native artery can avoid flow disturbance [7,8].

In vitro tissue regeneration is regarded as the most traditional approach used in the studies on tissue engineered vessels. According to the scheme proposed by MacNeill in 2002, autologous cells are expanded in vitro and organized on a suitable scaffold, cell culture is

performed in specifically designed bioreactors to produce an engineered functional tissue similar. The new tissue similar to the physiological one is implanted into the patient, without any rejection problem [25].

However, expansion of harvested autologous cells in vitro and cell growth onto the scaffolds are the time limiting steps. These reasons make this approach barely unfeasible in the normal clinical situations, and completely impossible in the case of acute diseases or trauma.

In the case of in vivo tissue regeneration, a scaffold is directly implanted either in the site of injury and the patient's body itself produces the new tissue, by invading the scaffold with cells, remodelling and sometime replacing it in the time.

## 1.4 Electrospinning as a method for preparing scaffolds for Tissue Engineering

### 1.4.1 Electrospinning history

Electrospinning is the most widely used method to generate nanofibers.

Fundamental electrospinning idea took its origin from Lord Rayleigh's observations on the electrospray phenomena in 1882 [26]. He found that a highly charged droplet was unstable and would break down into smaller droplets in presence of an high voltage: the so called "Rayleigh instability''. The electric Columbic repulsive forces, overcoming the surface tension, result in a rupture of the droplet surface. Later, Zeleny investigated the Instability of electrified of aqueous solutions [27]; in the late 60's, Dole et al. studied the electrosprays of dilute polymer solutions [28]. Electrospinning phenomenon is a similar to the electrospraying; the

substantial difference between the two is that electrospinning produces continuous fibers instead of small droplets.

In 1934, Formhals electrospun fine fibers from a cellulose acetate solution and registered a patent in U.S. on this new technology [29], [30]. Later, Simons signed another patent, in which he used concentrated solutions to increase the viscosity, having a more stable process and producing longer fibers [31]. In the early 80's, Larrondo and Manley performed an electrospinning process with polymer melts and produced polyethylene nanofibers [32].

The recent, rising interest in nanotechnology has renewed attention to this convenient, economical technology that enables engineers to produce nanofibers for various applications.

### 1.4.2 Electrospinning process

The electrospinning process enables to produce polymeric fibers with diameters in the range of a few nanometers to several microns. In electrospinning, a high voltage is applied to polymer solution (or a melt), saturating the solution with electrical unbalanced charges. The polymeric solution is stored in a reservoir and is forced out of a needle (or spinneret) at a constant rate. With increasing voltage, the surface charge on the polymer droplet increases, resulting in the formation of a conical shape (Taylor cone) at the tip of the spinnaret. As shown in Figure 1-1, once that a threshold voltage has been reached, the surface charge overcomes the surface tension and viscosity of the polymer droplet, a jet is initiated and ejected form the apex of the Taylor cone toward the grounded collector.

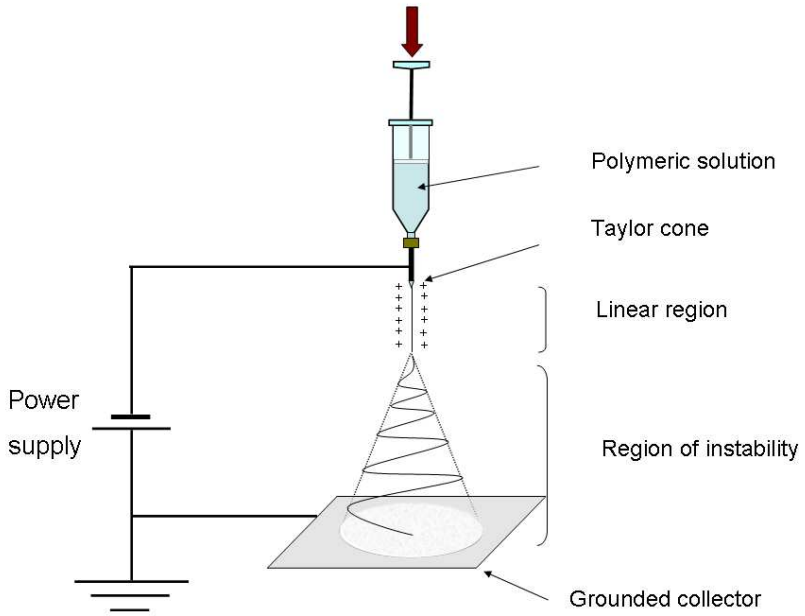


*Figure 1-1. Schematization of the electrospinning process*

The jet travels toward a region of lower electrical potential, that, for convenience, is a grounded collector. After being ejected from the apex of the Taylor cone, the jet travels linearly in a region, called linear region, whose extension can vary considerably between different polymer/solvent system. After that the high charge density results in a instability of the jet, that enters a so called instability region, where it undergoes to repeating bending and whipping rapid movements that contributed to elongate the fiber, narrowing its diameter down to the nanometric range. High speed photography have been used to image the fiber path and behavior along the air gap between spinneret and collector [33,34]**.** In addition. several studies applied mathematical models and numerical simulations to rationalize the shape of fiber track and the bending instability phenomenon [33,35,36].

In the small fraction of time, in which the jet travels from the needle to the grounded collector, the solvent evaporates, and dry nanometric fibers are deposited on the metal target plate, forming a non-woven nanofibrous mat. A fundamental step by step description of the electrospinning principles and the mechanisms of fiber formation have been presented by Rutledge and Fridrikh [37], and Detailed reviews on the topic of electrospinning for tissue engineering are given by several groups [35,38–41]. The electrospinning process can be manipulated by a number of variables for desired morphology and property of nanofibers. These variables include solution characteristics, process variables, and environmental parameters. Polymer solution characteristics, such as polymer molecular weight, concentration, solution viscosity, solution charge density, conductivity, dielectric constant and surface tension, are often difficult to isolate since varying one generally affects others. Process or system variables include:

- flow rate,
- field voltage,
- distance between tip and collector,
- needle tip design and placement,
- collector composition and geometry.

Environmental parameters, such as environmental temperature, humidity and atmosphere, are as important but less often explored [42], [43]. A general understanding of these parameters, allows one to set up a process to produce defect-free fibers with controllable nanofiber morphology. When electrospinning parameters are optimized, the obtained fiber

diameters should have a narrow distribution. Also, porosity of electrospun materials can be altered by changing the void spaces laying between the fibers through varying the mean fiber diameter, the diameter distribution and the degree of fiber packing.

### 1.4.3 Electrospinning in Tissue Engineering

Electrospinning is a simple and widespread technique for the production of nano- and micro-metric polymeric fibers that are deposited on a grounded collector to form a nonwoven material with regular nano-structured surface [44]. Electrospun nanofiber matrices are characterized by ultrafine continuous fibers, interconnected pores, high porosity and variable pore-size distribution similar to the dimensions of basement membranes. Those matrices present a dynamic system in which the pore size and shape can change when compared to other rigid porous structures.

Electrospun constructs can be produced that are particularly interesting as scaffolds for Tissue Engineering and as drug delivery systems [45–49]. A variety of degradable and resorbable materials have been processed, including degradable polyesters, such as poly(ε-caprolactone) (PCL), poly(lactide) (PLA), poly(glycolide) (PGA) and their copolymers poly(lactide-co-glycolide) (PLGA) , and natural polymers, such as collagen, silk fibroin, fibrinogen and other proteins [50–54].

Electrospun devices have been proposed for a multiplicity of applications where the scaffold is required to interact with different cells, tissues or even different organs at the same time. In those situations, the electrospun scaffold acts like an interphase between environments with diverse characteristics and requirements. For example, electrospinning have

been considered in the repair of the osteochondral defects, where integration with both the subchondral bone and the deep cartilage zone is required. The two regions are characterized by different cell types, different degree of vascularisation of the tissue, collagen distribution and porosity. Therefore, a scaffold with the ability to interact independently with the two tissues, in a particular selectively release different biomolecules, is required [Yang, engineering orthopaedic interfaces]. In the field of tissue engineered vascular grafts electrospun scaffold have been used to promote endothelial call attachment and proliferation on one side, while supporting the organization of new extracellular matrix generated by smooth muscle cells and fibroblasts on the other side. Selective release of Growth Factors that could target specifically the different types of cells has been prospected both for *in vitro* co-culture tests and for *in vivo* integration of tissue engineered vascular grafts. Control- and spatial-confinement of the released biomolecules can be obtained with graded materials and segregation of the delivery systems in particular regions of the scaffold.

#### *1.4.3.1 Nanofibers scaffolds*

Scaffolds made from nanofibrous materials using electrospinning techniques have been increasingly used for various tissue constructs, including those for replacement of intervertebral disk, meniscus, annulus fibrosus, blood vessels, and cartilage [55–61]. The advantages of using nanofibrous scaffolds for tissue engineering include their load-bearing functionality, porous structure, and nano- to micro- sized fibers, similar in the length scale to native extracellular matrix (ECM), to guide cell adhesion and proliferation [53,54,62–65]. The versatile use of electrospinning with a variety of natural and synthetic degradable polymers offers a large

repertoire for tissue engineering and drug delivery applications [66–69]. Additionally, electrospun biomaterials provide a wide range of mechanical and chemical properties via fiber composition, diameter, distribution and porosity, through control over a panel of engineering parameters in the process [45,47,49,70]. Further, collection of nanofibers onto a rotating mandrel or other collectors with specialized surfaces, can result in structural and mechanical anisotropy for the applications of vascular or fibrous tissue engineering [43,71].

#### *1.4.3.2 Nanofibers scaffolds for vascular Tissue Engineering*

Recent developments in nanofiber fabrication technology provide tremendous opportunities to improve vascular implant performances, because diverse fabrication methods and functionalization strategies allow one to design optimal material properties and environments for desired short-term and long-term performances that meet the needs of a specific treatment [72–75]. Specifically, nanofiber scaffolding materials offer a number of advantages for vascular grafting applications:

The nanofibers mimic the nanostructure of the extracellular matrix (ECM) of natural tissues. Cells live in a nano-featured ECM environment. They attach and organize better around fibers with diameters much smaller than cell diameter (>5μm). It is found that nanometric surface topography with a high surface area-to-volume ratio attracts more endothelial cells and promote their growth, thus, accelerating the re-formation of an endothelium to prohibit thrombosis of the artery [76].

Controllable porosity and interconnected pores together with biodegradable property could allow the materials to have large and ever increasing space for SMCs to grow, migrate and fulfill regeneration and for better integration of the host tissue in the long term.

Electrospinning of synthetic fibers and protein fibers have been demonstrated for vascular applications. Electrospun synthetic polymers such as PCL and PLGA have successfully been applied to engineer vascular tissues [50–52,77,78]. Electrospinning of natural-derived biopolymers such as collagen, elastin, silk fibroin, chitosan and fibrinogen have also been developed for vascular engineering [79–81].

A particularly interesting and promising area of electrospinning is creating composite scaffolds with mixed nanofibers or with a blended composition of polymers in the nanofiber. The benefit of scaffolds formed with a combination of different polymers is in the possibility of synergizing the favorable characteristics of each individual component to obtain a composite with superior mechanical and/or biological properties required for vascular grafts. Nanofibers with different physical or biological properties, such as hydrophobic/hydrophilic fibers, fibers with different degradation rates, and synthetic/biological fibers, can be combined to form hybrid fibers with desired properties. The hydrophilic/hydrophobic characteristic is a critical factor that affects protein adhesion thus influencing blot clotting formation and cell adhesion. It also affects biomolecule release and mechanical properties. Therefore, a composite made of hydrophobic and hydrophilic polymers can combine superior mechanical properties, better hydrolytic resistance and better thrombo-resistance that hydrophobic polymers provide with higher molecule incorporation potential that hydrophilic polymers provide [81]. Using fiber

composites with a polymer that degrades faster than the other can increase the porosity for tissue in-growth [82].

## 1.5 Drug delivering scaffolds for tissue regeneration

In addition to structural support, mechanical property and biodegradable feature, an ideal scaffold for tissue regeneration should provide molecular cues to guide regeneration of tissue structure and function. To incorporate regenerative or therapeutic molecules into biomaterials that sustain the molecule release in vitro or in vivo, various methods such as adsorption and covalent binding [83,84], encapsulation [85,86], and addition during scaffold formation [87], have been developed. A step forward could be moving from static cues of one molecule toward delivery systems that reproduce more closely the dynamically evolving microenvironment occurring in natural ECM [88–90]. The delivery systems incorporating molecules, mainly biodegradable particles, could offer distinctive advantages such as regulation of release rate while protecting their molecule cargo during all the stages of tissue regrowth [91,92]. Indeed, scaffolds that support tissue repair, regrowth or regeneration from cells, particularly from undifferentiated stem or progenitor cells, may have to partially recapitulate natural tissue morphogenesis, which is driven by the concomitant action of multiple factors working in concert. Growing evidence has shown that tissue morphogenesis is coordinated by the spatial arrangement and temporal duration of multiple molecules in the three-dimensional (3D) ECM [93,94]. For precise regulation, recent developments have demonstrated the benefits of using micro- and nano- structures [70,95–104]. The majority of newly-developed molecule-impregnated scaffolds, however, are capable of achieving sustained or temporally-controlled

molecule release. Few techniques are available to engineer 3D scaffolds that define spatial organization of molecules or control release in both space and time scale. Control of where and when a molecule acts can strongly contribute to provide spatially complex arrangements of cells in length scales ranging from nano-/micro- meters to centimeters. The spatial control over release is critical to coordinate cell behaviors for tissue pattern formation[92,102]. Selective release of molecules that target specific cell types or tissue formation without influencing the activity of other cell populations or tissue functions is important to establish both *in vitro* physiological tissue models and *in vivo* tissue regeneration [105–107]. Patterning or segregation of molecule delivery materials are important to spatially confine biomolecules [108–110]. To meet various physiological needs of different cell types during tissue regrowth, a 3D scaffold should present a multitude of regenerative biomolecules in a sustained manner at defined locations.

### 1.5.1 Nanofibers scaffolds as drug delivery systems

Recently, strategies that use electrospun fibers to encapsulate and deliver molecules have been established [46,87,104]. Due to inherently high surface area of electrospun materials, nanofiber constructs allow high molecule loading and efficient release *in situ*. However, the developed techniques have been limited to tune molecule release kinetics and often the structure and property of nanofibers are significantly influenced to facilitate molecule encapsulation. Herein, we report a new strategy of designing electrospun constructs, which utilize micropatterns of nanofiber to spatially define or temporally control delivery of molecules. We previously demonstrated the development of double-electrospinning system

that used a rotating mandrel collector to produce constructs composed of interpenetrating networks of nanofibers with diverse nanofibers in a tailored proportion to achieve anisotropic mechanical properties and engineered surfaces [43]. The incorporation of molecules which affect cell function and tissue regeneration must be designed to target at specific cell physiology process, dependent on cell type and cell differentiating state. Thus, an in-depth understanding of vascular cell biology and/or stem cell biology, particularly cell signalling, is important for the incorporation of the right molecular signals at the right location and time. Localized delivery of medicaments at a controlled rate over a specific period of time improves therapeutic efficacy and reduce toxicity of bioactive agents. In this view, a finely designed controlled-release device is required to spatially and temporally encounter the needs of the regenerating tissue [102,111,112].

## 1.6 Objectives of the thesis

Designing bioinspired vascular grafting materials through nanofiber fabrication techniques, such as electrospinning is an emerging field. To enhance the biomimicry of nanofibrous scaffolds, multi-functional nanofibers should be made by combining bioactive surface with spatiotemporal release of functional molecules and drugs. This is being explored by following techniques: (a) modifying the surface of nanofibers; (b) incorporating bioactive molecules in the nanofibers and achieving spatiotemporal control over the molecule release; (c) incorporating cells during the fiber-formation process; and (d) forming composite nanofibers that combine the different mechanical, bioactive and degradable properties of component materials.

The objective of this thesis is to develop a platform for producing a novel and innovative scaffolds for Vascular Tissue Engineering applications. Vascular tissue engineering offers a promising alternative approach to address the needs for small-diameter vascular grafts by overcoming the mechanical and/or biological problems associated with the current synthetic materials. The primary requirement is to design and manufacture with adequate mechanical property and deformational behavior and superior surface biocompatibility for endothelial cell adhesion and proliferation. To overcome the drawbacks related to materials and structures used in contemporary synthetic grafts, we will combine the superior biological properties of a natural polymer (silk fibroin) with higher mechanical stability and performance of a degradable and resorbable polyester (PCL). In Chapter 2, we will demonstrate a robust multilayered scaffolds with intermixing nanofiber structure, tunable anisotropy ratio, and surface properties which may hold great potential in tissue engineering applications.

Moreover, the present study intends to address the problem of spatial confinement of drug delivery in a specific region of the scaffold. Therefore, we will design scaffolds with capability of selectively releasing molecules in spatially- and temporally- controlled manner. Herein, electrospun composite scaffolds used to form materials with compositional and biochemical gradients along the scaffold thickness will be presented in Chapter 3, Chapter 4 and Chapter 5. We have characterized compositional and morphological changes as well as degradation behaviours of these composite scaffolds. More importantly, we will display a variety of tunable nanofiber micropatterns composed of degradable polymers PCL and PLGA

and characterized by compositional and biochemical gradients with the ability to control spatially and temporally the delivery of one or multiple molecules.

# 2 BIOHYBRID NANOFIBER COMPOSITE CONSTRUCTS WITH ANISOTROPIC MECHANICAL PROPERTIES


## Abstract

Synthetic implant materials often lack of the anisotropic mechanical properties and cell-interactive surface which are shown by natural tissues. For example, engineered vascular grafts need to be developed to address the mechanical and biological problems associated with the graft materials. The present study has demonstrated a double-electrospinning fabrication process to produce a poly(ε-caprolactone)-fibroin multilayer scaffold which shows well-integrated nanofibrous structure, endothelial-conducive surface and anisotropic mechanical property, suitable as engineered vascular constructs. Electrospinning parameters such as voltage, solution concentration, feed rate and relative humidity were optimized to obtain defect-free, uniform nanofibers. In order to mimic the different mechanical properties of natural vessels in the circumferential and longitudinal directions, a rotating cylinder was used as collector, resulting in the production of constructs with anisotropic properties. The combination of the collector shape and the collector rotation allows us to produce a tubular structure with tunable anisotropic mechanical properties. Fourier transform infrared

spectroscopy, differential scanning calorimetry and uniaxial tensile tests were used to characterize the electrospun constructs. Cell cultures with primary endothelial cells demonstrated that cells showed spread morphology and strong adhesion on fibroin richer surfaces. The platform for producing robust multilayer scaffolds with intermixing nanofiber structure, tunable anisotropy ratio, and surface with specific compositions may hold great potential in tissue engineering applications.

## 2.1 Introduction

The proper design of a scaffold that supports tissue regeneration has to take in account for a variety of factors such as mechanical properties, surface properties, morphology, pore size and distribution, biocompatibility and biodegradability [1,2]. Mechanical properties on tissue regeneration and cell growth are particularly important in tissues such as bone, muscles, cartilage, blood vessels and tendons [115].

Vascular grafts are currently used to replace damaged or occluded blood vessels for treatment of a number of vascular diseases such as coronary vascular diseases. Many patients that require vascular grafting do not have suitable autologous grafts and thus require synthetic grafts. Synthetic vascular grafting materials currently in clinical use are often made from stiff, bioinert materials such as expanded polytetrafluoroethylene (ePTFE) and dacron. When these synthetic grafts are used to replace small-diameter (<6 mm) vessels, low patency or high failure rates occur [116]. Grafting pathology is often characterized by anastomotic intimal hyperplasia and thrombosis, which are induced by improper hemodynamic, inflammatory or coagulatory conditions around grafts. A leading cause of these adverse conditions is the mechanical and biological properties of the synthetic graft materials [8].

Vascular tissue engineering offers a promising alternative approach to address the needs for small-diameter vascular grafts by overcoming the mechanical and/or biological problems associated with the current materials [1]. To avoid adverse hemodynamic conditions, mechanical properties of tissue engineering grafts must closely match those of native arteries,

meanwhile the grafts should be sufficiently strong. Many studies have demonstrated the anisotropic mechanical property of natural arteries; higher stiffness in the longitudinal direction can avoid an excessive stimulation of anastomotic regions, while being compliant in the circumferential direction to match the compliance of native artery can avoid flow disturbance [23,24].

Therefore, one of the goals in the present study is to create a structure that reproduces anisotropic mechanical properties of natural arteries. In addition, to provide anti-coagulatory and anti-inflammatory environments, the graft surface must be inherently anti-thrombogenic or conducive to endothelial cells. Furthermore, the presence of non-degradable grafts always imposes long-term concerns about the synthetic materials. Therefore, an ideal tissue engineering graft scaffold should not only closely match the mechanical properties of native arteries and be conductive to endothelial cells, but also be degradable as it provides a temporary scaffold to support the growing tissue substitute until cells produce their own extracellular matrix. It has been shown that a single material is difficult to simultaneously satisfy all these requirements.

Electrospinning is an attractive technique for fabricating tissue engineering scaffolds, due to the simplicity of the process and the capability of generating nanofibrous structures that mimic the natural extracellular matrix [40,45,117]. A variety of polymers have been electrospun for biomedical applications proposed in a wide range of areas including skin, nerve, tendon, cartilage, bone, and blood vessel [118–120]. Regenerated silk fibroin, one of the most promising biological polymers, is recently experimented in the field of tissue engineering because of its favorable interactions with cells and proteins [121–123]. Zhang et al. suggested

that electrospun fibroin scaffolds held potential for explorations of tissue-engineered vascular grafts because they sustained vascular cell viability, maintained cell phenotype and promoted cell reorganization [124]. In a recent study, Bondar et al. [125] have shown that endothelial cells recognize fibroin nanofibers through integrin-dependent mechanisms and, and the nanometric silk fibroin scaffolds did not interfere with the formation of a differentiated and interconnected endothelial layer. Poly(ε-caprolactone) (PCL) is a semicrystalline, bioresorbable, aliphatic synthetic polyester. A number of implantable medical devices are made of robust PCL. Electrospun PCL materials have been widely demonstrated for biomedical applications [126–128].

In the present study, we have demonstrated a novel multilayered biohybrid nanofiber scaffold made of silk fibroin and PCL. The scaffold is characterized by anisotropic mechanical properties, surface conducive to endothelial cells and degradation capacity. Anisotropic mechanical properties and surfaces with different functionalities are achieved by sequentially and simultaneously electrospinning fibroin and PCL on a rotational mandrel, which forms a robust multilayered structure with non-homogeneous compositions and an interpenetrating fibrous layer in the transition region.

## 2.2 Materials and Methods

### 2.2.1 Materials

Cocoons of Bombyx mori silkworm PN06 (Poli-ibrido Nazionale 2006) were kindly supplied by Centro Sperimentale di Gelsibachicoltura (Como, Italy). Poly-ε-caprolactone (PCL) with nominal average MW of 80,000 Da and poly(ethylene oxide) (PEO) with nominal average MW of 500,000 Da were purchased from Sigma Aldrich S.r.l (Milan, ITALY). Formic acid (98-100% purity) was also obtained from Sigma-Aldrich. N,N-dimethylformamide (DMF) minimum purity 99.9%, and methylene chloride (DCM) minimum purity of 99.5% were purchased from BDH Italia (Milan, Italy). All other substances were of analytical or pharmaceutical grade and obtained from Sigma-Aldric.

### 2.2.2 Preparation of regenerated Bombyx mori silk fibroin

Bombyx mori silk-fibroin water solutions were prepared as previously described [129]. Briefly, to remove sericin, cocoons were degummed by treating silk twice with 1.1 g/l and 0.4g/l $Na_2CO_3$ (anhydrous, minimum 99%) water solution at 98 °C for 1 hr each time. This resulted in 1 litre of solution containing 10 g of silk fibroin, which were then washed in de-ionized water and air-dried. The extracted silk fibroin was then dissolved in 9.3M LiBr (1 g fibroin in 10 ml LiBr solution) at 65 °C for 8-10 hr. After that, the solution was dialyzed in a Slide-A-Lyzer Cassette of 3500 MW (Pierce, Rockford, Illinoys, USA) against distilled water for three days in order to

remove the salt, and then filtered through a ceramic filter foam (porosity <5 μm). Finally, water-soluble powders of fibroin were prepared with a freeze-drying process.

### 2.2.3 Electrospinning

#### *2.2.3.1 Preparation of spinning solutions*

A series of fibroin solutions were prepared by dissolving regenerated silk-fibroin powders in formic acid at a concentration of 8-16% (wt%). PCL was dissolved at a concentration of 9% (wt%) in a mixture of DCM/DMF with 3-to-1 volumetric proportion. PEO was dissolved at a concentration of 5% (wt%) in water.

#### *2.2.3.2 Electrospinning of single-polymer materials*

In this study, single-polymer materials and composite materials were produced in flat sheet form or in tubular shape. The single-polymer nanofibrous materials were fabricated by a single electrospinning apparatus. A home-made electrospinning apparatus was composed of a Gamma High Voltage Research ES30P-10W power supply (Gamma High Voltage Research Inc., Ormond Beach, FL), a single syringe pump (Pump 11 Plus - Harvard Apparatus, Crisel Instrument, Rome, ITALY), and a flat aluminium collector to produce flat sheets or a rotating cylindrical collector to produce tubular-shaped materials. A cylindrical collector with 20 mm in diameter was rotated by a brushless rotating electric motor (BLF230C-A Oriental Motor Italia S.r.l., Milan, ITALY). Rotation speeds in the range of 50 - 2000 rpm were achieved. In addition. another collector with 4.96 mm in diameter rotating at 100 rpm was used to produce constructs with a smaller diameter. To facilitate the detachment of the scaffold materials

(fibroin or PCL), the collector was preventively coated with a thin veil of electrospun PEO. Fibroin and PCL fibers were collected with needle-collector distances of 12 cm and 22 cm, respectively. Syringes of 5 ml were filled with polymer solutions and fitted with a stainless-steel 18G blunt-ended needle which is then connected to 25 cm flexible PTFE tubing.

#### *2.2.3.3 Parametric study in the fibroin electrospinning process*

To produce good-quality silk-fibroin nanofibers, several electrospinning parameters were investigated and analyses were carried out on evaluating their effects on fiber morphology and diameter. The parameters of interest included applied voltage, solution concentration and feed rate, which varied in the range of 14-30 kV, 8-12% (wt%) and 1-12 µl/min, respectively. In addition, the effect of environmental relative humidity on fiber diameter was investigated. The electrospinning processes were thus carried out in two different environments with a relative humidity of 45% or 70%. Parameter configurations that resulted in defect-free fibers were carried further for morphology, chemical and thermal characterizations.

#### *2.2.3.4 Double-electrospinning system to produce nanofibrous composite scaffolds*

Multilayered composite scaffolds were produced by a new double-electrospinning system (Figure 2-1a and Figure 2-1b) through sequentially and simultaneously electrospinning fibroin and PCL on a rotational mandrel collector.

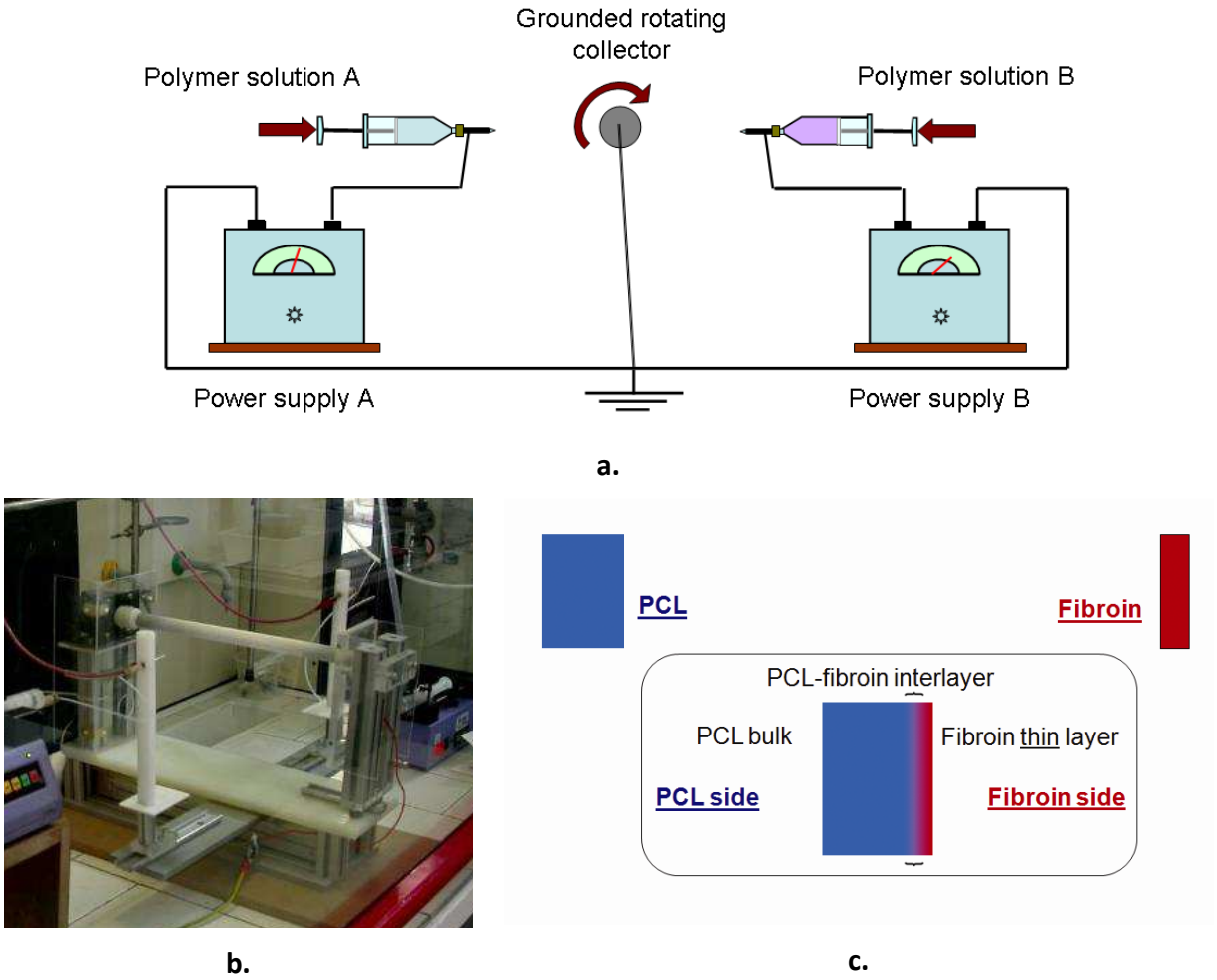


*Figure 2-1. (a) Schematic illustration of the double electrospinning system; (b) Actual setup of the system; (c) Illustration of the PCL_fibroin multilayered material.*

In sequence, a thin layer of fibroin nanofibers, an intermixed layer of fibroin and PCL nanofibers, and a thick layer of PCL electrospun fibers were deposited on the grounded cylindrical metallic collector (Figure 2-1c). Each solution (fibroin or PCL solution) was stored in a separate 5 ml syringe that served as a charged spinneret. The syringe was fitted with a blunt-ended needle and connected to PTFE tubing. Each spinneret were placed at the opposite side of the rotating mandrel, perpendicularly oriented with respect to the principal axis of the

collector, and connected to a separate high voltage power supply. Both spinnerets moved in concert over a 15 cm path with a speed of 5m/s along the mandrel under the control of a linear motorized stage (EZS3D025-C  Oriental Motor Italia S.r.l., Milan, ITALY). The feed rates of the two solutions were varied independently between 0 and an optimal flow rate over the deposition time via two different syringe pumps.

Using single-polymer electrospinning processes, electrospinning parameters were optimized for regenerated fibroin and PCL (Table 2-1).

| **Parameter** | **Fibroin** | **PCL** |
|---|---|---|
| Solvent | Formic acid | DCM/DMF (3:1) |
| Concentration | 10% (wt) | 9% (wt) |
| Voltage | 22 kV | 28 kV |
| Work distance | 12 cm | 22 cm |
| Feed rate | 7 µl/min | 15 µl/min |

*Table 2-1. Optimized electrospinning parameters.*

These fabrication parameters were used to produce fibroin-PCL composite scaffolds. Using the double electrospinning system described above, the silk-fibroin solution stored in syringe A was first electrospun on the collector at a feed rate equal to the optimal value of 7µl/min, while the PCL solution stored in syringe B were kept static. Thus, a thin layer of fibroin nanofibers was obtained. After 5 minutes, the PCL solution started to be electrospun and deposited onto the collector with a low feed rate of 1 µl/min. This was done simultaneously with the electrospinning and deposition of fibroin. During the next 10 minutes, the feed rate of

the PCL solution was gradually adjusted to the optimal value of 15µl/min, while the feed rate of the fibroin solution were gradually reduced to zero. As a result, an intermixed interlayer of fibroin and PCL nanofibers was deposited on the top of the thin fibroin layer (Figure 1b). Finally, electrospinning of the PCL solution was conducted for another 30-40 minutes, in order to obtain a thick PCL bulk layer. The obtained electrospun tubular constructs were cut along the longitudinal axis, resulting in a smooth flat sheet with a dimension of 6x12 cm and thickness approximately in the range of 90-120 µm.

*2.2.3.5 Post-treatment of scaffold materials containing fibroin*

A water/methanol mixture with 9:1 ratio was used for fibroin stabilization and detachment by dissolving PEO. Then, fibroin was rinsed with DI water and soaked overnight in DI water to eliminate solvent residuals.

### 2.2.4 Characterizations of the scaffold materials

Non-woven electrospun meshes were imaged with scanning electron microscopy (SEM). To investigate net morphology, samples were mounted on aluminium stubs and sputter coated with gold. Observations were made at 10 kV by using a Stereoscan 200 SEM (Cambridge Instrument Company, Cambridge U.K.). For nanofiber diameter analysis, three images were taken in different locations of each sample, and roughly 100 fiber diameters were measured and averaged using Image-J, an image analysis software. Results were presented as mean ± standard deviation.

Electrospun mats were analysed by FTIR in attenuate total reflectance (ATR) mode with a Perkin Elmer Spectrum One Spectrophotometer equipped with a diamond probe. In all cases 64 scans at a resolution of 2 $cm^{-1}$ were used to obtain the spectra.

Differential scanning calorimetry (DSC) was performed on 10 mg of material in an open crucible. The analysis was performed with a TA2920 calorimeter under flushing nitrogen (100 ml /min). A sample was first cooled down to -100 °C at the cooling rate of 50 °C/min, and was held at this temperature for 5 min. Subsequently, the first scan was performed by heating the sample up to 100 °C with the heating rate of 10 °C/min. This was followed by quenching the sample to -100 °C. The second heating scan was carried out by heating the sample from -100 to 315 °C with the heating rate of 10 °C/min and obtaining the thermogram. The melting peaks of PCL and PCL/fibroin samples were quantified by integration. Degree of crystallinity χc of PCL was calculated using $\chi c = 100*\Delta Hm/\Delta Hm°$, where ΔHm° was the theoretical heat of fusion for PCL with 100% crystallinity equal to 135 J/g.

### 2.2.5 Mechanical characterization

Mechanical properties were evaluated with uniaxial tensile tests on rectangular specimens (30x5 mm and 15x3 mm) cut along the circumferential (or transversal) direction and the longitudinal direction. Silk-fibroin nets were tested in a wet condition as well as in a dry condition. The fibroin nets were stored in water for 3 days at 4 °C before testing. For each specimen, three thickness measurements were taken using an electronic digital micrometer and averaged; three width measurements were taken using a custom digital caliper and averaged. Thickness of the specimens was in the range of 40-50 μm for fibroin electrospun

mats and 100-120 μm for PCL and composite samples. Mechanical tests were performed with an electromechanical Instron 4502 (Instrom, Canton, MA) universal tensile testing machine equipped with a 100 N load cell. Samples were first preloaded to 0.10 N, and the gauge length was recorded. The tensile test was carried to failure at a rate of 3 mm/min for fibroin samples and 10 mm/min for PCL samples and multilayered samples. Elastic modulus was calculated from the slope of the linear portion of the resultant stress-strain curve; maximum stress and failure deformation were also calculated from the measurement data. Four to five specimens were tested for each sample. The calculated values were averaged and reported as mean ± standard deviation. Students' t-test was carried out for statistic analysis of the data. A p value less than 0.05 was considered statistically different; a p value less than 0.01 was considered statistically very different.

### 2.2.6 Cell characterization

The endothelial cells used for characterization were cells isolated from proximal bovine pulmonary arteries and sub-cultured. Cells between passages three and six were used. Cells were cultured in Dulbecco's Modified Eagle's Medium (from Sigma-Aldrich) supplemented with 10% FBS, 2% L-Glutamine, and 1% penicillin-streptomycin at 37 ˚C and 5% $CO_2$ in the cell culture incubator. Circular electrospun nets (diameter of 1.5 cm) were sterilized in 70% ethanol, allowed to dry and briefly exposed to UV light before seeding. Cells were cultured to 90% confluency in the culture flask, detached and then seeded on the fibroin side with 1.0 ml of cell suspension per membrane at the concentration of 200,000 cells/ml. Culture medium was changed every other day. After 4 days of culture, the cell-seeded membranes were fixed with

4% formalin and stored in PBS at 4 °C. In order to prepare samples for SEM examination, electrospun nets were washed 2–3 times with distilled water, exposed to different grades of ethanol for 10 min. Finally, they were air dried under laminar flow hood. Samples were sputter coated with gold and the morphology was observed under SEM (JEOL 6480LV) at an accelerating voltage of 10 kV.

## 2.3 Results

### 2.3.1 Fibroin and PCL electrospun materials produced by a single-polymer electrospinning process

We have established single-polymer electrospinning processes to fabricate nanofibrous materials made of fibroin and PCL, respectively. The process parameters for each type of material have been optimized using a flat collector in the electrospinning system, and results are listed in Table 1. SEM images (Figure 2-2) demonstrate the microscopic morphology of nanofibrous fibroin nets and PCL nets electrospun with the optimized parameters. In both nets, the nanofibers appear to have a rounded cross-section and regular shape, with diameters in the nanometric range.

The average diameters of fibroin and PCL nanofibers are 192±79 nm and 421±105 nm, respectively. Because several studies have reported the electrospinning process of PCL structures [130], [78], the optimization of PCL electrospinning parameters is not detailed here. Parametric studies on the fibroin electrospinning process are presented below because of its unique setup. In addition, using a rotational cylindrical mandrel, we have developed the electrospinning processes for tubular structured fibroin and PCL, respectively. Parametric studies for these electrospinning processes, in particular, the effects of rotation speed on anisotropic mechanical properties of PCL nets and silk-fibroin nets, respectively, are presented.

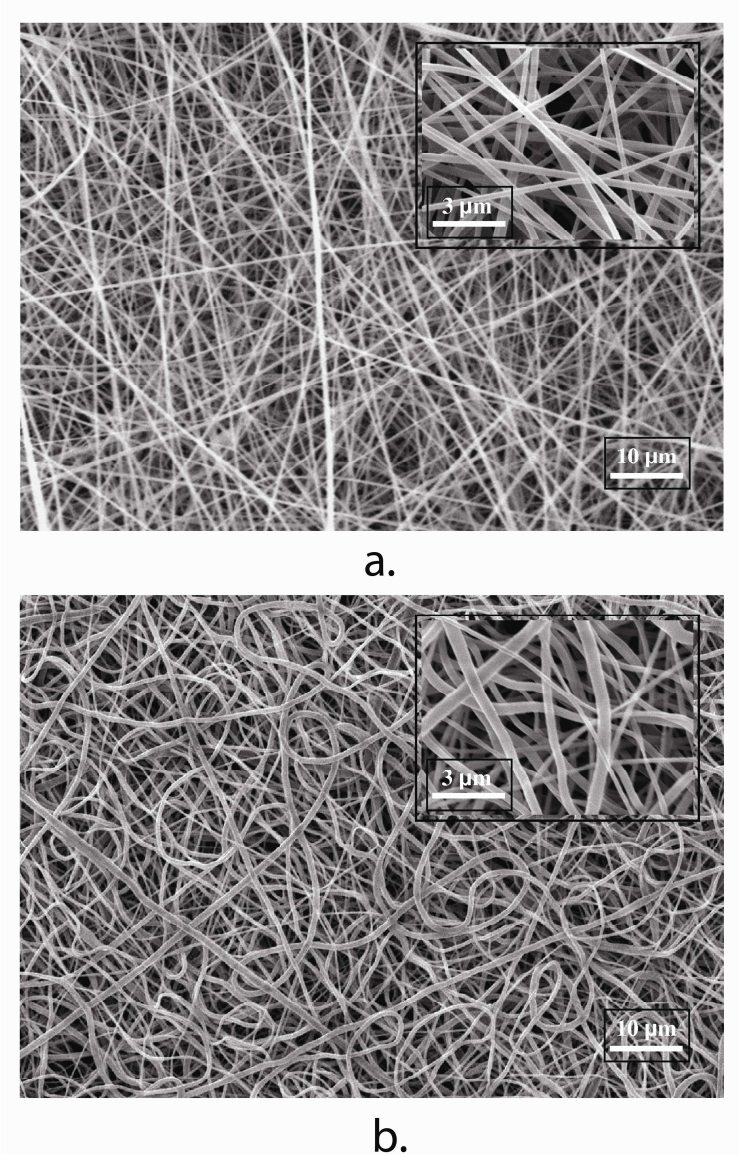


*Figure 2-2. SEM imaging graphs of silk-fibroin nanofibers (a) and PCL nanofibers (b) (scale bar = 10 µm). At a higher magnification, details of fiber morphology are shown (scale bar = 3 µm). The electrospinning processes were conducted on a flat aluminium collector with RH = 70% and optimized electrospinning parameters listed in Table 1.*

#### *2.3.1.1 Fibroin nets: parametric studies on nanofiber diameter*

Four electrospinning parameters, namely voltage, solution concentration, feed rate and relatively humidity, have been varied to investigate their influences on the fibroin fiber diameter. The electrospun fibers usually show diameters ranging from tens of nanometers to one micron. It is found that applied electric voltage in the tested range does not significantly influence the diameter of silk-fibroin nanofibers (Figure 2-3a), while the solution concentration plays an important role in determining the fiber diameter. No continuous defect-free fibers have been obtained with the fibroin solution at a concentration of 8% or lower in formic acid. When the solution concentration is 10% or higher, the mean fiber diameter increase exponentially with concentration; the mean fiber diameter increases from 192 nm at 10% to 325 nm at 14% (Figure 2-3b).

With our fabrication setup, it is not possible to obtain fibroin solutions in formic acid at a concentration higher than 14%. Another parameter, the feed rate at which the solution is forced out of the spinneret, does not significantly influence the mean fiber diameter when the feed rate is lower than 7 μl/min. Higher feed rates result in larger mean diameters (Figure 2-3c). Furthermore, environmental relative humidity (RH) shows a significant effect on the fiber diameter (Figure 2-3d). Electrospinning in a relatively humid condition (RH = 70%) results in much larger fibroin fibers compared to that in a less humid condition (RH = 45%).

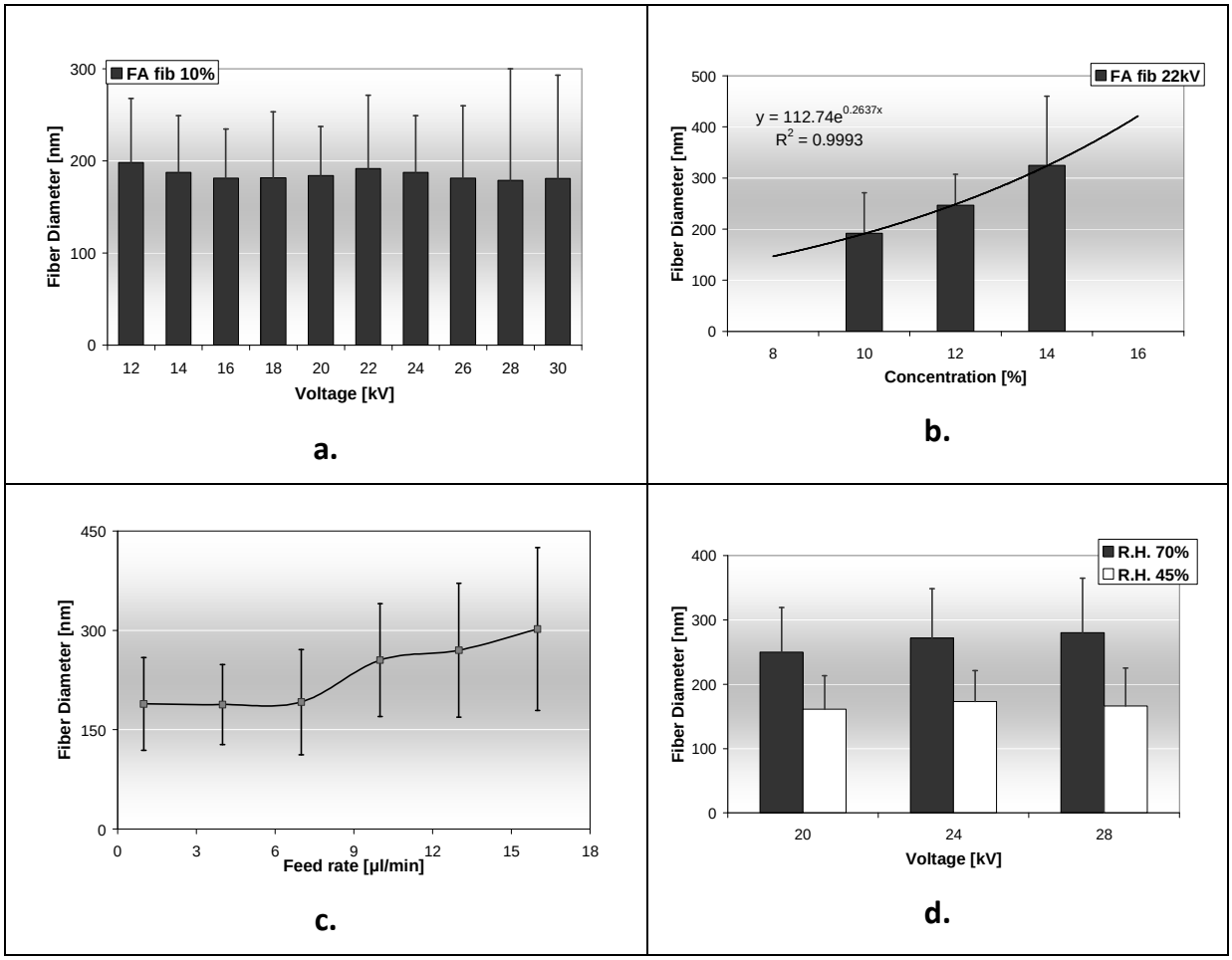


*Figure 2-3. Effects of electrospinning process parameters on the mean fiber diameter of electrospun silk-fibroin: (a) applied voltage; (b) solution concentration; (c) feed rate; and (d) environmental relative humidity (R.H.). Effects of R.H were studied at different electrospinning voltages: 20 kV, 24 kV, and 28 kV.*

Using the single-polymer electrospinning process with optimized parameters (Table 2-1) and a flat collector, fibroin nanofibers are characterized by an average diameter of 192 nm with a narrow normal-like distribution (Figure 2-4). The resultant electrospun nets contained a uniform array of randomly oriented fibers with smooth rounded surface.

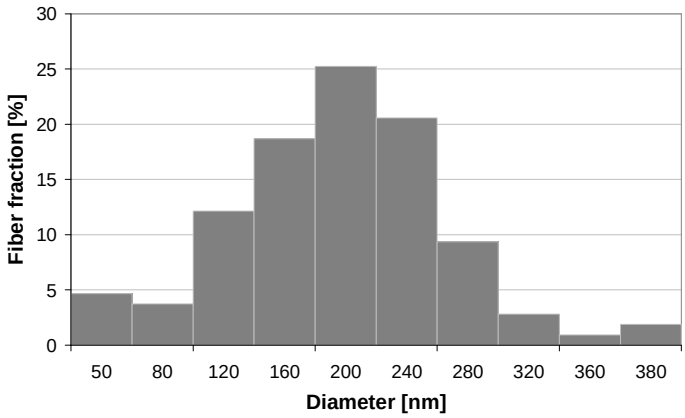


*Figure 2-4. Frequency distribution of the fiber diameter of silk-fibroin nets electrospun with optimized parameters shown in Table 2-1.*

*2.3.1.2 Fibroin nets: mechanical properties in a hydrated condition*

Fibroin nanofiber scaffolds were prepared by electrospinning fibers on a rotating cylindrical collector with a 20 mm diameter at varied rotation speeds including 100, 250, 500, 1000, 1500 and 2000 rpm. As a reference, electrospun samples for 0 rpm were prepared by using a rectangular collector with the same projected area as the cylindrical collector. Tensile tests were performed on the samples cut from the tubular constructs in the longitudinal direction and in the circumferential direction, respectively. Samples of a similar size from the rectangular scaffold materials were used as the reference (0 rpm). Figure 2-5 demonstrates that the mechanical properties, elastic modulus and maximum strength, change as function of the rotation speed of the mandrel. The samples collected at a high rotation speed, such as 500 rpm and 2000 rpm, show higher elastic modulus and mechanical strength in the circumferential direction.

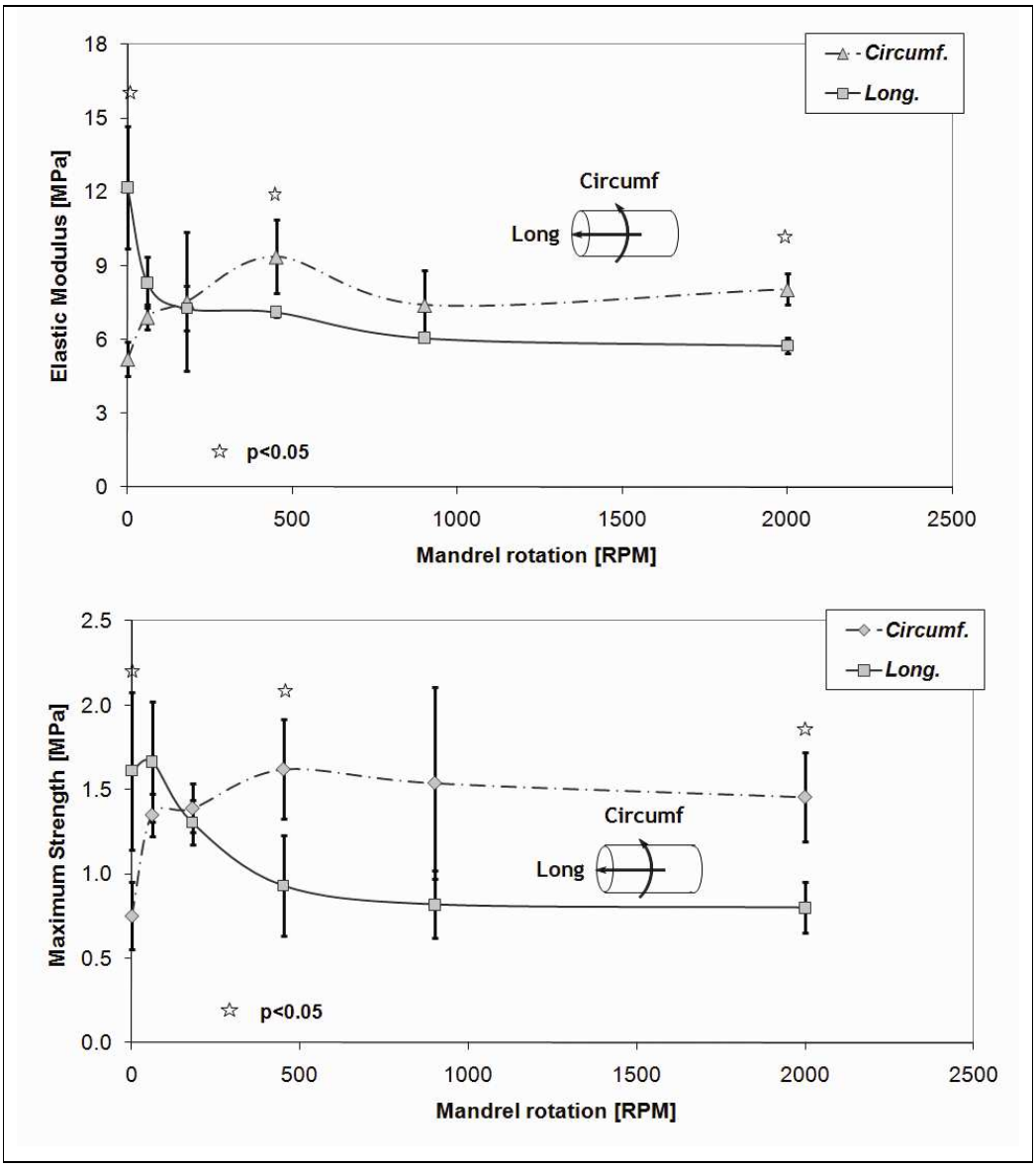


*Figure 2-5. Elastic modulus and ultimate strength of silk-fibroin electrospun nets produced with a rotating collector. These properties in both longitudinal and circumferential directions change with the rotation speed. "☆" shows that the mechanical property of the sample in the longitudinal direction is significantly different from that in the circumferential direction ($p<0.05$).*

On the contrary, the samples collected at a low rotation speed, such as 100 rpm, and those collected from a static rectangular collector (0 rpm) show higher elastic modulus and

mechanical strength in the longitudinal direction. According to the data, an inversion point for the anisotropy of mechanical properties is estimated to be around 200 rpm. However, at several rotation speeds, no statistically significant differences between the mechanical properties in the two directions are found. Results also show that the strengths of fibroin nanofiber scaffolds fabricated in various conditions were always low – no higher than 1.7 MPa.

#### *2.3.1.3 PCL anisotropic mechanical properties*

PCL nanofiber scaffolds were prepared by electrospinning fibers on a rotating cylindrical collector with a diameter of 20 mm at varied rotation speeds, including 100, 250, 500, 1000, 1500 and 2000 rpm. Similar as fibroin, electrospun PCL samples for 0 rpm were prepared by using a static rectangular collector with the same projected area as the cylindrical collector. Samples for mechanical testing were also collected in both longitudinal and circumferential directions. It is found that the mechanical properties of PCL samples show more anisotropic behaviors than fibroin samples. The anisotropy is also dependent on the rotation speed of the mandrel collector (Figure 2-6). The samples collected at a low rotation speed, such as 0, 100, 250, 500 and 1000 rpm, show higher elastic modulus and ultimate strength in the longitudinal direction. The samples collected at a high rotation speed, such as 1500 and 2000 rpm, show higher elastic modulus and ultimate strength in the circumferential direction. The estimated inversion point for the anisotropy is between 1000 and 1500 rpm.

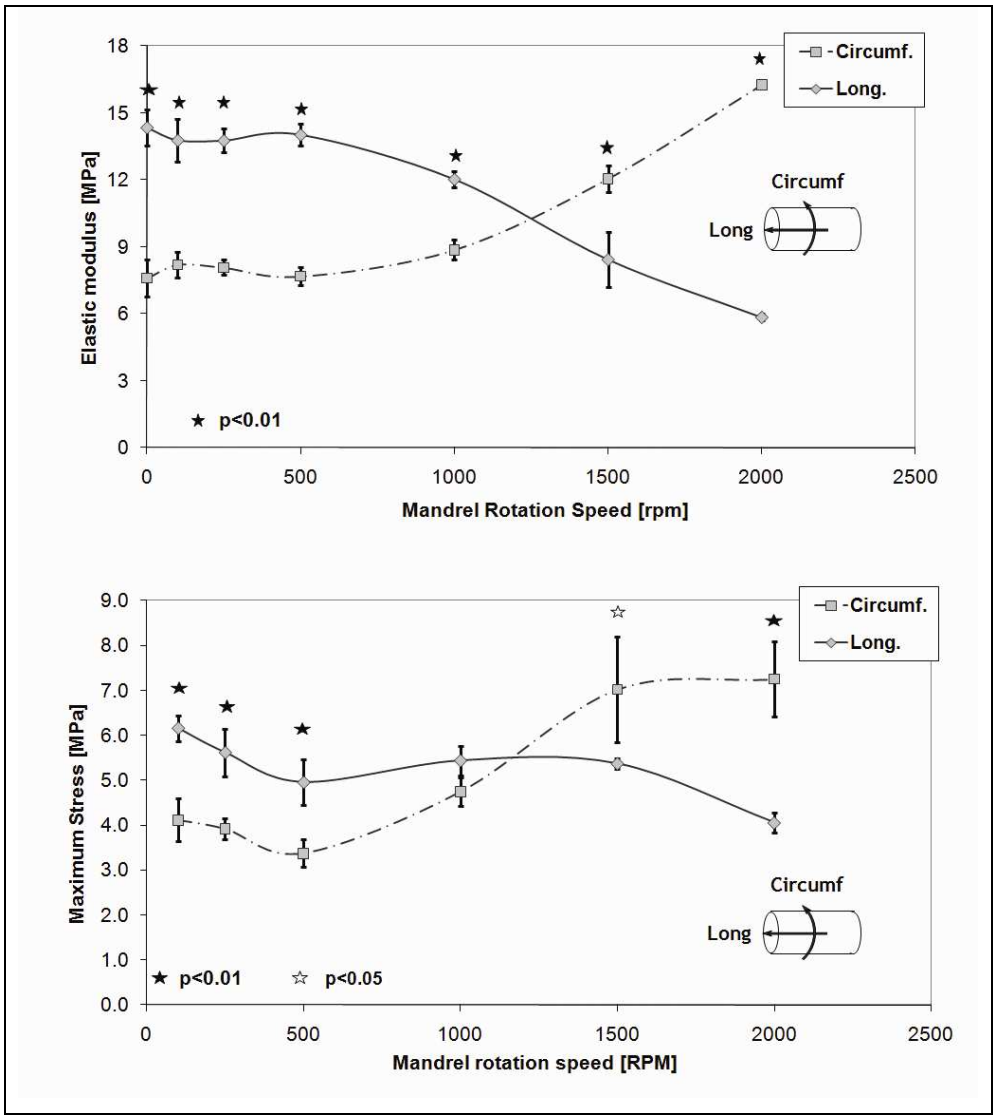


*Figure 2-6. Elastic modulus and ultimate strength of PCL electrospun nets produced with a rotating collector. These properties in both longitudinal and circumferential directions change with the rotation speed. "☆" and "★" show that the mechanical property of the sample in the longitudinal direction is significantly different from that in the circumferential direction ($p<0.05$ and $p<0.01$, respectively).*

*2.3.1.4 Mechanical properties of small diameter constructs*

PCL tubular constructs with a small diameter were prepared by electrospinning fibers on a cylindrical collector with a diameter of 4.96 mm rotating at 100 rpm (Figure 2-7). Specimens (15x3 mm) cut along the longitudinal and circumferential directions confirm the anisotropic mechanical behavior of the electrospun materials. In longitudinal direction, an elastic modulus of 11.82 ± 0.55 MPa and an ultimate strength of 7.25 ± 0.71 MPa were obtained; in the circumferential direction, the elastic modulus and ultimate strength were 4.04 ± 1.17 MPa and 3.55 ± 0.54 MPa, respectively. Thus, the mechanical anisotropic index (longitudinal-to-circumferential ratio of elastic modulus) results equal to 2.92.

*Figure 2-7. PCL tubular construct prepared by electrospinning.*

*2.3.1.5 Effect of collector shape*

In order to test the assumption that the anisotropic mechanical properties are related to the geometrical shape of the collector, we have designed a series of collectors which are characterized by different width-to-length aspect ratios (Figure 2-8). It was found that nets electrospun on a slender rectangular collector with higher width-to-length ratio present higher

modulus and strength along the length compared to those electrospun on a collector with lower width-to-length ratio. For example, for a width-to-length aspect ratio of 6, a mechanical anisotropic index of 2.27 was found.

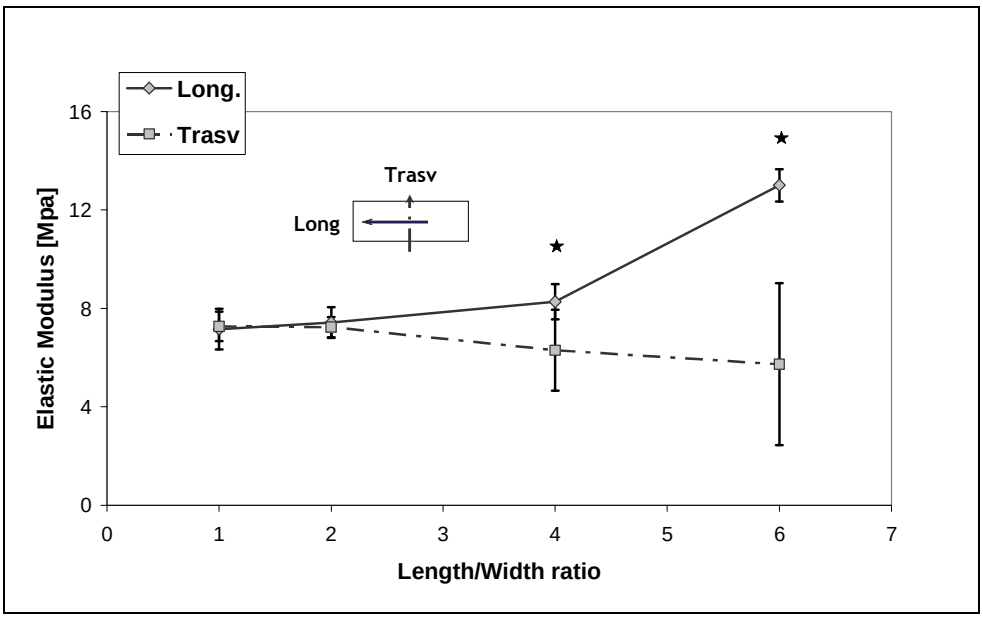


*Figure 2-8. Effect of collector shape on the mechanical property of PCL electrospun material. Elastic modulus along the two principal directions of the electrospun nets is reported as function of the length/width ratio of the collector.*

### 2.3.2 Multilayered PCL-fibroin scaffold produced by a double electrospinning process

*2.3.2.1* *Chemical and thermal characterizations of the structure*

PCL and silk-fibroin have been electrospun on a cylindrical collector rotating at a constant velocity to form a composite scaffold. With the new double-electrospinning apparatus described above, a multi-layered electrospun structure is formed and consists of an ultrathin layer of fibroin nanofibers, an interlayer of mixed nanofibers of fibroin and PCL, and a thick layer of PCL nanofibers. FT-IR analyses of the two opposite surfaces confirm that the layers are completely different in the composition (Figure 2-9). The ATR FT-IR spectra show the presence of pure PCL on one side (called PCL side) and fibroin on the other side (called fibroin side). Additionally, the shoulder at 1730 $cm^{-1}$ in the FT-IR spectrum of the fibroin side revealed a limited presence of PCL.

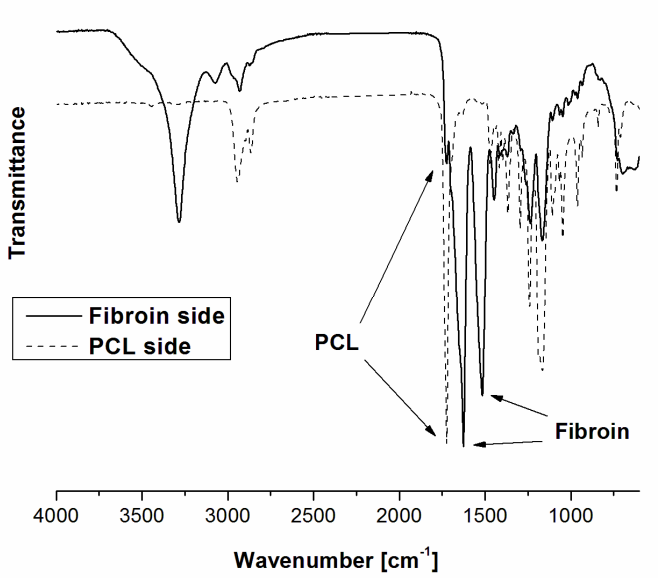


*Figure 2-9. ATR FT-IR analysis of the scaffold shows completely different compositions on the two surfaces. PCL side shows the characteristic spectrum of PCL, and fibroin side shows the characteristic spectrum of prevalent β-sheet fibroin and a small contamination of PCL due to the limited thickness of the fibroin layer.*

Figure 2-10 compares the DSC curve of a PCL-fibroin multilayered material with that of a pure electrospun PCL material. In the DSC analysis, the presence of fibroin is revealed by a small endothermic peak around 280 °C, which is corresponding to thermal degradation of silk-fibroin. It is known from previous results that the degradation peak area for a pure electrospun fibroin material is in the range of 230-250 J/g. Thus, using the area of the small peak shown in the composite scaffold (around 10-12 J/g), the overall content of fibroin inside the multilayered scaffold can be estimated to be around 5% in weight. The degrees of crystallinity of PCL for PCL and PCL/fibroin samples are equal to 40.4 % and 37.5 %, respectively.

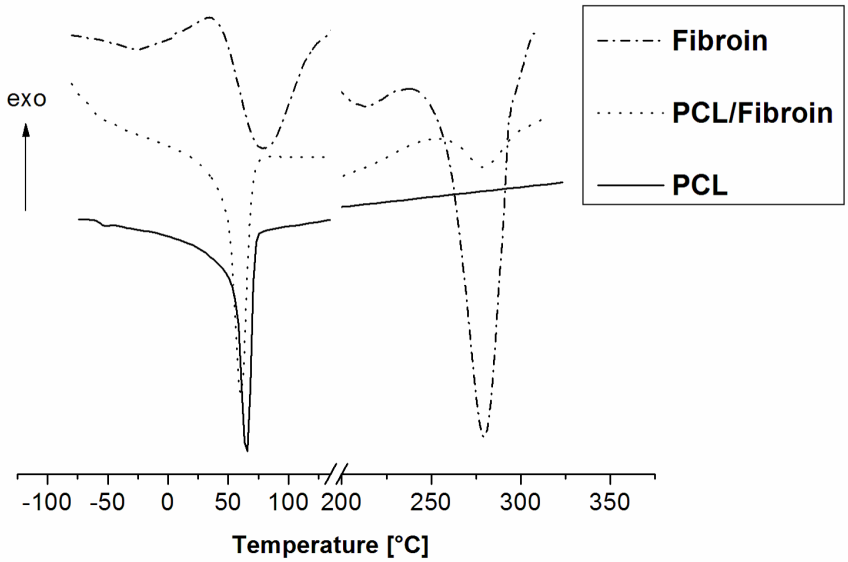


*Figure 2-10. DSC thermographs for PCL/fibroin multilayered material, pure PCL and pure Fibroin. The small endothermic peak at 280 °C, which is common to fibroin and PCL/fibroin multilayered material, is attributed to the thermal degradation of silk fibroin.*

*2.3.2.2 Anisotropic mechanical properties of the multilayered structure*

The mechanical properties of nanofibrous multilayered PCL-fibroin scaffolds have been studied and evaluated in comparison to the mechanical properties of pure PCL scaffolds prepared in the same conditions (Figure 2-11a). No significant differences in elastic modulus or in ultimate strength (data not shown) are found between multilayered PCL-fibroin scaffolds and pure PCL scaffolds in both circumferential and longitudinal directions. This is found on the samples collected at a low rotation speed (150 rpm) and on those collected at a high rotation speed (1500 rpm).

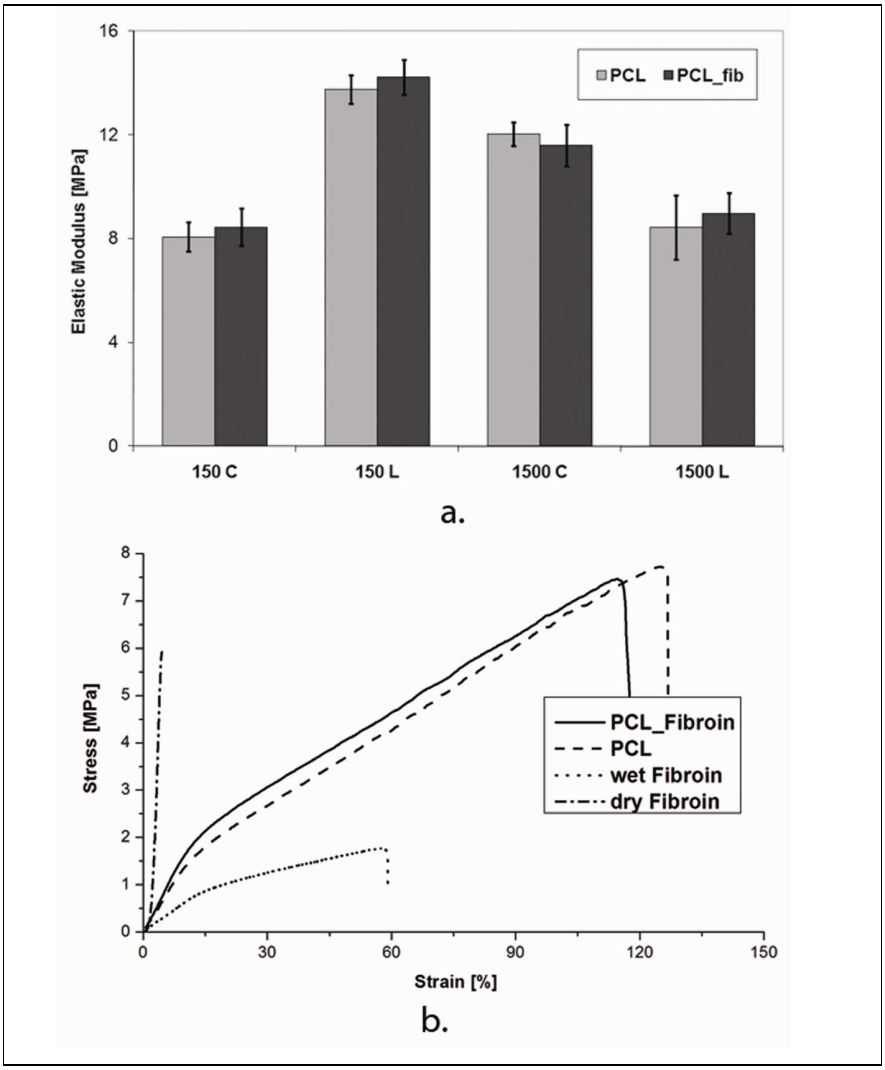


*Figure 2-11. a) Elastic modulus of multilayered PCL-fibroin materials and pure PCL materials. The material fabrication used a cylindrical collector rotating at a low speed (150 rpm) and a high speed (1500 rpm). All the tests were performed on the circumferential direction "C" and the longitudinal direction "L" of the samples. No significant differences in elastic modulus were found ($p>0.05$). b) Representative stress-strain curves of hydrated fibroin, dry fibroin, PCL, and PCL-fibroin electrospun nets. The material fabrication used a cylindrical collector rotating at a high speed (1500 rpm). All the tests were performed on the circumferential direction of the tubular scaffolds.*

Therefore, fibroin does not significantly contribute to the mechanical property of the multilayered composite scaffold. This is also shown by representative stress-strain curves for multilayered PCL-fibroin material and pure PCL electrospun material using specimens cut in the circumferential direction (Figure 2-11b). These curves also show that the mechanical property of fibroin electrospun material is dependent on the humidity; it is much stiffer and stronger in a dry condition than it is in a hydrated condition.

*2.3.2.3 Endothelial cell characterization*

Endothelial cell culture test was performed on flat electrospun constructs using primary arterial endothelial cells (Figure 2-12).

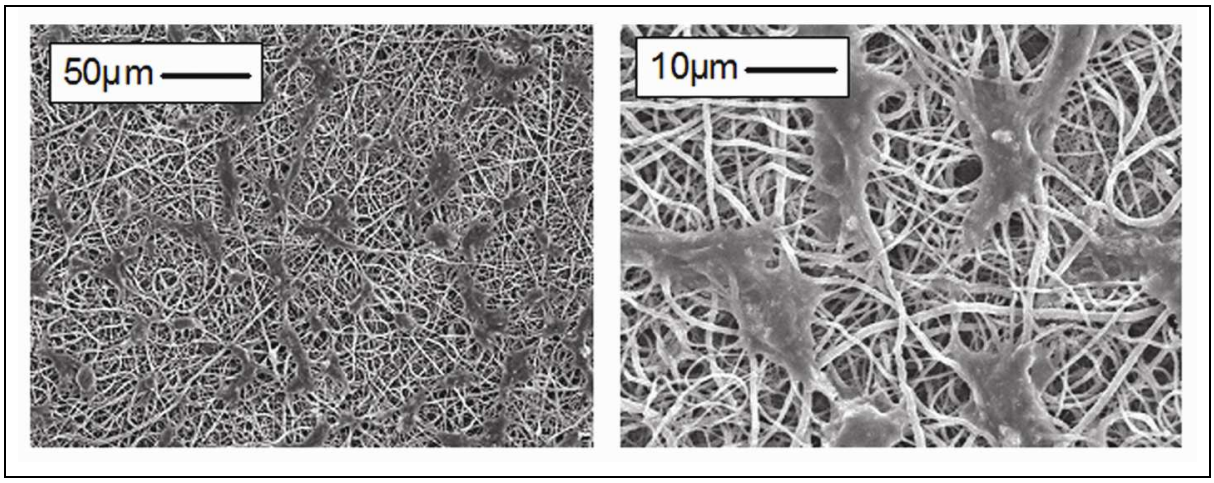


*Figure 2-12. SEM images of bovine pulmonary artery endothelial cells seeded on the fibroin side of the multilayered structure (4 days in culture).*

A low concentrated cell suspension was seeded on the two different surfaces of the multilayered electrospun structure. Cell morphology and adhesion site were examined after 4 days of culture. Endothelial cells seeded on the fibroin side resulted in a highly spread

morphology, protruding cytoplasmic interconnections between the cells along a larger number of electrospun fibers.

## 2.4 Discussions

The present study has reported the development of electrospinning processes of silk-fibroin, PCL and PCL-fibroin multilayer scaffolds for engineered vascular construct. Using a single-spinneret electrospinning system with a flat collector, we have optimized electrospinning parameters to obtain defect-free, uniform nanofibers from pure PCL and pure silk-fibroin, respectively. In particular, the effects of applied voltage, protein concentration, feed rate and environmental humidity on the fibroin fiber diameter are demonstrated. Using a rotating cylindrical collector, anisotropic mechanical behaviors of these pure nanofiber materials are obtained and the anisotropy is found to be dependent on the rotation speed of the collector. In addition, we have developed a new double-electrospinning system, and have achieved a promising combination of mechanical property and biological property with a biohybrid nanofibrous scaffold made from PCL and silk-fibroin.

### 2.4.1 Electrospinning of silk fibroin

A major difference in fibroin electrospinning and characterization presented here from previous studies [131,132] is that we have taken the environmental relative humidity (RH) and the hydration state of a fibroin sample into consideration. We have shown that the diameter of fibers electrospun at 45% RH were about half of that at 70% RH (Figure 2-3d). It is likely because water molecules reduce the electric charge density on the developing fibers, thus reducing the driving force for fiber elongation and diameter reduction. Also, a single fiber can be stretched

more in a dry environment because the viscosity remains low for a longer time, an effect equivalent to extending the distance from the needle, while a fiber in a more humid environment becomes solid faster and experiences a lower degree of stretching. In addition, we have demonstrated the difference in mechanical properties between dry and hydrated fibroin nets (Figure 2-11b). It is found that hydration highly reduces stiffness and strength of the electrospun material. Because the scaffold is often used in the hydrated state, the majority of mechanical characterizations performed here are based on hydrated samples. The ultimate tensile strengths reported in this study are comparable to the values reported by Soffer et al. [133] who electrospun hydrated fibroin nets from a PEO/fibroin water solution, but the elastic modulus reported here are much higher, ranging from 5.32 to 12.11 MPa. The difference is likely attributed to a much higher testing rate (3 mm/min compared to 0.2 mm/min) and the preconditioning cycles used in the present study.

### 2.4.2 Effect of the rotation speed and the collector shape on anisotropic mechanical properties

The present study have shown that varying rotation speed leads to changes in the material mechanical anisotropy index which is defined as the ratio of the mechanical property in the longitudinal direction to that in the circumferential direction. With the rotation speed varying from 0 to 2000 rpm, anisotropy indices of elastic modulus range from 1.7 to 0.35 for PCL material, and anisotropy indices range from 1.2 to 0.70 for fibroin material. PCL shows more gradual changes in the anisotropy index with the rotation speed, and a wider range of anisotropy indices is achievable with PCL. In addition, no significant differences are found

between pure PCL nets and multilayered PCL-fibroin nets both at 150 rpm and at 500 rpm. This suggests that mechanical properties of a PCL-fibroin bi-layered system are similar to those of a pure PCL electrospun material. This could be due to the small amount of fibroin (~5% in weight) in the composite construct according to the DSC analysis results. The dependence of the mechanical anisotropy index on the rotational speed could be explained by the relationship between fiber alignment and rotational speed, according to previous studies which showed that a rotational collector tended to align the fibers along the circumferential direction at higher rotation speeds [134]. The nanofiber alignment in the circumferential direction happens when the tangential velocity at the collector surface exceeds the velocity at which the nanofibers approach the collector, particularly when the rotation speed becomes higher. Additionally, many studies have shown a strong correlation between mechanical properties and fiber alignment in non-woven electrospun materials [135–137]; progressive alignment of the fibers in one direction improves elastic modulus and tensile strength of the material in the same direction.

It is also noticed in this study that at 0 rpm and at lower rotation speeds, both PCL and fibroin materials show higher modulus and strength in the longitudinal direction than in the circumferential direction. Because there is no mandrel rotation, it may involve the effect of collector shape. In order to test the assumption that the anisotropic mechanical properties are related to the geometrical shape of the collector, we have designed a series of collectors which are characterized by different width-to-length aspect ratios (Figure 2-8). It was found that nets electrospun on a slender rectangular collector with higher width-to-length ratio present higher modulus and strength along the length compared to those electrospun on a collector with

lower width-to-length ratio. The distortion of the electric field in the air gap might induce the alignment of fibers along the prevalent geometrical direction and thus higher mechanical properties along that direction (See Figure 2-13). The collector shape effect on the mechanical anisotropic index is also important at lower rotation speeds when the effect of mandrel rotation is negligible. The inversion point, where the anisotropic index is equivalent to 1, suggests the balance between the collector shape effect and the rotation speed effect. It is about 1200rpm for PCL and 150rpm for fibroin.

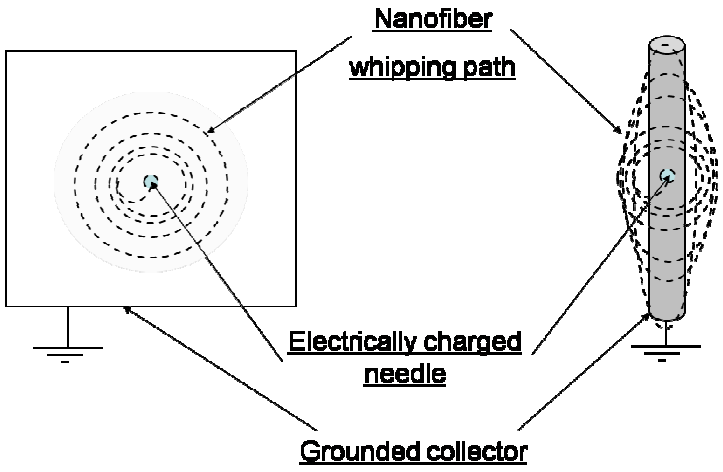


*Figure 2-13. Effect of the shape of the collector. A distortion of the electric field in the air gap might induce a preferential alignment of nanofibers along the prevalent geometrical dimension of the collector*

At low rotation speed of the mandrel the material in the longitudinal direction is stronger and stiffer than in circumferential direction. This property is desired for vascular grafts. Therefore, we also produced constructs with a smaller diameter (4.76 mm) at a low rotation speed of 100 RPM. After mechanically testing the construct in longitudinal and in

circumferential directions we found that the anisotropic behaviour was also demonstrated by small diameter constructs. In particular, elastic modulus and ultimate strength in the longitudinal direction are higher than the respective values in the circumferential direction. The longitudinal-to-circumferential ratio was 2.92.

### 2.4.3 Double electrospinning system

Double electrospinning combines the advantageous properties of two types of materials, but more importantly, it better integrates their nanofibers compared to a simple overlapping of nanofibers. We have shown that the multilayered structure resulted from double electrospinning improves biological properties of PCL as endothelial adhesion potential on the scaffold surface increases with a natural cell-conducive polymer (fibroin), while it retains superior mechanical properties of the synthetic slow degradable polymer (PCL). Furthermore, as shown in Figure 9b, the stress-strain behaviors of fibroin and PCL are quite different, which result in completely different behaviors during deformation. As no strong adhesion exists at the PCL and fibroin interface, a simple overlapping of a PCL layer and a fibroin layer leads to delamination of the construct during deformation. Therefore, the fundamental importance of the double electrospinning system resides in the possibility to produce a mixed fiber interlayer. The intermixed region acts like an active interphase that transmits interfacial forces and avoids delamination. Different from the other recently developed double electrospinning system by Baker et al. [137], the system established in the present study designs two charge needles, from which the polymers solutions are ejected, to move concurrently along the rotating mandrel, thus resulting in a more effective mixing of the different materials. In addition, there are no

charged shields placed perpendicularly to the mandrel, thus preventing any modifications of the electric field in the region between the charge spinnerets and the collector.

### 2.4.4 Application of the scaffolds in tissue engineering

Mechanical property and surface biological property are both important for vascular scaffolding materials. To reproduce anisotropic mechanical property of arteries, engineered vascular scaffolds need sufficient radial compliance and relatively higher longitudinal stiffness (anisotropy index > 1). Thus electrospinning processes at lower rotation speeds of the mandrel are likely useful to produce these anisotropic scaffolds, and changing the mandrel rotation speed makes the anisotropy tunable, particularly with PCL bulk materials. Using a multilayer structure with bulk PCL and limited amount of fibroin on the surface, we can obtain not only an optimized combination of anisotropic mechanical property, but also surface properties for cells. Compared to PCL, a fibroin-based matrix better supports endothelial cell growth due to the favorable biological properties of the silk protein. Besides the composition, the net morphology is also important for the formation of effective endothelial layer. Other studies also demonstrated that three-dimensional silk-fibroin nets derived from the cocoons of the silk worm, *Bombyx mori*, support the attachment, spread and growth of a variety of human cell types of diverse tissue origins [138]; in particular, it has been reported that the regenerated silk-fibroin maintains normal cell phenotypes and functions of primary human macro- and micro-vascular endothelial cells as well as endothelial cell lines [138], and has anti-thrombogenic potential [124].

## 2.5 Conclusions

We have demonstrated a double-electrospinning technique to produce a robust tubular scaffold with well-integrated nanofibrous structure, anisotropic mechanical behaviour and endothelial-conducive surface, for vascular tissue engineering. A thick bulk PCL mesh of nanofibers, an intermediate intermixed fibrous layer, and a thin layer of silk-fibroin nanofibers have been combined to form a multilayered structure which is stable against mechanical delamination. The structure can be stiffer in the longitudinal direction and more compliant in the circumferential direction, and reach up to 2.5 in the longitudinal-to-circumferential ratio in this study. The combination of the collector shape and the collector rotation allows us to produce a tubular structure with tunable anisotropic mechanical properties. The phenomenon has been extensively demonstrated in the case of electrospinning on a 20 mm mandrel, while can be generally applied. In fact, samples obtained with a 4.96 mm mandrel rotating at 100 rpm confirm the anisotropic behavior reaching a longitudinal-to-circumferential ratio higher than 2.9. In addition to vascular scaffolds, the system and technique developed in this study will be important for many other tissue engineering applications as well.

# 3 BIOMOLECULE GRADIENT IN MICROPATTERNED FIBROUS SCAFFOLD FOR SPATIOTEMPORAL RELEASE


## Abstract

Delivery of drugs, growth factors or other biomolecules dramatically increases the scaffold ability to direct and sustain cell attachment, migration, proliferation and, ultimately, cell activity both in vitro and in vivo applications. Moreover, spatial confinement, temporal control and specificity of drug presentation are pivotal factors in directing cell behaviour and tissue repair and remodelling.

Using a modified double-electrospinning system, we have demonstrated heterogeneous nanofibrous scaffolds composed of degradable polymers poly(ε-caprolactone) (PCL) and poly(lactide-co-glycolide) acid (PLGA) characterized by compositional and biochemical gradients along the scaffold thickness. We have revealed the different behaviours of acid terminated PLGA (PLGAac) and ester terminated PLGA (PLGAes) during degradation in an isotonic phosphate solution.

By means of fluorescent molecules and fluorescently-labeled albumins encapsulated in the nanofibers, we have successfully visualized the concentration profile of the scaffold

constituents. Spatially-confined delivery was demonstrated for a variety of micropatterned PCL-PLGAac scaffold with a novel side-by-side release test. These electrospun composite graded scaffolds have shown programmable delivery of the model molecules to one specific surface of the device with efficiency of separation as high as 95%. In addition, we obtained simultaneous and sequential release of two different model proteins on the two surfaces of the newly engineered, composite electrospun scaffolds, and we showed that release kinetics can be influenced by changing the initial pattern of drug distribution and the composition of the scaffold. We believed that scaffold preparation and release micropatterns presented in this work may represent the platform for the development of novel multifunctional matrices able to control and direct the process of tissue regeneration.

## 3.1 Introduction

Growing evidence has shown that tissue morphogenesis is coordinated by the spatial arrangement and temporal duration of multiple molecules in the three-dimensional (3D) extracellular matrix [93,94]. This has stimulated recent advances in the design of a new generation of biomaterials, which aim to mimic the spatio-temporal regulatory mechanisms of molecules for tissue regeneration or other therapeutic purposes [92,105,108]. To incorporate biomolecules into biomaterials and sustain the biomolecule release in vitro or in vivo, methods, such as adsorption and covalent binding [83,84], encapsulation [85,86], and addition during scaffold formation [87], have been developed. To deliver biomolecules in a more specific or spatiotemporally-controlled manner, recent developments in the area have demonstrated the advantages of micro- and nano-structured devices [70,100,101] and material scaffolds [102–104]. For tissue engineering and regenerative medicine, the need of precisely regulating regenerative molecule microenvironments is ever increasing. The majority of newly-developed molecule-impregnated scaffolds, however, are only capable of achieving sustained or temporally-controlled molecule release. Few techniques are available to engineer 3D scaffolds that define spatial organization of molecules or spatially-controlled release. The spatial control over release is critical to coordinate cell behaviors for tissue pattern formation [92,102]. Also, because the functions of many biomolecules such as proteins are cell- and tissue- specific, selective release of molecules that target specific cell types or tissue formation without influencing the activity of other cell populations or tissue functions is important to establish

both *in vitro* physiological tissue models and *in vivo* tissue regeneration [105–107]. Currently, techniques of 2D on-chip patterning or 3D segregation of molecule delivery materials are available to spatially confine biomolecules [108–110]. However, to meet various physiological needs of tissue regeneration, a 3D scaffold should not only present a multitude of regenerative biomolecules in a sustained manner at defined locations, but also be capable of precisely programming spatiotemporal control to meet physiological needs as well as satisfying other tissue-specific requirements such as mechanical properties. This is a challenging task, given the fact that it is difficult to simultaneously build multiple functional features into one scaffolding material.

Electrospinning of biomaterials has been increasingly used to fabricate tissue engineering scaffolds in the last decade, because they offer adequate mechanical property for implantation [65], and nanostructure guidance to cell adhesion and proliferation [53,54]. Electrospun biomaterials, consisting of nanofibers that mimic the structure of the native extracellular matrix, provide a wide range of mechanical and chemical properties via fiber composition, diameter, distribution and porosity [45,47,49,70]. Recently, various methods using electrospun fibers to encapsulate and deliver molecules have been established [46]. This could dramatically increase the scaffold ability to regulate various cell activities. Due to inherently high surface area of electrospun materials, these constructs allow high molecule loading and efficient release *in situ*. However, the developed techniques have been limited to tune molecule release kinetics. As far as we know, no electrospun constructs with capability of spatially-defined or spatiotemporally-controlled delivery of biomolecules have been demonstrated before.

We have previously developed double-electrospinning technique to fabricate interpenetrating networks of nanofibers from different polymers [43]. We also demonstrated the use of diverse nanofibers in a tailored proportion to engineer the surfaces or anisotropic mechanical properties of tissue scaffolds. By furthering the techniques to program micropatterns of molecule-impregnated nanofibers, the present study aims to demonstrate composite, electrospun biomaterials that are capable of selectively releasing molecules in spatially- and temporally- controlled manner. Herein, heterogeneous nanofibers composed of degradable polymers poly(ε-caprolactone) (PCL) and poly(lactide-co-glycolide) acid (PLGA), have been used to form scaffolds with compositional and biochemical gradients along the scaffold thickness. Using PLGA nanofibers to encapsulate small molecules or proteins, we have characterized compositional and morphological changes as well as degradation behaviours of these composite scaffolds for up to 50 days *in vitro*.

## 3.2 Materials and Methods

### 3.2.1 Materials

LACTEL® 50:50 poly(d,l lactide-co-glycolide) acid with a carboxylate end group and intrinsic viscosity of 0.67 dL/g, hereinafter referred to as PLGAac, was purchased from DURECT Corp. (Pelham, AL). PURASORB® 50:50 poly(d,l lactide-co-glycolide) acid with an ester end group and intrinsic viscosity of 0.32-0.48 dL/g, hereinafter referred to as PLGAes, was obtained from Purac Biomaterials (Lincolnshire, IL). PCL with molecule weight of 80 kDa, chloroform (CF), N,N-dimethylformamide (DMF), methylene chloride (MC), methanol (MetOH), 1,1,3,3,3-hexaflouro-2-propanol (HFIP), sodium phosphate ($NaH_2PO_4$), sodium phosphate dibasic ($Na_2HPO_4$) and sodium azide were all purchased from Sigma Aldrich (St. Louis, MO). Polymers were used as received. Solvents were of analytical grade and used without any further purification. Isotonic phosphate buffer solution was prepared by mixing a 0.13 M solution of $NaH_2PO_4$ with 0.002% sodium azide and a 0.13 M solution of $Na_2HPO_4$ with 0.002% sodium azide, and then adjusting pH and osmolarity to 7.4 and 290-300 mosmol/L, respectively. Sodium azide was used to prevent bacterial contamination.

Fluorescent dyes, rhodamine 123 (Rh123) with green emission, rhodamine-B (RhB) with red emission, coumarin with blue emission, as well as fluorescently-labelled proteins, fluorescein isothiocyanate conjugate bovine serum albumin (AlbF) with green emission and tetra-methyl-rhodamine isothiocyanate conjugate bovine serum albumin (AlbT) with red emission were all obtained from Sigma Aldrich. The molecular weight, chemical formula,

excitation/emission wavelength and usage in this study of fluorescent dyes and fluorescently-labelled albumins are summarized in Table 3-1.

| Dyes | Molar Mass [g/mol] | Chemical formula | Excitation /Emission [nm] | Use |
|---|---|---|---|---|
| **Rhodamine 123 (Rh123)** | ≈760 | 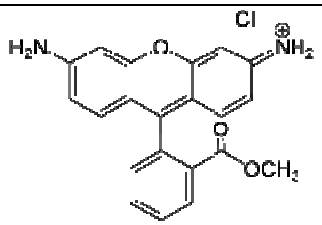 | 485/535 | Release/ Imaging |
| **Rhodamine-B (RhB)** | 479.02 | 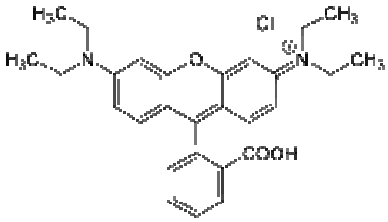 | 560/590 | Imaging |
| **Coumarin** | 146.14 | 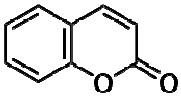 | 360/450 | Imaging |
| **Albumin-Fluorescein isothiocyanate (Alb F)** | 66000/ 389.4 | 7 to 12 moles of FITC per mole of albumin | 485/535 | Release |
| **Albumin-Tetra-methylrhodamine isothiocyanate (Alb T)** | 66000/ 364.2 | About 1 mole of TRITC per mole of albumin | 560/590 | Release |

*Table 3-1. Fluorescent dyes, fluorescent-labeled albumins properties and their uses*

### 3.2.2 Preparation of electrospinning solutions

PCL was dissolved in 75/25 CF/DMF at a concentration of 10% (wt). For both PLGAac and PLGAes, the pre-spinning polymer solutions were prepared by dissolving the polymer in the mixture of HFIP and DI water with a ratio of 7:1 (vol) with a final concentration of 17% (wt). To

visualize the compositional gradients across the thickness of electrospun scaffolds and to characterize the molecule release profiles, fluorescent dyes or fluorescently-labelled albumins were added to pre-spinning solutions. DI water was used to dissolve fluorescent dyes. A solution of Rh123 or RhB with a concentration of 1 mg/ml was prepared with DI water, and then mixed with HFIP (7:1). Subsequently, the mixture was used to dissolve PLGAac and PLGAes. A PCL/coumarin pre-spinning solution was obtained by dissolving the polymer at a concentration of 8% (wt) in a ternary solvent mixture of MC:DMF:MetOH with a ratio of 5:3:2 (vol), where MetOH served as the carrier for coumarin. This was done by first dissolving 10 mg of coumarin in 300µl of DI water to obtain the stock solution, and subsequently adding MetOH to the stock solution to obtain a 5 mg/ml solution of coumarin, and finally preparing the pre-spinning solution with the ternary solvent mixture. To prepare PLGAac nanofibers for *in vitro* release of fluorescent-labelled albumins, 5 mg of AlbF or AlbT was dissolved in 90 µl of DI water. Then, 630 µl of HFIP was added to the solution, forming a mixture to dissolve 220 mg of PLGAac, resulting in a 17% (wt) polymer solution. The overall content of albumin was 2.3% with respect to the mass of the dry polymer. During the entire process, the dye-containing solutions were always shielded from light to preserve the activity of fluorescent species.

### 3.2.3 Double-electrospinning process

The electrospun composite with the compositional gradient of distinct materials across the composite thickness was prepared through programming the sequential and/or simultaneous electrospinning processes of PCL and PLGA on a rotating mandrel collector, using a modified double-electrospinning system previously described by us [43]. Briefly, a layer of PCL

nanofibers, an intermixed layer of PCL and PLGAac (or PLGAes) nanofibers, and a layer of PLGA electrospun fibers were deposited in sequence on the grounded cylindrical aluminum collector. The design of the compositional patterns along the thickness of the scaffold was achieved by controlling 3D movements of a collector, in coordination with spinning processes separately programmed. The cylindrical collector, with 8 mm in diameter, rotated at a constant velocity by a brushless rotating electric motor (BLF230C-A, Oriental Motor, U.S.A. CORP., Torrance, CA). Each solution was individually stored in a 5 ml syringe. The syringe was connected to a blunt-ended needle that served as a charged spinneret. Each spinneret placed at the opposite side of the rotating collector, were perpendicularly oriented with respect to the principal axis of the collector, and connected to a separate high voltage power supply (ES30P-10W, Gamma High Voltage Research Inc, Ormond Beach, FL). Both spinnerets moved in concert over an 18 cm path with a speed of 5m/s along the collector mandrel which was under the control of a linear motorized stage (EZS3D025-C, Oriental Motor). The feed rate of each solution varied independently via separate syringe pumps (NE-300, New Era Pump Systems, Farmingdale, NY) during the course of deposition. The electrospinning flow rates that allowed the formation of defect-free nanofibers were determined beforehand for each solution, and used to define the maximum flow rates, which were 0.6ml/hr for PLGA fibers and 1.1ml/hr for PCL fibers. The collector geometry, the concentration of polymer solutions, and apparent density of pure PCL and PLGA electrospun nets were used to establish a correlation between the feed rate and the deposition rate of each polymer per unit of surface area. Detailed information of the solution compositions and electrospinning parameters is listed in Table 3-2.

| Polymer | Loaded dye | Solvent mixture | Polymer conc. [% wt] | Dye content [%] $wt_{dye}/wt_{pol.}$ | Voltage [kV] | Work Distance [cm] | Feed rate [ml/h] |
|---|---|---|---|---|---|---|---|
| **PLGAac PLGAes** | / | HFIP/water 7/1 vol. | 17 | / | 26 | 20 | 0.15-0.6 |
| **PLGAac PLGAes** | Rh123 RhB | HFIP/water 7/1 vol. | 17 | ≈ 0.012 | 24 | 20 | 0.15-0.6 |
| **PLGAac** | AlbF AlbT | HFIP/water 7/1 vol. | 17 | 2.23 | 22 | 20 | 0.15-0.6 |
| **PCL** | / | CF/DMF 3/1 vol. | 10 | / | 26 | 24 | 0.3-1.1 |
| **PCL** | Coumarin | MC/DMF/MetOH 5/3/2 vol. | 8 | ≈ 0.05 | 20 | 20 | 0.3-1.1 |

*Table 3-2. Characteristics of polymer/dye solutions and electrospinning parameters*

The electrospinning process was performed at room temperature in open atmosphere with a relative humidity of 20-25%. The overall thickness of the electrospun nets was measured using a micrometer screw gauge. The design thickness of PCL-PLGA materials was 150 µm; samples with actual thickness outside of the range 135-165 µm were discarded. When fluorescent molecules were used, the entire apparatus was shielded from light to preserve the dyes. Electrospun samples were stored in a dessicator and kept in the dark.

### 3.2.4 Characterization of nanofiber morphology

The morphology of the electrospun fibers was observed using a JSM-6480LV scanning electron microscope (SEM) (JEOL Ltd., Tokyo, Japan) at 5.0 kV. Samples were sputter-coated with gold prior to analysis.

### 3.2.5 Characterization of compositional micropattern

Scaffolds loaded with fluorescent dyes were embedded in cryo-optimum-cutting-temperature compound (Andwin Scientific, Schaumburg, Germany) or in paraffin for histology. A series of 15 µm-thick sections were obtained with a cryostat or rotary microtome for confocal imaging. The cross-sections of the nanofiber scaffolds loaded with fluorescent species were examined under a Zeiss LASER Scanning 510 confocal microscope equipped with AR, HE/Ne and diode laser sources (Carl Zeiss Inc, Jena, Germany). The images were used to assess the dye distribution in the nanofibers and along the thickness of the nets. Compositional profiles of scaffolds were determined by measuring the color intensity of dyes in the confocal images, using ImageJ software (http://rsbweb.nih.gov/ij/). Fluorescent profiles were obtained by averaging at least 6 profiles acquired from 3 different samples.

### 3.2.6 Thermal analysis

The thermal analyses were performed using a differential scanning calorimeter (DSC) (DSC 204 F1 Phoenix®, Aurora, IL, USA) under flushing nitrogen (100 ml/min). Each sample was first heated from -110°C to 120°C with an incremental rate of 10 °C/min and held at each temperature for 3 min. The sample was then slowly cooled to −110°C with liquid nitrogen at a cooling rate of 5 °C/min and reheated for a second scan to 120°C at a rate of 10°C/min. For the PCL-PLGA composites, the glass transition of PLGAac and PLGAes were measured from the first heating scans. The transformation was clearly visible and was accompanied by an appreciable enthalpic relaxation effect due to the aging of the polymer. Therefore, the onset point and inflection point were both reported. In the second heating scan, the glass transitions of PLGA

were not visible, due to the melting peak of PCL. The peak temperature of the melting transition of PCL was recorded and melting peaks of PCL in pure PCL sample and PCL-PLGA samples were quantitatively determined by integration. The crystallinity degree of PCL ($\alpha_{PCL}$) was determined by comparing the melting enthalpy of PCL ($\Delta H_{PCL}$) for PCL nanofibers with the theoretical value of a sample with 100% crystalline PCL ($\Delta H_{100\%}$), which equals to 139.4 J/g [139]. Thus, $\alpha_{PCL} = 100*(\Delta H_{PCL} / \Delta H_{100\%})$. The melting enthalpy was determined by calculating the area of the endothermic melting peak of PCL. Under the assumption that melting enthalpy of PCL remained constant in PCL-PLGA samples, $\alpha_{PCL}$ was used to determine the fraction of PCL nanofibers.

### 3.2.7 Hydrolytic degradation analysis

Hydrolytic degradation analyses were performed on electrospun scaffolds at 37 °C in phosphate buffer solution (pH = 7.4) under constant mild agitation up to a maximum of 6 weeks. For each electrospun net, specimens were immersed in 5 ml of phosphate buffer solution in separate test tubes. Triplicate samples for each experimental condition were withdrawn at a predetermined time, carefully washed in DI water and dried under vacuum in a dessicator for 48 hours. Then, the samples were weighed on an analytical balance. Using the gravimetric method, weight loss of each sample was then determined and averaged. Corresponding changes of nanofiber morphology were monitored using SEM micrographs. Molecular weights of PCL, PLGAac and PLGAes were determined by gel permeation chromatography (GPC) (GPCmaxTM, Viscotek, Houston, TX, USA) with a differential refractive index (RI) detector (Viscotek 3580), and a set of Viscotek viscogel columns with THF as the

eluent at 30 °C. The analytical GPC was calibrated using monodisperse polystyrene standards. Molecular weights of the as-spun scaffolds and those after each degradation time were measured. The GPC curves of the materials presented a bi-modal distribution. The overlapped peaks were thus deconvoluted into two separate asymmetric peaks with the least-squares method and assigned to PCL and PLGAac (or PLGAes). The peak-fitting parameters were conditioned using the peak parameters of the parent materials. The molecular weights corresponding to individual deconvoluted peaks were also determined.

### 3.2.8 Release profile characterizations

For molecule release characterizations, the circular samples with 24 mm in diameter were cut from PCL-PLGAac and PCL-PLGAes scaffolds loaded with fluorescent dye or fluorescently-labelled albumin. For each experimental condition, 3 samples were used for analyses. Samples were placed in a custom-made diffusion chamber in which each surface of the electrospun scaffold faced a different reservoir chamber filled with 1ml of buffer solution. The two reservoirs used SecureSeal hybridization chambers (Grace Biolabs, Bend, OR) to seal the surface. Each reservoir had small holes for sampling and changing solutions. The holes were covered with silicone sealing tap during experiments to prevent evaporation. Thus, the molecule movements between the reservoirs could only be through the pores of the electrospun materials. The release tests were performed at 37 °C. Samples of buffer solutions in both reservoirs were collected every day during the first 16 days, and subsequently once a week. After samples were taken, the reservoir chambers were rapidly rinsed with DI water and refilled with fresh phosphate buffer at 37°C. Samples of 200 µl in triplicates were analyzed in

96-well microplates with a Victor 2 microplate reader (PerkinElmer, Santa Clara, CA) to quantify the amount of Rh123, AlbF and AlbT released daily. The concentration and net amount of released Rh123, AlbF and AlbT were determined using the respective calibration curves (**Table 3-3**). The geometry and porosity of the molecule-releasing scaffolds kept constant for all the experimental samples. As various fluorophores were simultaneously released by some samples, the possibility of the overlap of the fluorophore emission spectra was examined; no evidences of any undesired overlap were found. An efficiency of separation (S) was introduced to quantify the capability of confining molecule release to one specific side of the scaffolds. The efficiency of separation of a particular molecule between Side A and Side B ($S_{molecule\_A\text{-}B}$) was defined as the percentage of molecules released on Side A over the total amount of molecules released on Sides A and B for the whole duration of the test.

| | | | |
|---|---|---|---|
| **Rh123** | x < 45000 | y = 4.248*10^7 x + 1014 | $R^2$ = 0.987 |
| **Alb F** | x < 20000 | y = 639.9 x + 366.9 | $R^2$ = 0.998 |
| **Alb F** | 20001 < x < 60000 | y = -2.432 $x^2$ + 687.7 x + 327.4 | $R^2$ = 0.999 |
| **Alb T** | x < 20000 | y = 457.4 x + 389.3 | $R^2$ = 0.996 |

*Table 3-3. Calibration curves for Rh123, AlbF and AlbT with the respective coefficient of determination. "x" is to the measured fluorescence intensity and "y" is the concentration of the molecule in solution expressed in µg/ml. The net mass released can be calculated taking into account the known capacity of the release chamber.*

## 3.3 Results

### 3.3.1 PCL/PLGA scaffolds with micropatterned nanofibers demonstrated custom-designed compositional gradients

Using the double-electrospinning apparatus with capability of precisely programming the 3D position of different nanofibers, we have formed electrospun multi-component structures showing designed micropatterns. Figure 3-1 illustrates a structure which consists of a 25 μm-thick PCL nanofiber layer, a 100 μm interlayer with mixed nanofibers of PCL and PLGA, and a 25 μm PLGA nanofiber layer. The design shows a pattern of pure PCL and PLGA on the opposite sides of the surfaces, and an intermediate region in which the PLGA content varies gradually between 0 and 100% along with a reversed change of PCL content. This compositional gradient across the material thickness was achieved by progressively decreasing the feed rate of PCL to 0 while simultaneously increasing the feed rate of PLGA to the maximum value. The pattern was designed to produce scaffolds with equal amount of PCL and PLGA in weight.

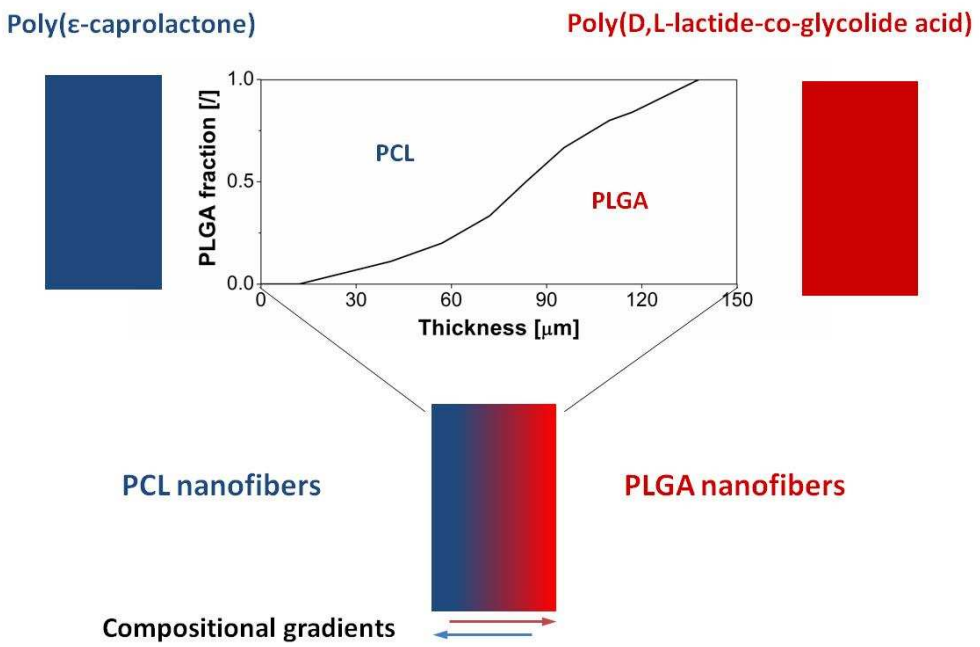


*Figure 3-1. Schematic illustration of the cross-section of a PCL-PLGA electrospun scaffold with internal compositional gradient. The fraction of PCL nanofibers (shown in blue) decreases along the thickness of the material from 1 on the left side (PCL side) to 0 on the right side (PLGA side), while the PLGA fraction (shown in red) increases along the thickness of the scaffold from 0 to 1.*

To assess the actual composition of scaffolds, DSC analysis was used. Results demonstrated that the material composition closely matched the design. The comparison between the endothermic melting enthalpies of PCL in the scaffolds and the melting enthalpies of pure electrospun PCL, was used to determine the actual amount of PCL and the PCL/PLGA ratio in the scaffolds (**Table 3-4**). PCL nanofibers showed crystallization enthalpy of 55.9 J/g during cooling and melting enthalpy of -58.5 J/g in the second scan. As the melting enthalpy of 100% crystalline PCL is 139.5 J/g, the resulting crystallinity of electrospun PCL nanofibers was 42%. Also, results from the crystallization and melting enthalpies of PCL-PLGAes and PCL-

PLGAac scaffolds revealed that the actual PCL content was around 55% in both cases. Therefore, the actual PLGA contents were around 45%. Also, the glass transition temperatures of PLGAac and PLGAes, determined from the inflection point in the first DSC scan curves of PCL-PLGA scaffolds, were 39.7 and 38.5 °C, respectively. We also noticed that the glass-rubber transition for PLGAes (onset point) started at 35.2 °C, below the working temperature of 37°C. The transition zone for PLGAac started at 37.8 °C, just above the working temperature.

| Sample | PCL | | | | | |
|---|---|---|---|---|---|---|
| | **Tm** (II scan) [℃] | **$\Delta H_{PCL}$ melting** (II scan) [J/g] | **PCL content** [%wt] | **Tc** (cooling) [℃] | **$\Delta H_{PCL}$ crystal.** (cooling) [J/g] | **PCL content** [%wt] |
| **PCL nanofibers** | 60.0 | -58.5 | **100.0** | 27.1 | 55.9 | **100.0** |
| **PCL-PLGAes** | 61.3 | -31.9 | **54.5** | 27.9 | 29.7 | **53.1** |
| **PCL-PLGAac** | 59.1 | -32.2 | **55.0** | 26.7 | 30.5 | **54.6** |

| Sample | PLGA | | | |
|---|---|---|---|---|
| | **PLGA content** (from melting) [%wt] | **PLGA content** (from crystal.) [%wt] | **Tg** (I scan, Onset) [℃] | **Tg** (I scan, Inflection) [℃] |
| **PCL-PLGAes** | 45.4 | 46.9 | **35.2** | 38.5 |
| **PCL-PLGAac** | 45.0 | 45.4 | **37.8** | 39.7 |

*Table 3-4. Thermal properties of PCL and PLC-PLGA electrospun materials.*

Confocal images of the cross-sections of molecule-impregnated nanofiber materials further demonstrated that the compositional gradients of composites matched the designed nanofiber micropatterns (Figure 3-2). Herein, PCL nanofibers were loaded with a blue fluorophore coumarin, while PLGAac nanofibers were loaded with red fluorophore RhB and/or green fluorophore Rh123. Figure 2 demonstrated the molecule pattern in a two-component scaffold and a three-component scaffold. Figure 3-2a showed the confocal image of a PCL-

PLGAac material, in which PCL and PLGAac were loaded with blue and red fluorophores, respectively. The gradual increase in the red color intensity from the left to the right side of the image demonstrates the increase of PLGAac content across the material thickness, whereas the attenuation of blue intensity shows the reduction of the PCL fraction in the same region. Also, no red signals were found close to the surface on the PCL side, and no blue signals close to the surface on the PLGAac side. This reflects the pure polymer design in these regions. However, due to the saturation of fluorescent signals, the fluorescent profiles in the high intensity range could not be accurately assessed. Figure 3-2b illustrated the design of a three-component scaffold, where PLGAac nanofibers were used to impregnate two molecules in the respective regions: green Rh123 in the inner region and red RhB in the outer region of the scaffold. Similar to the pattern observed in the two-component scaffold, the fluorescent intensity profiles in the confocal image reproduced the designed micropattern across the scaffold thickness with accuracy except in the high intensity range.

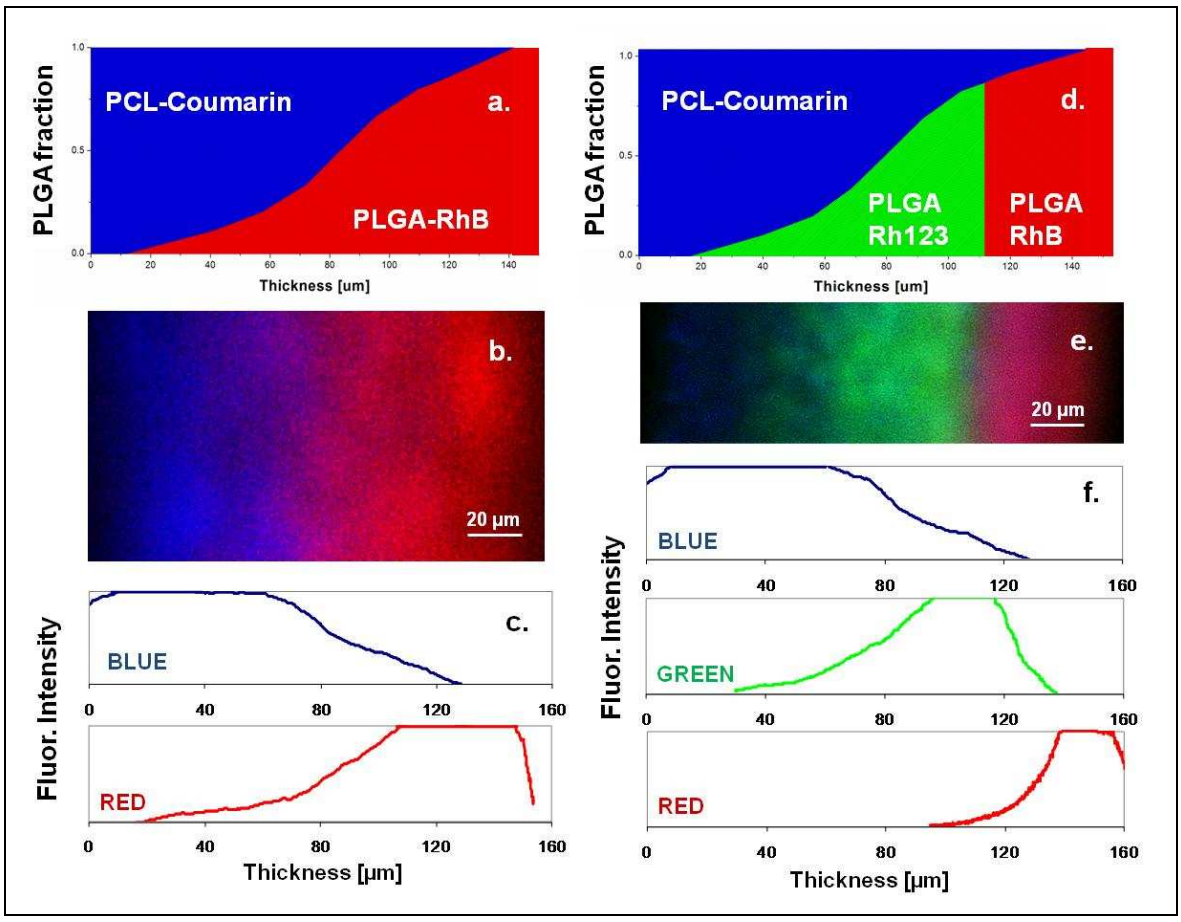


*Figure 3-2. Design illustrations and confocal images of the gradient micropatterns over the thickness of PCL-PLGAac scaffolds. In the design illustrations (a, d) and confocal images (b, e), blue color shows PCL nanofibers loaded with fluorophore coumarin, red shows PLGAac nanofibers loaded with RhB, and green shows PLGAac nanofibers loaded with Rh123. The color intensity profiles (c, f), quantitatively determined from the confocal images, demonstrate the changes in the signal intensity of each fluorophore molecule across the sample thickness. Results demonstrate good agreement between the design patterns and the actual concentration profiles of the molecules or fibers.*

### 3.3.2 Hydrolytic analyses of PCL-PLGA scaffolds demonstrated the different degradation behaviors and morphological changes of PLGAac and PLGAes

To compare the hydrolytic degradation behaviors of PCL-PLGAac and PCL-PLGAes scaffolds, samples were analyzed with the gravimetric method for weight loss, GPC for changes in the polymer molar weight distribution, and SEM for the nanofiber morphology. The results demonstrated significant differences between PLGAac and PLGAes during the 6-week hydrolytic degradation process. SEM micrographs in Figure 3-3 and Figure 3-4 demonstrate the evolution of PCL-PLGAac and PCL-PLGAes scaffolds during degradation. Figure 3-3a and Figure 3-3b shows that the morphology and network of PLGAac nanofibers remained virtually unchanged after 1 week of buffer exposure. During this time period, the average fiber diameter increased about 25%, from 0.62 ± 0.27 μm to 0.78 ± 0.28 μm. After 3 weeks, PLGAac nanofibers exhibited more significant increase in diameter with an average diameter of up to few microns, and the fiber network was characterized by soldering-like attachments at the junctions (Figure 3-3c). From the SEM images, it was noticed that by week 3, the fibers on the sample surface had partially lost their cylindrical and smooth morphology. Also, the PCL nanofibers started to emerge in the SEM images; they were underneath the PLGA fibers, exhibiting unaffected cylindrical and smooth morphology. Overall, the deformed and swollen PLGAac nanofibers seemed to be collapsed onto, and wrapped around, the more stable PCL fibers after 3 weeks of degradation. After 5 weeks, the fibrous structure of PLGAac almost disappeared, and a film of PLGAac covered the web of PCL nanofibers which were unscathed after degradation (Figure 3-3). From

a macroscopic view, it was found that the PCL-PLGAac scaffolds remained dimensionally stable and flat for the entire experimental period.

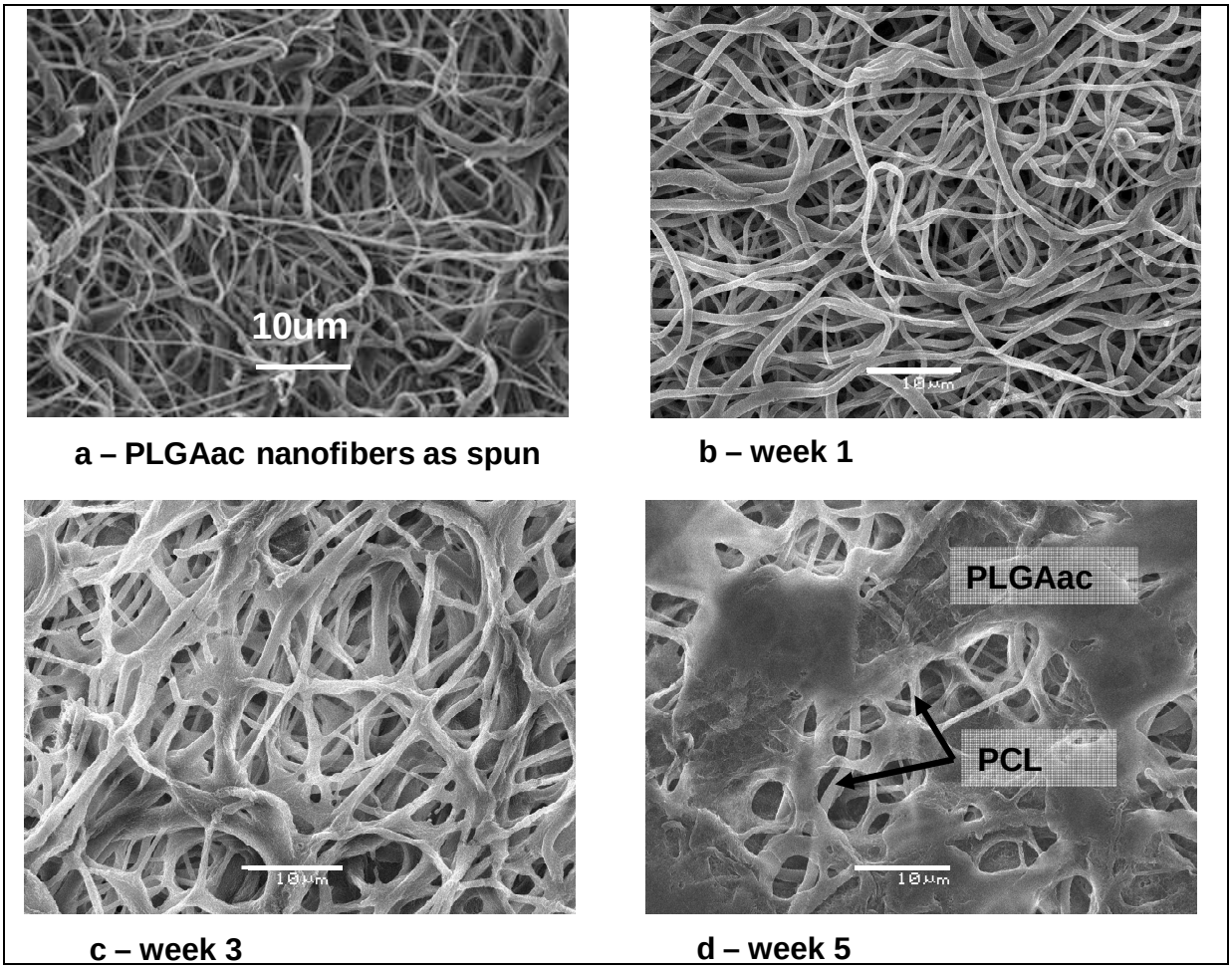


*Figure 3-3. Representative SEM micrographs of the PCL-PLGAac nanofibrous scaffold with an internal compositional gradient. Images were taken from the PLGA side. (a) Morphology of PLGAac nanofibers as spun. (b-d) Changes in the nanofiber morphology after 1 week (b), 3 weeks (c), 5 weeks (d) of degradation in phosphate buffer solution at 37°C. The unchanged PCL nanofibers underneath the PLGAac layer were found after 5 weeks of degradation (d). Scale bar shows 10µm. Scale bar shows 10 µm.*

Compared to PLGAac, the morphology of PLGAes nanofibers altered much faster (Figure 3-4). After only 1-day exposure to buffer, the electrospun PLGAes nanofiber network started to collapse with extensive soldering-like attachments at the junctions (Figure 3-4b).

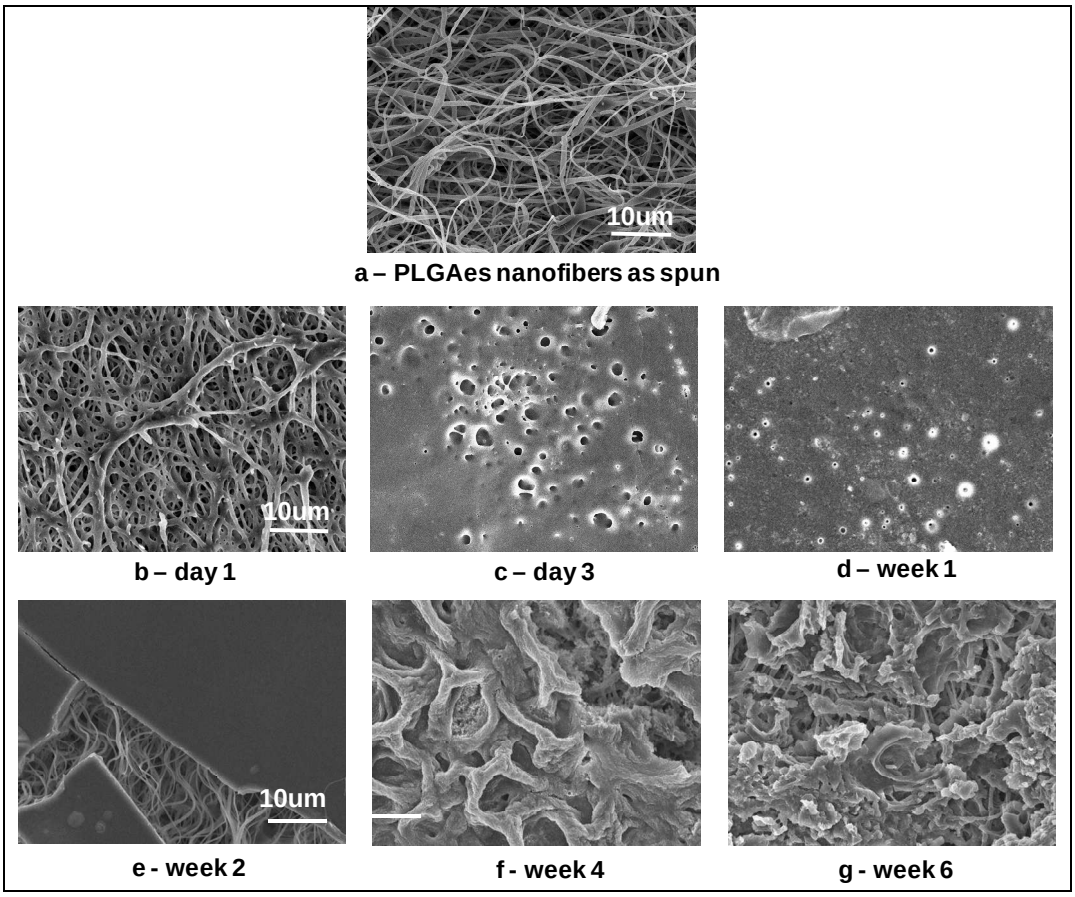


*Figure 3-4. Representative SEM micrographs of the PCL-PLGAes nanofibrous scaffold with an internal compositional gradient. Images were taken from the PLGA side. (a). Morphology of PLGAes nanofibers as spun. (b-f) Changes in the PLGAes nanofiber morphology after 1 day (b), 3 days (c), 1 week (d), 2 weeks (e), 4 weeks (f) and 6 weeks (g) of degradation in phosphate buffer solution at 37°C. The unchanged PCL nanofibers underneath the PLGAes layer were found in all these images (b-d). Scale bar shows 10μm.*

Within one day, the average fiber diameter increased nearly 80%, from 0.50 ± 0.17 μm to 0.88 ± 0.10 μm. After 3 days, no fiber-like morphology remained in the PLGAes layer. The layer turned into a membrane with an array of small circular pores (Figure 3-4c) whose diameter continued to decrease in the first week (Figure 3-4d). At the end of the second week, the PLGAes layer was entirely re-structured and became a solid substrate without pores lying on the bed of PCL nanofibers.

Figure 3-4e demonstrated the structure of PCL fibers lying under a fractured portion of the PLGAes layer. From then on, the surface of PLGAes layer appeared to be continuously eroded by the buffer, and after 6 weeks, a significant amount of material still remained on the surface (Figure 4f-g). From a macroscopic view, it was found that the PCL-PLGAes scaffolds shrunk and bent toward the PLGAes side, which might be due to the loss of PLGAes pores reducing the volume of the PLGAes material. Similar to PCL-PLGAac, in the PCL-PLGAes composites, the morphology and network structure of the nanofibers on the PCL side remained unchanged during the degradation process.

To gain further understanding of the hydrolytic degradation processes of the composite scaffolds, we characterized changes in overall weight and molecular weight of different PCL-PLGA scaffolds. Using GPC curves of the component polymers (Figure 3-5), we first determined the weight-average molecular weight (Mw), number-average molecular weight (Mn) and polydispersity (pdi) of pure PCL, PLGAac and PLGAes materials.

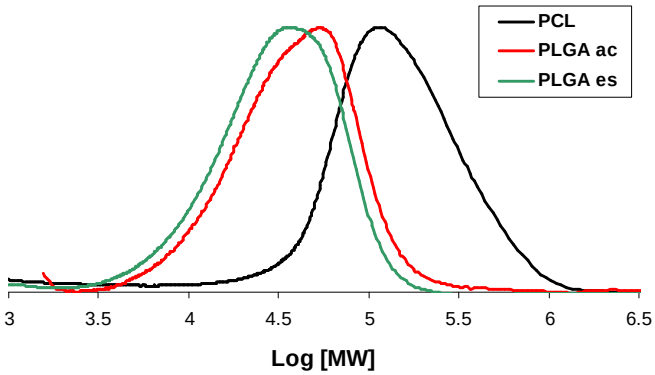


| Polymer | $M_w$ [kDa] | $M_n$ [kDa] | pdi |
|---|---|---|---|
| **PCL** | 137 | **78** | 1.8 |
| **PLGAac** | 43 | **26** | 1.6 |
| **PLGAes** | 36 | **22** | 1.7 |

*Figure 3-5. GPC curves and molecule weight analyses of pure PCL, PLGAac, PLGAes materials. The weight-average molecular weight ($M_W$), number-average molecular weight ($M_n$) and polydispersity (pdi) are reported.*

Figure 3-6 demonstrated the differences between PCL-PLGAac and PCL-PLGAes scaffolds in GPC curves, molecular weight changes and weight loss during hydrolytic degradation. The GPC curves exhibited a bimodal distribution. The peak at higher molecular weight was assigned to PCL, whereas the peaks at lower molecular weights were assigned to PLGA. GPC results from both PCL-PLGAac and PCL-PLGAes materials (Figure 3-6a-b) showed that the PLGA peak gradually decreased and shifted towards lower molecular weights, while the PCL peak remained unaffected during the hydrolytic degradation. Using deconvolution analysis of GPC curves, the contributions of PCL and PLGA, the PLGA content in the scaffold and the number average molecular weight of the polymer were determined. As shown in Figure 3-6c, the molecular weight of PLGAac slightly decreased between week 2 and week 3 before getting steady at

21kDa. The PLGAac content in the scaffold steadily dropped to approximately 22% of the original amount after 6 weeks. Compared to PCL-PLGAac, the molecular weight of PLGA in PCL-PLGAes scaffolds dropped more progressively from 22 to 9 kDa during the experimental period (Figure 3-6d). The PLGAes content decreased accordingly. However, when compared to PCL-PLGAac, there was a higher amount of PLGA content present in PCL-PLGAes scaffolds after 6 weeks, approximately 40% of the original amount of polymers. Therefore, compared to PLGAac, PLGAes degraded more slowly, but underwent chemical breakdown during degradation, showing immediate reduction in molecule weight and more rapid loss of nanofiber morphology. The weight loss curves for the PCL-PLGAac and PCL-PLGAes scaffolds were presented in Figure 3-6e and Figure 3-6f, respectively. The remaining mass of the scaffolds was determined by the gravimetric method and by measuring the overall area under the GPC curve; both results in similar curves of weight loss.

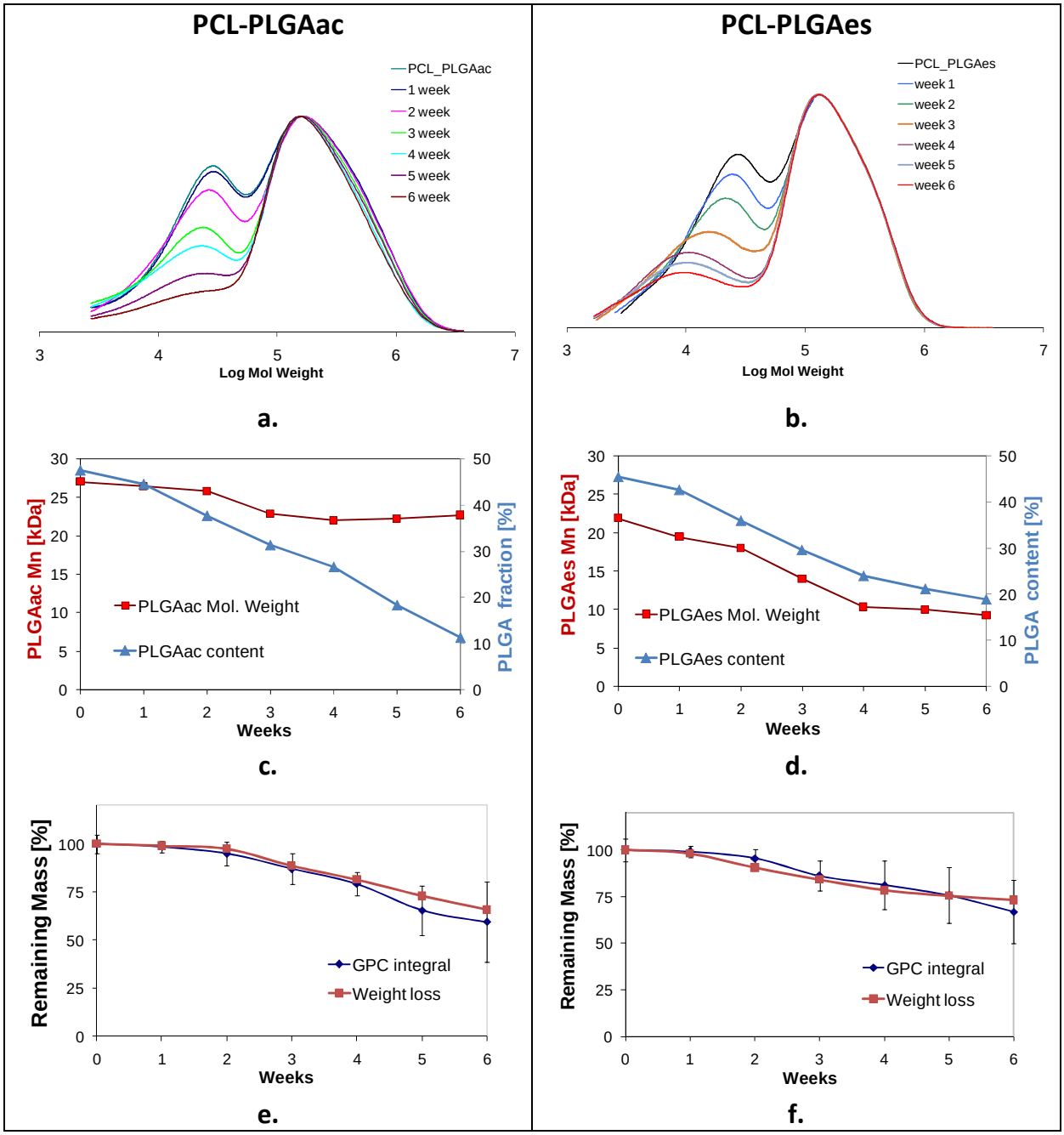


*Figure 3-6. GPC analyses of PCL-PLGAac and PCL-PLGAes scaffolds as spun and after the hydrolytic degradation tests. (a - b) GPC curves of PCL-PLGAac and PCL_PLGAes; (c - d) Changes in number average molecular weight and remaining PLGA content determined by the deconvolution of the GPC curves; (e -f) Overall remaining mass percentage of the scaffolds determined by the gravimetric method and measurement of the total area under the GPC curves.*

### 3.3.3 Spatially-controlled release of small molecules from PCL-PLGAac and PCL-PLGAes scaffolds

To assess the capacity of PCL-PLGAac and PCL-PLGAes materials for spatially controlled release of active molecules, we first performed release experiments using Rh123. PCL and PLGA/Rh123 solutions were electrospun to prepare scaffolds following the pattern described in Figure 3-1. Release studies were carried out in custom-made diffusion chambers illustrated in Figure 3-7a. The two sealed reservoirs filled with phosphate buffer solution were placed on the opposite sides of the electrospun scaffolds. The PCL side of the scaffold was set to face the buffer reservoir chamber on the "A" side; the Rh123-impregnated PLGA side was placed in contact with the buffer reservoir on the "B" side. Daily measurement results of the Rh123 dye concentrations in both reservoirs for the first 9 days are shown in Figure 3-7. Figure 3-7b demonstrated that the majority of the encapsulated fluorescent molecules were released from the PLGAac side. Thus, the electrospun PCL-PLGAac scaffolds demonstrated the capability of confining sustained molecule release to one side of the scaffolds.

The separation efficiency of Rh123 between the two surfaces ($S_{Rh123\_B\text{-}A}$) of the PCL-PLGAac scaffolds was 81 ± 5 % during 16-day release experiment. On the contrary, PCL-PLGAes samples displayed a mixed release behavior. Figure 3-7c showed that more molecules were released from the PCL side, when compared to PCL-PLGAac. In addition, after day 3, the molecule concentration measured on the PCL side exceeded that on the PLGAes side. This resulted in an overall separation efficiency of around 50%; thus, no separation of Rh123 between the two surfaces of the PCL-PLGAac scaffolds was found.

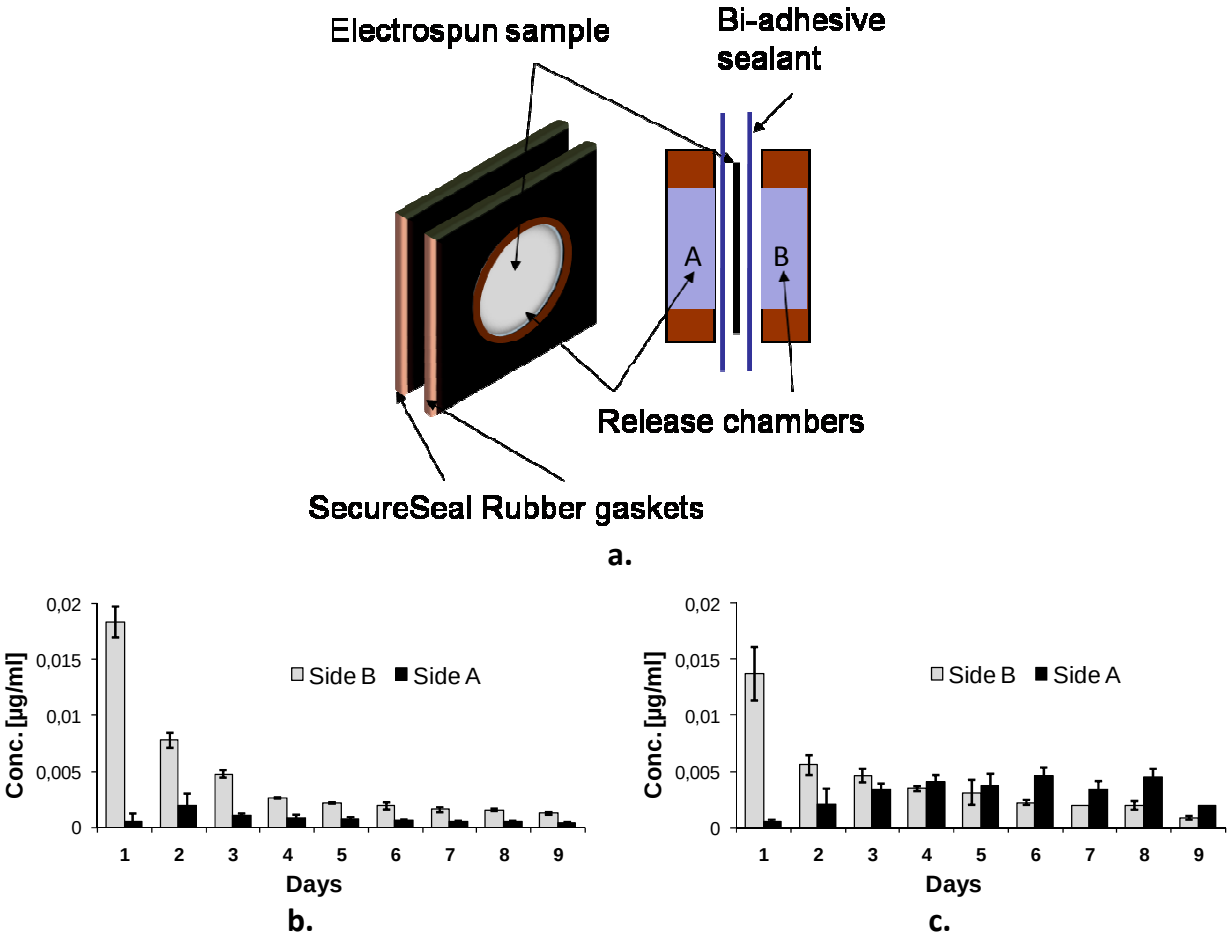


*Figure 3-7. Double-sided release test on PCL-PLGAac and PCL-PLGAes with Rh123 impregnated in the PLGA fibers. (a) Schematic illustration of the custom-made diffusion chambers with independently sealed reservoirs facing the two surfaces of the electrospun samples. (b) Release of Rh123 from the two surfaces of PCL-PLGAac scaffolds. (c) Release of Rh123 from the two surfaces of PCL-PLGAes scaffolds. The release was determined by measuring the fluorophore concentration in the chamber reservoirs. Herein, "Side B" indicates the fluorophore-loaded PLGA surface and "Side A" indicates the PCL surface.*

Therefore, the PCL-PLGAac scaffold was chosen for the release of biomolecules; though interesting, PCL-PLGAes scaffolds were not further used to study spatially-controlled protein release.

### 3.3.4 Spatially-controlled protein release from PCL-PLGAac scaffolds

A variety of micropatterned composite scaffolds made up of PCL nanofibers and protein-impregnated PLGAac nanofibers were designed to demonstrate the use of nanofiber micropattern for spatially-controlled, sustained releases of single or dual molecules. PLGAac nanofibers loaded with fluorescently-labeled albumins were prepared by one-phase, solution electrospinning. Albumin was dissolved directly in the polymeric solution prior to electrospinning and appeared to be homogeneously distributed in the PLGAac nanofibers (Figure 3-9).

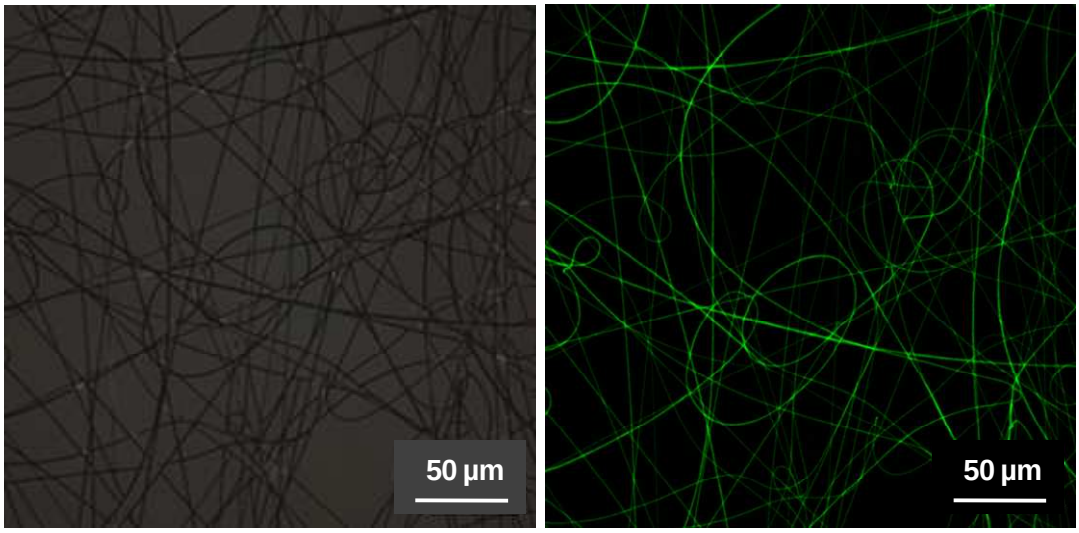


*Figure 3-8. Optical and confocal images of PLGA nanofibers prepared by one-phase, solution electrospinning. Fluorecently-labeled, AlbF was dissolved directly in the polymeric solution and was homogeneously distributed along the nanofibers.*

#### *3.3.4.1 Spatially-controlled sustained release of one molecule*

Figure 3-9 demonstrates the cumulative release of AlbT from the PCL-PLGAac electrospun scaffolds. The scaffolds were prepared according to the micropattern presented in

Figure 2. AlbT was encapsulated in the PLGAac nanofibers. The scaffolds were characterized by a nanofiber gradient and thus AlbT gradient. Results showed that sustained release of AlbT was highly confined to the PLGAac side of the scaffolds (Side B), and the release of AlbT from the PCL surface (Side A) was limited. The separation efficiency for AlbT between side B and side A of PCL-PLGAac scaffolds was 90 ± 4%, higher than the efficiency for small molecules (i.e. fluorophores). Results also showed that approximately 88% of the total amount of entrapped AlbT was released during the 50-day experiment.

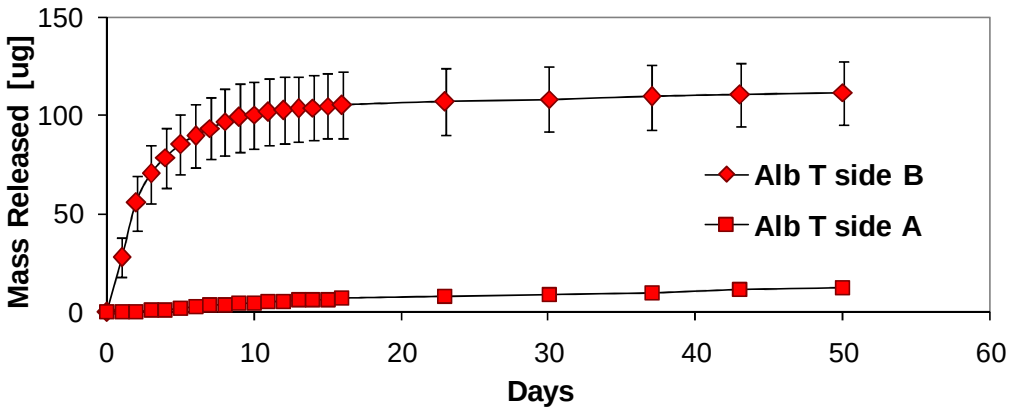


*Figure 3-9. Cumulative release of AlbT from the two surfaces of PCL-PLGAac composite scaffolds. The scaffolds were prepared following the compositional pattern presented in* ***Errore. L'origine riferimento non è stata trovata.****. AlbT was encapsulated in PLGAac and it was released mainly from the PLGAac-rich side. "Side A" refers to the PCL-rich side, whereas "Side B" refers to the AlbT-loaded PLGAac side.*

This estimation was made using an overall PLGAac content in the scaffold equal to 48%, as obtained from DSC analysis of this specific AlbT-loaded PCL-PLGAac scaffold. Approximately 20% of the total loaded proteins were released in the first 24 hours, 80% were released in 9

days. After day 9, the low-slope release curve indicated a small amount of sustained release at a constant rate (about 1% per week). In addition, it was found that the release rates on the two sides of the scaffold were similar after day 9.

#### *3.3.4.2 Controlled releases of dual molecules to one side*

Using electrospun scaffolds with a similar compositional micropattern as shown in Figure 2d, we also demonstrated the concurrent release of two proteins from the same side of the PCL-PLGAac composite scaffolds. Instead of dye-impregnated nanofibers, as illustrated in Figure 3-10a, PLGAac nanofibers in the inner part of the scaffolds were loaded with AlbF (green), while those in the outer region were loaded with AlbT (red). Results of cumulative release curves (Figure 3-10b-c) showed that both AlbT and AlbF were preferentially released from one side of the scaffolds with high efficiency. The separation efficiencies of AlbT and AlbF were 91 ± 4% and 87 ± 5%, respectively. To compare the release kinetics of AlbT and AlbF during the first 10 days, the cumulative release on Side B was normalized with respect to the respective total amount of delivered proteins (Figure 3-10d). The curves suggested that AlbF initially was released at a slower rate when compared to AlbT which was located closer to the surface, but the differences were not statistically significant.

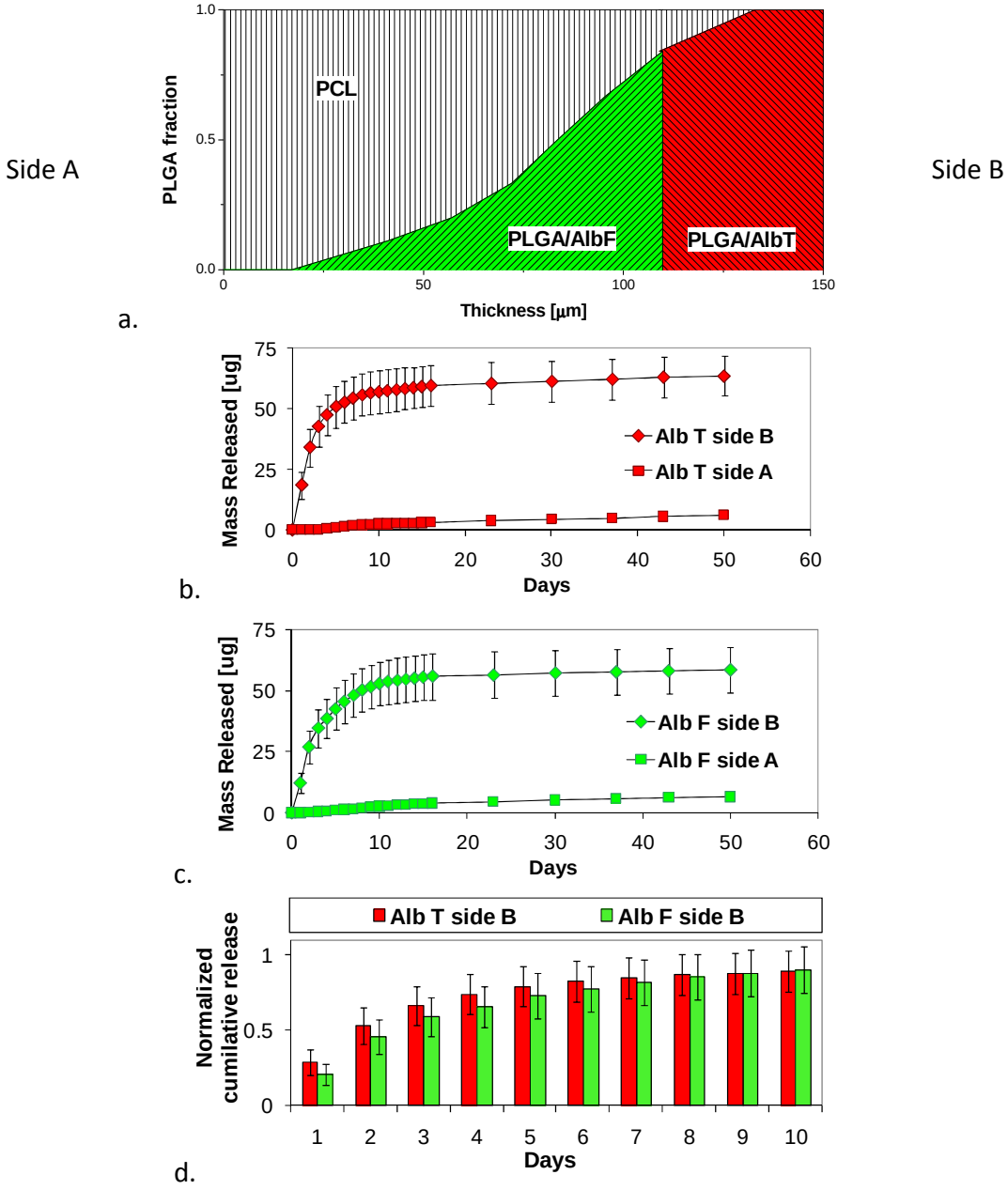


*Figure 3-10. Dual-drug release from one surface of the scaffold. (a) Illustration of the compositional pattern of nanofibers. (b) Cumulative release curve of AlbT. (c) Cumulative release curve of AlbF. (d) Comparison of AlbF and AlbT release during the first 10 days.*

#### *3.3.4.3 Controlled releases of dual molecules to the opposite sides*

The compositional gradient micropattern was further used as building-blocks of a more complex scaffold design for bi-directional release-control purposes. As illustrated in Figure 10a, the new pattern was generated by duplicating gradient patterns on both sides symmetric with respect to PCL. Herein, PLGAac was used to encapsulate either AlbF or AlbT. The designed pattern consisted of a 25 µm-thick layers of PLGAac electrospun nanofibers loaded with different fluorophore-tagged molecules on both surfaces, a 50 µm layer of PCL nanofibers in the core of the scaffold, and two PCL-PLGAac inter-layers characterized by a similar compositional gradient pattern. As a result, a precisely-controlled distribution of two biomolecules was generated across the scaffold thickness. Results from molecule release showed that AlbF and AlbT were selectively released from the opposite sides of the PLGAac-PCL-PLGAac composite scaffolds. The cumulative release curves for AlbF and AlbT are shown in Figure 3-11b and Figure 3-11c, respectively. AlbF was predominantly delivered to the reservoir on Side A, while AlbT was released to that on Side B. The separation efficiency of AlbF between Side A and Side B ($S_{AlbF\_A\text{-}B}$) was equal to 0.91 ± 0.04, while the separation efficiency of AlbT between Side B and Side A ($S_{AlbT\_B\text{-}A}$) was equal to 0.92 ± 0.03.

Side A

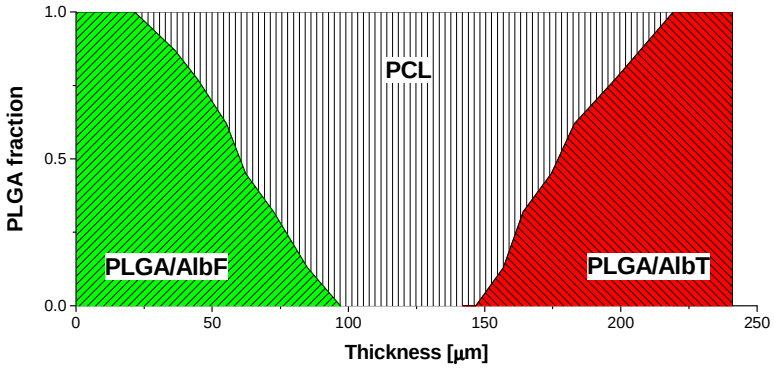


Side B

a.

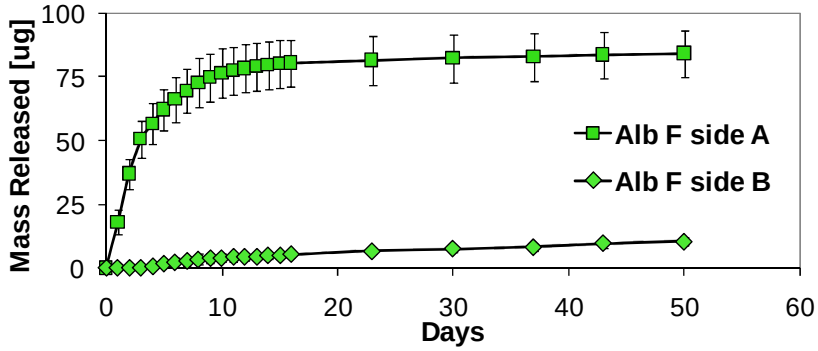


b.

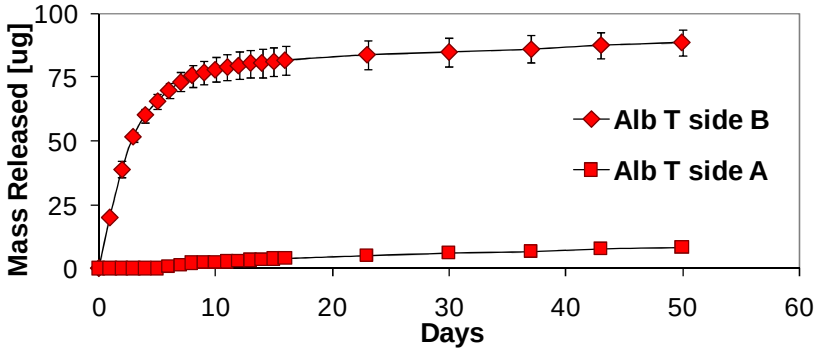


c.

*Figure 3-11. Dual-drug release from the opposite surfaces of the PLGAac-PCL-PLGAac scaffold. (a) Illustration of the compositional pattern of nanofibers. (b) Cumulative release curve of AlbT. (c) Cumulative release curve of AlbF. Release of green-emitting AlbF was mainly confined to side A, whereas release of red-emitting AlbT is mainly confined to side B.*

## 3.4 Discussion

This study has developed and characterized a hierarchically-structured biomaterial platform, in which tunable nanofiber micropatterns are designed to control spatio-temporal release of molecules. Herein, the molecule release from the materials was illustrated with electrospun scaffolds whose micropattern over the thickness was characterized by complementary density gradients of diverse molecule-impregnated fibers. The scaffolds consist of PLGA fibers, an “active” component that encapsulates and releases model molecules, and PCL fibers, a “passive” component that provides mechanical integrity of the structure and sequesters molecule release. Various compositional patterns were designed and imaged with confocal microscopy which demonstrated good correlations between the designed and actual patterns. Additionally, we have revealed the differences of PLGAac (acid terminated PLGA) and PLGAes (ester terminated PLGA) during degradation, by showing that PLGAac is more stable and PLGAac nanofibers more gradually increase the diameter during hydrolytic degradation. Thus, spatially-confined release was demonstrated with PCL-PLGAac scaffolds but not PCL-PLGAes scaffolds. Using the precise graded composition and the interplay between PCL and PLGAac, we showed that the hierarchically-structured composite was capable of sustaining selective release of small molecules or larger proteins on one side of the scaffold.

### 3.4.1 Selection of PLGA material for controlled release

PLGA is a biodegradable polymer that has been used in a wide range of medical implants, tissue engineering products and drug delivery devices, because of its slow degradation, good biocompatibility and mechanical property [50–52]. Also, both PLGAac and PLGAes are often used for preparing degradable scaffolds or controlled release materials; however, no studies have examined the influence of their chemistry difference on their capability of encapsulating and releasing molecules. Different from previous studies, this study is the first to compare the use of low-molecular-weight PLGAac and PLGAes nanofibers for controlled release. There were large differences between the two PLGA materials in physiochemical properties and nanofiber morphology alterations during degradation. Our results suggested that these differences could be attributed to the polymer state transition as determined from the DSC thermo-analysis. PLGAes nanofibers changed dramatically since the beginning of degradation, lost fibrous features, and turned into a dense, continuous polymeric film in a week. Conversely, PLGAac nanofibers showed delayed morphological changes to much later stages of degradation. The rapid morphological evolution of PLGAes nanofibers can be explained by the fact that the onset point of the glass transition transformation for PLGAes (35.2°C) was lower than the experimental temperature (37°C). Although the glass transition temperature of PLGAes as measured from the inflection point of the DSC curve was 38.5°C, vast regions of PLGAes nanofibers undergo glass-rubber transitions at 37°C. Due to the phase transition, highly mobile polymer chains in the rubbery state allow polymer relaxation and

water uptake. Acting as the plasticiser, the water molecules could contribute to further reduction of the glass transition temperature of PLGAes. PLGAes also underwent chemical breakdown during degradation, showing immediate reduction in molecule weight. Increased mobility of polymer chains caused nanofibers to start soldering together at their junctions and then coalesce to form a continuous film. In contrast, PLGAac whose glass transition onset point was at 37.8°C, resulted in more stable nanofiber morphology. The glass-rubber transition likely was deferred, preventing water uptake. The PLGAac fibrous structure thus retained for a longer time, showing open, interconnected pores during degradation. The structural characteristics likely contributed to different behaviours of PCL-PLGAes and PCL-PLGAac in controlling release of molecules impregnated in the PLGA fibers, as shown in the results. The early formation of continuous, non-porous PLGAes layer might reduce the diffusion of biomolecules toward the PLGA surface, resulting in no confined release of Rh123 from PCL-PLGAes scaffolds after day 2, while PCL-PLGAac scaffolds maintained sustained, spatially-controlled molecule release over a 6-week long period. Therefore, molecule release from the nanofiber composite scaffold is largely determined by the degradation behaviours and morphological changes of PLGA fibers.

### 3.4.2 Sustained, spatially-confined molecule release

Release of fluorescently-labeled albumin from PCL-PLGAac composite scaffolds were monitored up to 50 days in our study. Our prolonged release study demonstrated fast release in the first 9 days and limited amount of sustained release over the rest of the experimental period. In particular, the release profile of albumin showed modest burst release (~20% of total amount) on the first day. The initial burst release and subsequent fast release during the first

few days could be attributed to: (a) the nanofiber gradient pattern, in which higher density of molecule-impregnated fibers is closer to the surface for earlier release, and (b) the molecule distribution in the nanofiber. As suggested by previous studies, direct dissolution of molecules in the pre-spinning organic solution, as used in this study, could result in a non-uniform distribution of molecules with a large portion segregated at the nanofiber surface [140]. Therefore, modifications of temporal release kinetics might be approached by altering either the fiber pattern or the molecule encapsulation in the nanofiber. Encapsulation techniques other than one-phase blending might result in different release kinetics [141], [142]. Different from the molecule diffusion in the initial stage, the prolonged slow release in the later stage of the assay in this study may be attributed to the polymer degradation behaviour.

In addition to sustained release, our release profiles of single small molecules or larger proteins as well as multiple proteins all demonstrated high separation efficiency of molecule release on the side with higher molecule concentration. Diffusion to the side with lower or zero concentration of molecules was minimal. The distribution of molecule-impregnated PLGAac nanofibers was thus effectively translated to sequestration of molecule release. The compositional gradient across the scaffold thickness confined molecule release in the proximity of a surface of the scaffold, thus leading to a spatially-defined preferential release. In addition, our results suggested that the rate of water penetration in the scaffold may strongly influence release profiles and distribution. However, further explorations are required for a better understanding of the water penetration/drug transport coupled phenomena.

### 3.4.3 Release mechanisms

The most important mechanisms governing molecule release from polymeric scaffolds are diffusion, degradation and erosion of the polymer matrix [143], [144], [145]. To understand the underlying mechanisms, several mathematical models of mass transport have been developed. In this study, because PLGAac nanofibers exhibited modest swelling, the polymer molecular weight remained unchanged and the weight loss was small during the first week, diffusion was likely the leading mechanism of molecule release from PLGAac nanofibers during this period of time. A simple semi-empirical model proposed by Ritger and Peppas in 1986 describes drug release behavior from polymer by taking into account both Fickian and non-Fickian diffusion mechanisms, and is mathematically written as

$$\frac{M_t}{M_\infty} = kt^n \qquad \text{(Eq 1)}$$

where $M_t$ is the mass of drug released at time $t$, $M_\infty$ is the mass of drug released as time approaches infinity, $k$ is a constant that incorporates characteristics of the polymer and the drug, and n is the diffusional exponent, which reflects the transport mechanism. Using Eq 1 to model our experimental data, we found this model was valid for the first 60% of the fractional release. Electrospun nanofibers can be modeled as a random array of mono-dispersed cylinders with diameters much smaller than their lengths. According to Ritger and Peppas, one-dimensional radial release from a cylinder, under perfect sink conditions, can be described with

pure Fickian diffusion using Eq 1 ($n$ = 0.45). For n = 1, drug release is independent of time (zero-order release); for 0.45 < n < 1, drug release follows a non-Fickian anomalous transport mechanism. In this study, we showed that loaded molecules were released unevenly from the two surfaces of the scaffold. Approximately 90% of the total drug released in 50 days was delivered to one side of the scaffold. The release from the other surface was close to zero in the first week of the experiment and could be neglected. By fitting the first 60% of the release profile of AlbT from side B of PCL-PLGAac scaffolds (Figure 8), we obtained n equal to 0.59 ± 0.07, with a high correlation coefficient ($r^2$ = 0.983). The curves were normalized with respect to the total amount of loaded drug. Because diffusion is largely dependent on the water permeation through pore-to-pore movement in the non-uniform scaffold, release of molecules impregnated in PLGA fibers may be activated at different time points according to the location in the scaffold. In addition, due to the high surface-to-volume ratio of electrospun materials, the molecule distribution in the nanofibers may significantly influence the release. Herein, the use of one-phase molecule dissolution yielded a large amount of molecules on the surface of nanofibers [140], which was likely released during the first day and thus could be separately modeled. Excluding the first day data resulted in a much lower "n", 0.46 ± 0.04, with a higher $r^2$, 0.998. The value of the diffusional exponent "n" was close to the theoretical value of 0.45. In light of the modeling results, we can divide the release profiles in three regions, based on the widely-used release mechanism. In the first day of the experiment, a modest burst release of about 20% of the total loaded molecules was obtained due to the molecules segregated near the nanofiber surface. Between day 2 and day 8, the scaffold released additional 60% of the

loaded molecules by Fickian diffusion. After day 9, the steady release of AlbT with a constant rate was found, which could resulted from PLGAac degradation and nanofiber swelling.

### 3.4.4 Potential applications for regenerative scaffolds

A new generation of scaffolding materials for tissue engineering and regenerative medicine seeks to combine the material scaffolding function such as structural guidance and mechanical support with the regenerative function such as molecule release to guide cell dynamics and organization [92]. We thus demonstrate a promising scaffolding biomaterial using programmable nanofiber structure to meet various mechanical and biological needs [43] Because tissue regeneration is a highly regulated process involving differentiation and spatial organization of multiple cell types in 3D, sustained release of cell-specific molecules in a spatially-defined arrangement, as demonstrated here, could spatially guide cells and their commitment to regeneration. Uniform presentation of a regenerative molecule may not satisfy regeneration needs in many situations [146], because over-expression of a regenerative molecule at a wrong place or a wrong time may lead to abnormal or diseased tissues. For example, PDGF is an important growth factor stimulating vascular SMC ingrowth and proliferation to build vascular medial layer, but it is also a major contributor to vascular intima dysfunction leading to intima hyperplasia and stenosis. Also, in some circumstances, biomaterials need to interface different tissues to stimulate regeneration [147].

Though we have demonstrated the potential of micropatterned nanofiber composite scaffolds using model fluorescent-labelled molecules or proteins, the material platform developed here can be applied to a wide range of applications, including therapeutic implants,

tissue engineering, and drug delivery. In these applications, spatial confinement and temporal control of various molecules are pivotal to the improvement of therapeutic efficacy and the reduction of biomolecule toxicity or side effects. Additionally, the gradient pattern structure could be further used as a building-block to design more complex molecule-fiber structures for spatially-defined, sequential release of multiple biomolecules. To achieve more complex structures or designs, one can take advantage of the programmable nanomaterial fabrication developed here, which involves separate control over the fabrication of different nanofibers and their positions in 3D. Because the bioactivity of proteins is a critical issue in the controlled release, future studies should involve the use of more environment-sensitive molecules. Electrospinning of molecule-impregnated nanofibers using a simple solution-based method as demonstrated here, has been used to release bioactive growth factors [39]. Also, other molecule encapsulation methods have been developed for electrospun materials to retain protein bioactivity [46], [141], [142], which might be used in conjunction with the techniques developed here in the future.

## 3.5 Conclusion

We have developed and characterized micropatterned nanofiber composites made from biodegradable materials. This is the first demonstration of using nanofiber patterns in 3D biomaterials to achieve sustained, spatiotemporally-controlled release of multiple molecules or proteins. The hierarchically-structure composite may be used to define 3D dynamic microenvironments and likely find broader applications in tissue engineering and therapeutic device.

# 4 PROGRAMMABLE DUAL-RELEASE PROFILES OF MODEL PROTEINS FROM ELECTROSPUN GRADED MATERIALS

## 4.1 Introduction

Nanofibrous scaffolds have demonstrated excellent potential for guiding the formation of new tissues in many tissue engineering fields [148–150]. In recent years, the regenerative potential of scaffolding materials has dramatically improved by encapsulation and release of proper biochemical signals in a controlled manner. Therefore, there is a great interest in developing scaffolds with the capability of selectively exposing cells and tissues to an assortment of active molecules with controlled dosage, timing and duration. Effective interplay between scaffolding materials and controlled release strategies is critical. In general, scaffold functions of can be extended to the delivery of signaling molecules either by using drug releasing scaffold or by incorporating drug delivery devices into the scaffold itself [151,152].

Bulk- and surface-eroding polymeric devices can serve as programmable drug delivery systems to generate pulsatile release of one protein or sequential release of multiple

biomolecules. Effective multipulse drug delivery system has been demonstrated using materials based on resorbable polyesters [153,154], polyanhydride-based laminates [155] and crosslinked hydrogels [156]. Chen and Mooney [157] developed PLGA scaffolds for spatially confined delivery and sequential release of VEGF and PDGF; Suciati et al. demonstrated the release of different bioactive molecules by sintering alternative layers of drug-loaded PLA microparticles plasticized with PEG and unloaded microparticles [158]. Alternatively, PLGA microparticles have been used to obtain delayed release after an initial lag-time [92]. In addition, several drug delivery materials have been recently developed for dual GF delivery. Burdick et al. demonstrated dual release of GFs for neural regeneration by encapsulating PLGA microspheres loaded with NT-3 in a PLA-PEG-PLA hydrogel with free CNTF [159]. Instead, porous scaffolds were shown that promoted neo-vascularization as a result of the release of known pro-angiogenic GFs, such as VEGF and PDGF [160].

In the previous chapter, we designed and established a material platform with electrospun composite scaffolds consisting of PCL and PLGA nanofibers with the ability to selectively deliver model biomolecules to one side of the scaffold. A precise gradient of composition through the scaffold thickness was created, which allowed one to tailor the initial distribution of small molecules and fluorescent-labeled proteins inside the device. We demonstrated that encapsulated molecules were released from one side of the scaffold with high efficiency of separation. We demonstrated that the composite structure could serve as a building-block to generate complex multilayered devices for controlled release of multiple biomolecules. This chapter thus further illustrates how different patterns and kinetics of release of two separate biomolecules can be achieved just by combining two of the basic elements. We

also seek to better understand the mechanism of the controlled release by providing the evidence about the critical role of PCL nanofibers in limiting water permeation in the scaffold for modulating the release pattern. This is then applied to guide the design of new composite scaffolds with the capability of control the timing and the kinetics of molecule release.

## 4.2 Experimental part

### 4.2.1 Materials and preparation of multi-component, electrospun scaffolds

As described in the previous chapter, Poly(d,l lactide-co-glycolide) acid (PLGA) with a 50:50 ratio of lactide/glicolide and a carboxylate end group from LACTEL®, was selected as the carrier for fluorescein isothiocyanate conjugate bovine serum albumin (AlbF, green emission) and Tetra-methyl-rhodamine isothiocyanate conjugate bovine serum albumin (AlbT, red emission). Poly-ε-caprolactone (PCL, 80 kDa) from Sigma Aldrich (St Louis, MO) and PLGA solutions with ALbF and AlbT were electrospun with a double electrospinning apparatus to obtain scaffolds with gradients of composition though their thickness. Electrospun nanofibers of pure PLGA were also prepared from PLGA solution without loaded molecules. Rhodamine B (RhB) was used as a fluorescent marker to study water penetration through electrospun scaffolds. Details about fluorescent molecules, solution preparations for electrospinning and parameters for the electrospinning process are provided in the previous chapter (please refer to sections 3.1, 3.2 and 3.3 of Chapter 3). Electrospinning conditions of PLGA were slightly modified to overcome the problem of unreliable spinning conditions at low flow rate, by limiting the duration of the spinning stages at the lowest rates.

The electrospun composite materials with internal compositional gradients were prepared through sequential and/or simultaneous electrospinning of PCL and drug-loaded PLGA on a rotational mandrel collector. A previously described double-electrospinning system was used. In some cases intermixed layers of PCL and pure PLGA were integrated in the design to

modify water diffusion characteristics of the scaffolds. In general terms, electrospun structures consisted of layers of single polymer nanofibers and layers of mixed nanofibers made of different polymers. Fibers in different layers were obtained through the continuous spinning process following the designed micropatterns, in order to integrate materials with variable composition and uneven distribution of biomolecules inside the scaffold. More details of the compositional profile and the biomolecule distribution along the thickness of the different scaffolds are given in the Results section. The double-side molecule release was described in section 3.3 of chapter 3.

### 4.2.2 Water permeation into the scaffolds

PCL and PLGA were individually electrospun to prepare mats with an uniform composition. Circular samples were obtained with a 25 mm punch cutter from each electrospun net and were placed between 2 cylindrical chambers made out of PMMA to form a custom made diffusion cell. The actual thickness of all the samples was within 10% of the designed thickness. Each chamber, with 2.2 mm in diameter and 2 ml in volume, was sealed to one side of the scaffold with bi-adhesive rubber gasket. Small holes were drilled on the side of the PMMA chambers and were used to add or remove the liquid from the diffusion cell. The chamber on one side of the scaffold, or named sink reservoir here, was filled with phosphate buffer solution; the other chamber, or named source reservoir here, was filled with a concentrated solution of RhB in phosphate buffer (2 mg/ml). With predetermined intervals, 200 µl of solution were withdrawn from the sink reservoir and replaced with fresh medium. The collected medium was analyzed for RhB concentration with a microplate spectrophotometer. A

total of 4 PCL disks and 6 PLGA disks were tested. The results were expressed as average ± standard deviation.

## 4.3 Results and Discussions

In this study, we designed electrospun scaffolds for controlled release of multiple active molecules. In the previous chapter, we demonstrated electrospun scaffolds with variable composition and graded micro-patterns of nanofibers along the thickness of the scaffold. We also demonstrated that electrospun scaffolds were capable of confining the release of model proteins to one side of the materials. Herein, we aimed to study whether the spatial patterns of nanofibers had the capacity of programming release kinetics. By using the basic patterns developed before as building blocks, we engineered the scaffolds for various release patterns. This was done through modifying the distribution and proportion of PCL and PLGA nanofibers along the thickness of the scaffold. The newly designed scaffolds maintained the ability to localize the delivery of each loaded biomolecule and demonstrated the capability of controlling the release kinetics.

### 4.3.1 Sequential release

Using PCL as the matrix, electrospun composite scaffolds with dual PLGA gradient patterns were designed for the sequential release of two proteins. The materials were prepared by continuous electrospinning in sequence of a 50 μm-thick layer of PCL nanofibers, a mixed layer of PCL and AlbF-loaded PLGA nanofibers with varied PCL/PLGA ratios, a 25 μm-thick transitional layer of PCL nanofibers, and a mixed layer of PCL and AlbT-loaded PLGA nanofibers with varied PCL/PLGA ratios. Figure 4-1a shows a schematic illustration of the pattern. The

micro-pattern was characterized by an equal amount of AlbF-loaded PLGA and AlbT-loaded PLGA, and consequently, an equal amount of AlbF and AlbT. The overall composition was 55% (wt) of PCL, 22.5% (wt) of AlbF-loaded PLGA and 22.5% (wt) of AlbF-loaded PLGA.

Figure 4-1b showed the cumulative release profiles of AlbF and AlbT released from both sides of the scaffold. It was found that both AlbF and AlbT were delivered preferentially to the chamber on side B. The separation efficiencies of AlbF and AlbT between side B and side A were 0.92 ± 0.03 and 0.85 ± 0.04, respectively. The scaffold was highly efficient in spatially confining the delivery of both AlbT and AlbF. The spatial confinement was more efficient for AlbT than for Alb F. AlbF was also released mainly on side B, although it was originally localized in a central region of the scaffold. Daily net release of AlbF and AlbT to side B in the first 12 days were shown in Figure 4-1c. The release kinetics of AlbF and AlbT are different from the previous study on dual protein release in Chapter 3. The net release of AlbT peaked on day 1 and day 2, and the net release of AlbF peaked on day 5.

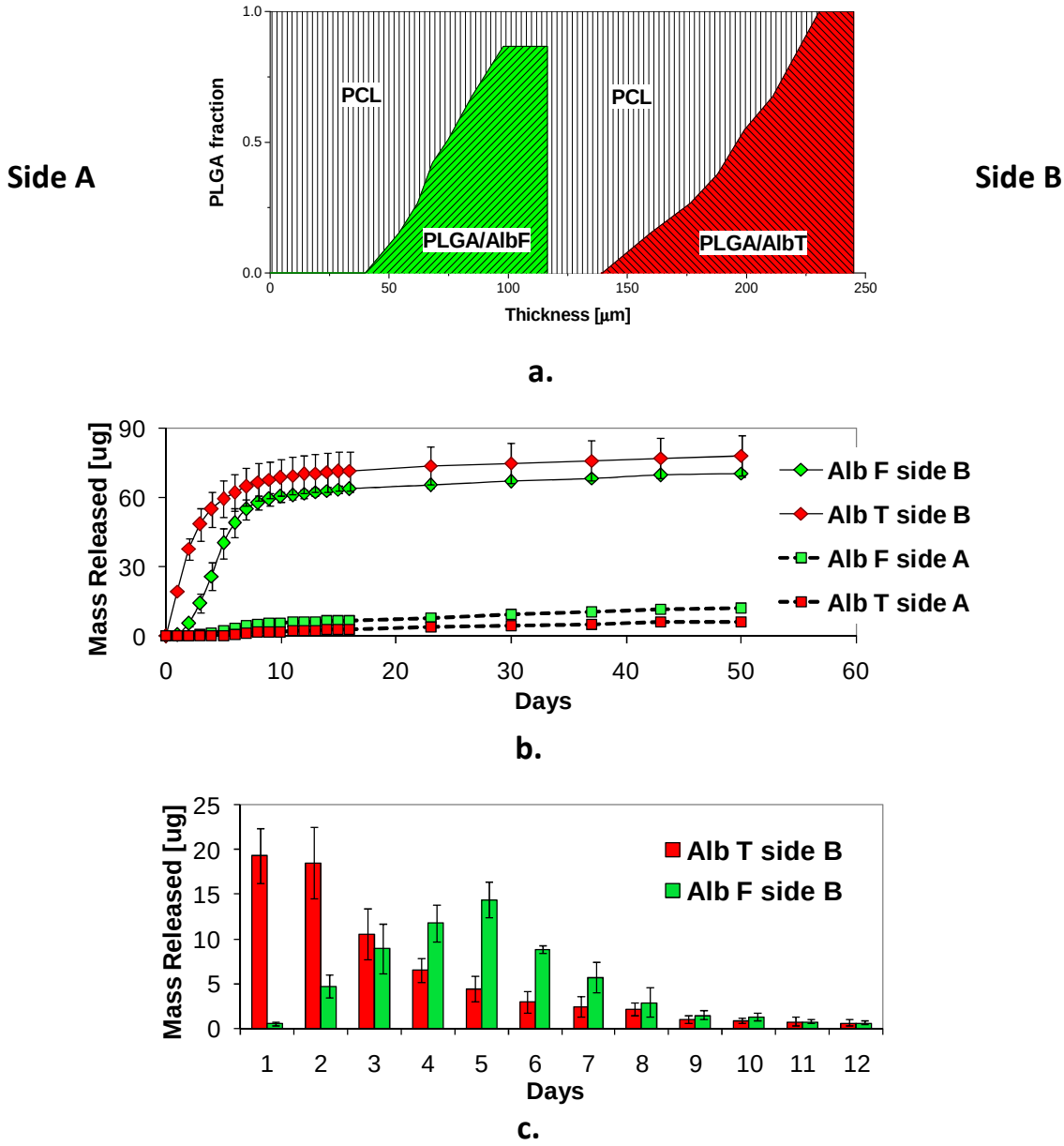


*Figure 4-1. PCL-PLGA scaffold for the sequential release of proteins. (a) Illustration of the compositional pattern of nanofibers. AlbF-loaded PLGA nanofibers were confined in the middle of the scaffold, while AlbT-loaded PLGA nanofibers were close to side B; (b) Cumulative release profiles of AlbF and AlbT from the two surfaces of the scaffold; (c) Net release profiles of AlbF and AlbT to side B during the first 12 days*

Furthermore, to explore the effect of the material pattern on the spatio-temporal release kinetics, a scaffold structure of modified dual gradients for the sequential release was designed (Figure 4-2a).

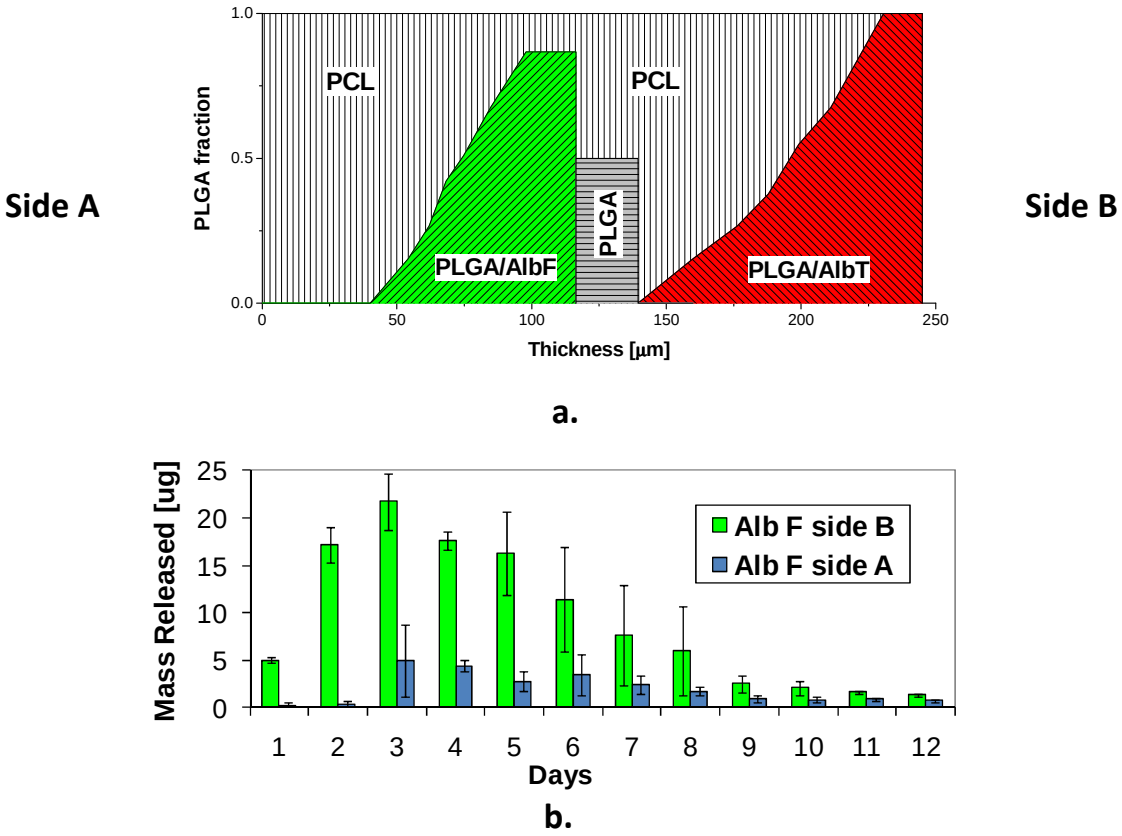


*Figure 4-2. PCL-PLGA scaffold with PLGA in the transitional layer of the pattern to modify the sequential release of proteins. (a) Illustration of the compositional pattern of nanofibers. PLGA and PCL nanofibers were combined in the transition zone between AlbF-loaded PLGA and AlbT-loaded PLGA nanofibers. (b) Net release profiles of AlbF and AlbT to both sides during the first 12 days*

In the modified design, the 25 μm-thick transitional layer of PCL nanofibers was replaced by a layer of intermixed PCL and PLGA nanofibers (PCL/PLGA ratio of 50/50). Compared to Figure 1, the release profile for AlbF was different: the net release of AlbF to side B peaked on day 3, much earlier than the similar pattern without PLGA in the transitional layer (Figure 4-2b). Meanwhile, the ability of the scaffold to confine the release on one specific side remained unaffected.

Therefore, various release kinetics of combined biomolecules could be achieved by modulating the nanofiber micropattern and the composition profile including the thickness of the PCL layer, thickness and composition of transitional layer. Regulating the timing and release kinetics of different molecules from scaffolds is critical to successful tissue regeneration. For example, there are different molecules influencing the process of neovascularization at different stages. In particular, VEGF contributes to initiate angiogenesis, while PDGF promotes vessel maturation in a later stage [161], [162]. For this reason, porous PLGA scaffolds for the sequential release of VEGF and PDGF were prepared by subsequently entrapping PDGF-loaded nanoparticles and integrating free VEGF into a scaffold by gas foaming and particulate leaching [160]. The nanofiber-based materials developed here may more readily program the desired molecule release kinetics for regeneration of mechanically strong tissues such as artery. For instance, it has been shown that PDGF guide the migration of smooth muscle cells, while transforming growth factor beta (TGF-β) is able to accelerate the proliferation of smooth muscle cells.

A sequential release of PDGF and TGF-β with proper timing (Figure 4-3) may promote regeneration of arterial media.

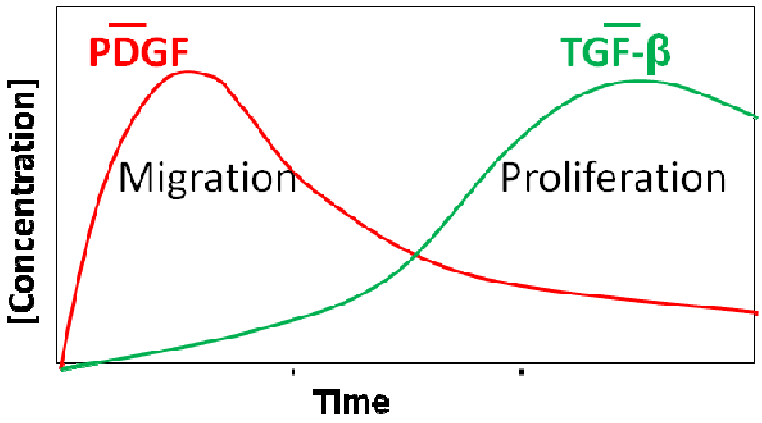


*Figure 4-3. Schematic illustration of a possible pattern for the sequential release of PDGF and TGF-β to regenerate vascular media.*

Currently, the optimal release kinetics for tissue regeneration in vitro or in vivo is largely unexplored. Using scaffolds to program release kinetics as demonstrated here, could be instrumental to identify an optimal condition from a large variety of release patterns and to study the underlying molecule mechanism. In addition, this method could be applied to the preparation of drug delivery devices for pulsatile release of active molecules.

### 4.3.2 Dual molecule release to the opposite sides of a scaffold

In order to demonstrate the effect of nanofiber composition on spatial control over biomolecule release from the scaffold, we have modified the pattern for dual molecule release to the opposite sides of a scaffold, which was demonstrated in Chapter 3. As shown in Figure 4-4a, the modified pattern comprised a 25 μm-thick layer of AlbF-loaded PLGA electrospun nanofibers on one surface of the scaffold, an inter-layer of PCL and AlbF-loaded PLGA with variable composition, a 50 μm-thick transitional layer of intermixed PCL and PLGA nanofibers in the core of the scaffold, an inter-layer of PCL and AlbT-loaded PLGA with variable composition, and 25 μm-thick layers of AlbT-loaded PLGA electrospun nanofibers close to the other surface. The micro-pattern was characterized by an equal amount of AlbF-loaded PLGA and AlbT-loaded PLGA, and consequently, an equal amount of AlbF and AlbT. The material composition was 35% (wt) of PCL, 25% (wt) of AlbF-loaded PLGA, 25% (wt) of AlbF-loaded PLGA and 15% (wt) of PLGA. Overall, the scaffold consisted of 65% of PLGA nanofibers and 35% of PCL nanofibers.

The cumulative release curves for both AlbF and AlbT were shown in Figure 4-4b and Figure 4-44c, respectively. The separation efficiency of AlbF between side A and side B ($S_{AlbF\_A\text{-}B}$) was 0.82 ± 0.04, while the separation efficiency of AlbT between side B and side A ($S_{AlbT\_B\text{-}A}$) was 0.81 ± 0.05.

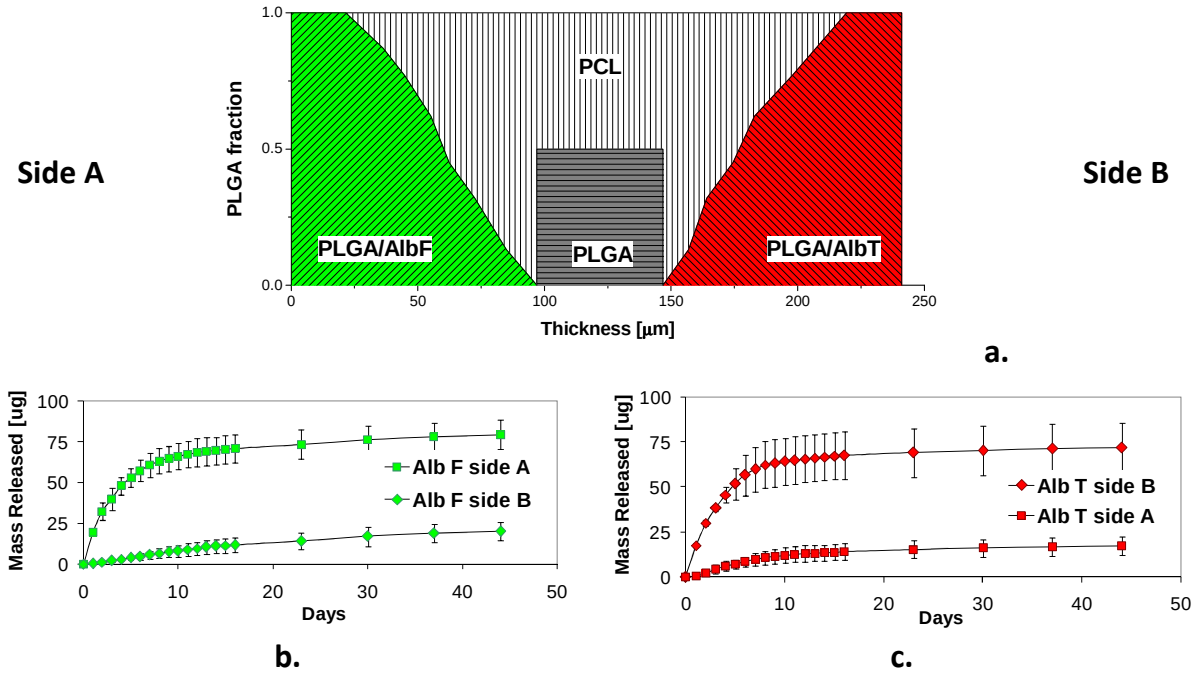


*Figure 4-4. PCL-PLGA scaffold with PLGA in the transitional layer of the pattern to modify the spatially-controlled release of proteins. (a) Illustration of the compositional pattern of nanofibers. PLGA and PCL nanofibers were combined in the transition zone between AlbF-loaded PLGA and AlbT-loaded PLGA nanofibers. (b) Cumulative release profiles of AlbF to both sides of the scaffold; (c) Cumulative release profiles of AlbT to both sides of the scaffold.*

As shown in the previous chapter (Chapter 3, Section 3.4), when the transitional region consisted of only PCL nanofibers, the separation efficiencies of AlbF and AlbT ($S_{AlbF\_A\text{-}B}$ and $S_{AlbT\_B\text{-}A}$) were 0.91 ± 0.04 and 0.92 ± 0.03, respectively. Here, we showed the scaffold pattern with the presence of a considerable amount of PLGA nanofibers in the transitional layer retained the ability to confine the protein release to one side, but the separation efficiency was significantly reduced. This molecule-releasing scaffold may be used in the applications where coordination of different molecule activities is needed. In the last 10 years, electrospun scaffolds have been explored for a number of applications such as wound dressing materials,

anti-adhesion membranes, vascular and cardiac patches, vascular grafts, neural conduits and repair of osteochondral defects. In these applications, the materials often interact with different cells, tissues and even organs. Scaffolds that selectively provide proper biochemical cues to different cell populations on two surfaces of the scaffolds may help simultaneous and coordinated regeneration of tissues. In the case of vascular tissue engineering, for example, a scaffold releasing VEGF and TGF-β respectively to the two surfaces, as illustrated in Figure 4-5, might simultaneously promote the formation of an endothelial layer on one side while inducing the proliferation of smooth muscle cells on the other side.

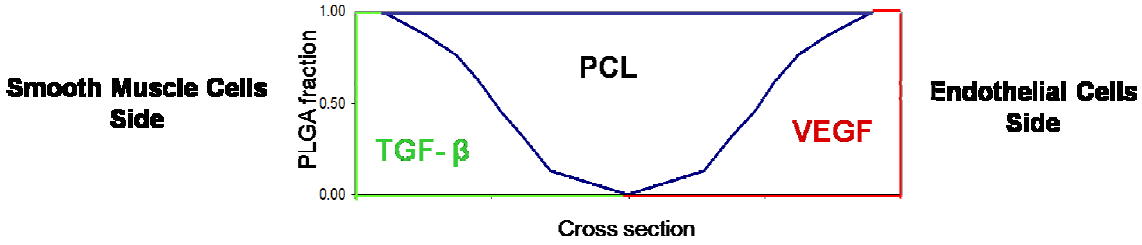


*Figure 4-5. Schematic illustration of a possible pattern for the separate release of VEGF and TGF-β on different sides of a vascular graft to regenerate artery. The delivery of each growth factor is spatially confined to one of the opposite surfaces of the scaffold to meet the specific requirements of different cell populations.*

### 4.3.3 Delayed release of AlbF and AlbT from opposite sides

To further modulate the release patterns for delayed protein release, another pattern with two symmetric compositional gradients inside the scaffold was designed and characterized (Figure 4-6a). In this design, the fraction of albumin-loaded PLGA nanofibers was higher in the internal region of the construct, rather than near the surfaces. Starting from side A, the

molecule delivery scaffold consisted of a 20 µm-thick layer of PCL nanofibers, an interlayer of mixed PCL and AlbF-loaded PLGA nanofibers with PLGA content varying from 0 to 0.8, a 50 µm-thick transitional layer of intermixed PCL and PLGA nanofibers, a interlayer of mixed PCL and AlbT-loaded PLGA nanofibers with PLGA content gradually varying from 0.8 to 0, and a second 20 µm-thick layer of PCL nanofibers on Side B. The scaffold contained equal amount of AlbF-loaded PLGA and AlbT-loaded PLGA. As a result, the scaffold was composed of approximately 40% (wt) of PCL, 22.5% of AlbF-loaded PLGA, 22.5% of AlbF-loaded PLGA and 15% of PLGA. Overall, the scaffold consisted of 65% of PLGA nanofibers and 35% of PCL nanofibers.

The cumulative release curves for AlbF and AlbT are shown in Figure 4-6b and Figure 4-6c, respectively. With this configuration, the scaffold maintained the ability to localize the release of each drug on one surface, but the separation efficiency was dramatically reduced: $S_{AlbF\_A\text{-}B}$ and $S_{AlbT\_B\text{-}A}$ was reduced to 0.66 ± 0.05 and 0.63 ± 0.05, respectively. Also, it resulted in a different release pattern: a near-zero order release was obtained instead of a power law behavior. Compared to the release profiles shown before, the initial burst release on the first day dramatically diminished. The stage of fast release due to diffusion was also delayed and kept over a longer period.

In general, we have demonstrated the capability of modifying the release kinetics with programmable the pattern and/or the fiber composition. Unfortunately, modulating temporal kinetics may reduce the spatially confinement of the molecule delivery to one side. However, this might be mainly due to the presence of PLGA nanofibers in the transitional layer along with PCL fibers. For the applications that require a high separation efficiency of a molecule to one side, a pattern without PLGA nanofibers in the transitional region is suggested.

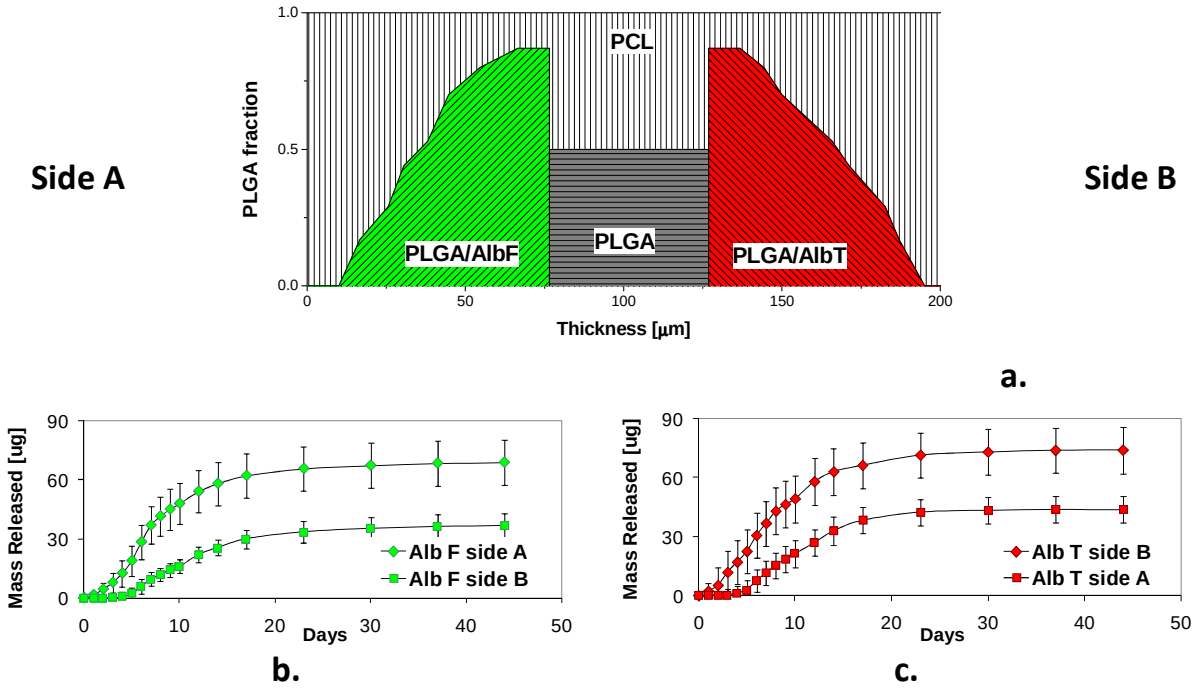


*Figure 4-6. Modified PCL-PLGA scaffold with inverse gradient for dual molecule release from opposite sides of the scaffold and in vitro release profiles of AlbF and AlbT from the two surfaces of the scaffold. a.) Schematic representation of a PCL-PLGA graded scaffold with two reversed gradients. The content of albumin-loaded PLGA nanofibers was 0 near the surfaces and maximum in the internal part of the scaffold. PLGA and PCL nanofibers were combined in the transition region between AlbF-loaded and AlbT-loaded PLGA nanofibers . Cumulative release curves for AlbF (b.) and AlbT (c.)*

### 4.3.4 Mechanism of drug release

In the previous chapter, we suggested that the protein release was divided into 3 stages: (1) the initial burst release on the first day, which resulted from a non-Fickian diffusion mechanism (anomalous diffusion); (2) the stage of fast release, which can be described by a semi-empirical equation developed by Rittger and Peppas using a network of mono-disperse infinite cylinders to model nanofibers; and (3) the final stage of steady slow release. Despite a number of approximations in the Rittger and Peppas equation, this approach has been widely used in order to describe the release behavior of electrospun nanofibers. However, the understanding of the molecular diffusion through the scaffold was still limited. The role of PCL nanofibers and the water diffusion or permeation into the scaffold remained unclear. In this chapter, we thus designed and characterized several different scaffolds to better understand the regulatory mechanisms of release through nanofiber patterns. By comparing all the release profiles, we could reach the following conclusions:

First, the integration of PLGA nanofibers and PCL nanofibers in the transitional regions of the scaffold resulted in a reduced capability of the scaffold to spatially confine the molecule delivery (Figure 4-4 and Figure 4-6). In other words, the diffusion of biomolecules, limited by PCL nanofibers, was expedited with the presence of PLGA nanofibers. In the case of sequential release, the movement of AlbF toward side B was faster in the presence of PLGA in the transitional region.

Second, when the fluorophore-labeled albumin is located close to the surface of the scaffold, a relatively faster release is obtained with a larger portion released in the first days (Figure 4-5). If albumin-loaded PLGA nanofibers are covered by a layer of PCL fibers, delayed release is found (Figure 4-1b, Figure 4-2b, Figure 4-6).

Third, the thickness of the PCL layers is important. For example, as shown in Figure 4-1, a 50 µm-thick layer of PCL nanofibers almost completely prevents AlbF from releasing to side A, while a 25 µm-thick transitional layer of PCL nanofibers only delays the molecule diffusion toward side A.

In summary, the role of PCL nanofibers that play in the pattern-controlled spatiotemporal release is likely to prevent molecule diffusion, while PLGA nanofibers seems to favor the transfer of biomolecules. To study this hypothesis, we compared the water diffusion through PLGA nanofibers and PCL nanofibers (Figure 4-7). Macroscopically, we found that within less than two days, the appearance of a 150 µm-thick layer of PLGA nanofibers turned from white to completely translucent, a sign of complete water uptake. Also, small molecules dissolved in the water can freely move from one side of the material to the other. On the contrary, in the case of PCL nanofibrous materials, no small molecules (RhB) were detected for almost 2 days in the sink reservoir, showing that there was no molecule movement between the opposite chambers. After 6 days, the concentration still increased slowly. Macroscopically, the material retained its white color. Therefore, the results suggested that water diffusion through a thin layer of PCL nanofibers was difficult. This is probably due to the hydrophobicity of PCL nanofibers, which hinder the movement of water molecules.

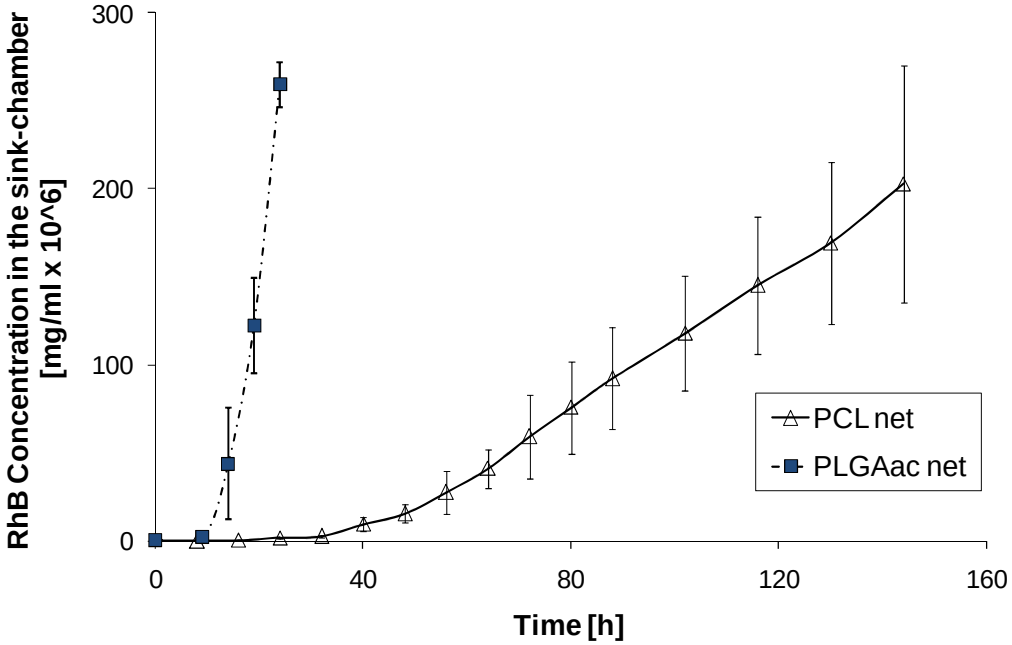


*Figure 4-7. Water permeation into PLGA and PCL electrospun scaffolds.*

Because the molecule diffusion or release through the nanofibrous scaffold was via the water permeation, to fully describe the release behavior of the composite electrospun scaffolds, both the molecule diffusion from the nanofibers and the water movement through the scaffold have to be taken into account. With a finite velocity of water uptake, the molecule diffusion and dissolution are activated at different time points in different scaffold regions. The diffusion pathways of the molecules toward the surface of the device are limited by the presence of air-filled pores.

### 4.3.5 Modeling the release

A full understanding of the material performances could help to guide the design of programmable molecule delivery systems with desired release profiles. This will only be possible with the development or identification of a mathematical model that properly describe the release. This is a challenging task. Herein, we propose a possible modeling approach using a basic gradient pattern (Figure 4-8).

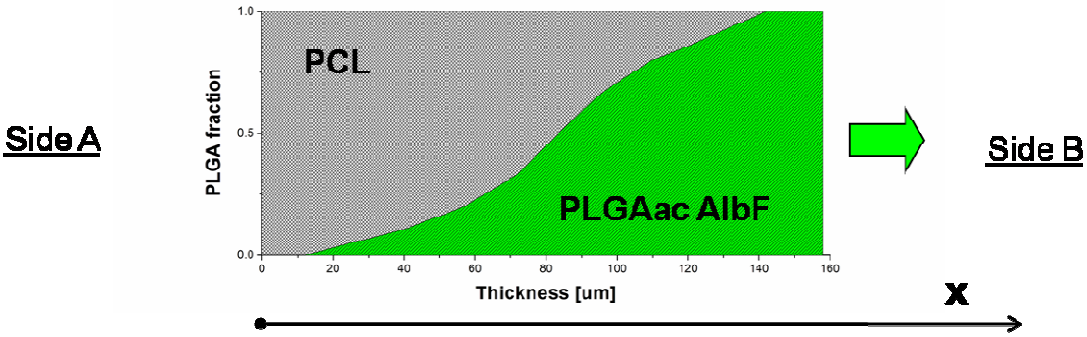


*Figure 4-8. Design pattern for composite scaffold with compositional and biochemical internal gradient*

The diffusion coefficient for water ($D_{water}$) is required to describe the water movement in the scaffold. According to our experimental results, the diffusion coefficient of water in PLGA nanofibers ($D_{water\text{-}PLGA}$) defines the higher end of $D_{water}$, while the diffusion coefficient of water in PCL nanofibers ($D_{water\text{-}PCL}$) defines the lower end of $D_{water}$. $D_{water\text{-}PLGA}$ and $D_{water\text{-}PCL}$ can be determined from diffusion studies or derived from thermodynamic principles. As the micropattern is characterized by a gradient structure with varied PCL/PLGA ratios, $D_{water}$ varies with the composition in the intermixed layers of nanofibers. Thus, a linear relationship between

$D_{water}$ with the PCL/PLGA ratio or the position x over the scaffold thickness is expected. The rate of water uptake in the scaffold (w) at a specific time point can be determined with Eq.1.

$$\frac{\partial w}{\partial t} = \frac{d}{dx}\left( D_{water}(x) \frac{dw}{dx} \right) \quad \text{Eq. 1}$$

In alternative, we could also determine with the relationship with the percolation theory. The amount of encapsulated molecules in the scaffolds and the amount of mobile molecules at each time point may be quantified with Eq. 2 and Eq. 3, where K is a constant that depends on the molecule and the material. Eq. 2 describes the variation of encapsulated molecules in the scaffold, while Eq. 3 describes the rate of molecule release.

$$\frac{\partial \rho_{fix}}{\partial t} = -K \rho_{fix} \cdot w \quad \text{Eq. 2}$$

$$\frac{\partial \rho_{mob}}{\partial t} = K \rho_{fix} \cdot w + \frac{d}{dx}\left( D(x,w) \frac{dw}{dx} \right) \quad \text{Eq. 3}$$

In summary, the dependence of the diffusion coefficient (D(x,w)) on the material composition point by point (x) and on the water content (w) has been used to describe the molecule diffusion in the scaffold. The diffusion problem can be solved with boundary conditions that depend on the specific compositional pattern and D(x,0) = 0, at t = 0. To our knowledge, there is no analytical solution for this problem, and thus a numerical solution should be expected.

## 4.4 Conclusions

Taking advantage of multi-functional scaffolds produced by a double electrospinning, we demonstrated programmable drug delivery devices able to deliver different active molecules in a controlled fashion. We obtained simultaneous and sequential release of two different model proteins on the two surfaces of a newly engineered, composite electrospun scaffolds, and we showed that release kinetics can be influenced by changing the initial pattern of drug distribution and the composition of the scaffold. We believed that scaffold preparation and release micropatterns presented in this work may represent the platform for the development of novel multifunctional matrices able to control and direct the process of tissue regeneration.

# 5 SOLUTION AND EMULSION ELECTROSPINNING FOR VASCULAR ENDOTHELIAL GROWTH FACTOR ENCAPSULATION AND RELEASE

## 5.1 Introduction

In the previous chapters we presented a number of electrospun scaffolds with a potential as specialized drug delivery systems. We designed and prepared by electrospinning nanofibers mats characterized by a novel compositional and biochemical micropattern for encapsulation and release of biomolecules. By taking advantage of a smart distribution of encapsulated species and differential water penetration rates throughout the scaffold, we demonstrated spatially- and temporally-programmable delivery of model biomolecules, such as fluorescent dyes and fluorescently-labeled proteins. Previously in this thesis work, we used one-phase, solution electrospinning process to encapsulate model molecules in the nanofiber scaffolds; however, our findings can be extended to any encapsulation methods and any drug-carrier polymers. The usage of different polymer/drug systems will result in different release rates and profiles of the specific loaded molecules, but the overall release scheme, involving

locally-confined and temporally-programmable deliveries, will be respected. In fact, the release profile of a particular drug depends just on the specific mechanism of release from nanofibers, while the overall release pattern depends essentially on the peculiar compositional pattern and the initial drug distribution that we designed.

Growth factors (GF) are proteins specific for cell-to cell and cell-extra cellular matrix communication. During tissue morphogenesis GFs influence cellular behavior, tissue formation and organization. Growth factors are stored in the extra cellular matrix in insoluble, inactive forms via specific binding with glycosaminoglycans like heparins. Upon specific activation GFs are readily released in the intercellular fluid, where they can express their biological activity. Confinement of inactivated GFs within the ECM is an amazingly efficient solution for rapid, extracellular signal transduction. Concentration and spatial distribution in the extracellular environment are key factors for GFs efficacy. In particular, it has been shown that gradients in the concentration of free GFs can direct cell adhesion and migration, differentiation of multipotent cells and organization of cells into complex structure [163,164].

Vascular endothelial growth factor (VEGF) is a potent mitogen for micro- and macro-vascular endothelial cells and it is considered to be one of the most critical aspects in vascular formation and regeneration, particularly regulating the function of endothelium. Dosage of these biomolecules must be carefully regulated in a quantitative, spatial, and temporal manner in order to control cellular behaviors. Efficiently engineered VEGF delivery systems are required to minimize drug loss, degradation and denaturation, to assure a release within the concentration range in which the maximum benefit is provided. As VEGF has a short half-life in the body, a

smart drug delivery system have to maximize the medicament availability in the most required zone and limit the release in the near-by region [165].

In one-phase, solution electrospinning biomolecules are directly mixed within the polymer solution, and the mixed solution is electrospun to fabricate drug-loaded nanofibers. Researchers have used solution electrospinning to incorporate various types of proteins and genes in nanofiber scaffolds, including bovine serum albumin (BSA) [166], lysozyme [167] and growth factors [49]. Although solution electrospinning is relatively easy to perform, a possible issue with activity loss of incorporated biomolecules can arise. This is a quite severe problem for proteins, because they may lose their bioactivity due to conformational changes in the organic solution. For this reason, emulsion electrospinning has been proposed as an alternative technique for the preparation of drug-loaded nanofiber materials. Emulsion electrospinning is relatively novel and simple method of encapsulating biomolecules in biomaterials and has attracted increasing interest in the recent years [142,168]. It was also pointed out that nanofibers prepared by emulsion electrospinning could protect the structural integrity and bioactivity of encapsulated protein [166,168].

In this part of the work we used both one-phase solution electrospinning and emulsion electrospinning to encapsulate VEGF in nanofiber scaffolds and we monitored VEGF release with a short-term in vitro release experiment. In addition, by using fluorescent molecules, we showed how the specific encapsulation method strongly influences drug distribution inside the nanofibers.

## 5.2 Experimental part

### 5.2.1 Materials

LACTEL® 50:50 poly(d,l lactide-co-glycolide) acid with a carboxylate end group and intrinsic viscosity of 0.67 dL/g, hereinafter referred to as PLGA, was purchased from DURECT Corp. (Pelham, AL, USA).

RESOMER® R207S poly(d,l lactide) acid with inherent viscosity of 1.3 - 1.7 dL/g, hereinafter referred to as PdlLA, was obtained from Pharma Polymers (Darmstadt, Germany)

Poly(ε-caprolactone) (PCL) with molecule weight of 80 kDa, chloroform (CF), N,N-dimethylformamide (DMF), methylene chloride (MC), 1,1,3,3,3-hexaflouro-2-propanol (HFIP), as well as emulsifiers, Span™ 80 and Tween™ 80 were all purchased from Sigma Aldrich (St. Louis, MO, USA).

Bovine serum albumin (BSA), fluorescein isothiocyanate conjugate bovine serum albumin (AlbF) with green emission and vascular endothelial growth factor human recombinant (VEGF) were also obtained from Sigma Aldrich (St. Louis, MO, USA).

Quantikine® Human VEGF ELISA kit was purchased from R&D Systems (Minneapolis, MN, USA) and used for the quantitative determination of VEGF content in the release medium, kit following the manufacturer's protocol.

### 5.2.2 Preparation of pre-spinning solutions and electrospinning

Protein-loaded electrospun PLGA and PdlLA nanofibers were prepared by conventional solution electrospinning. Flourescently-labeled albumin AlbF was encapsulated in PLGA and PdlLA nanofibers for visualization of the distribution of the loaded biomolecules. A solution of AlbF in DI water with a concentration of 5 mg/ml was prepared and then mixed with HFIP in a 1:7 volumetric proportion. The HFIP:DI water mixture with AlbF was used to dissolve PLGA with a final concentration of 17% (wt) and PLGA nanofibers loaded with AlbF were prepared from a homogeneous, one-phase solution by solution electrospinning. Nanofiber mats prepared with this technique were indicated hereinafter as **PLGAsol_AlbF**. Electrospinning parameters for all the electrospun nanofibers prepared by solution electrospinning are listed inTable 5-1.

The HFIP:DI water mixture with AlbF was also used to dissolve PdlLA to a final concentration of 10% (wt) and PdlLA nanofibers loaded with AlbF were prepared by solution electrospinning (hereinafter indentified as **PdlLAsol_AlbF**). Thin layers of PLGA and PdlLA electrospun nanofibers loaded with AlbF were deposited on glass slides for confocal observation.

Lyophilized VEGF was reconstituted with DI water at a concentration of 0.1 mg/ml to prepare the VEGF batch solution. By dilution of the VEGF batch solution in DI water and addition of BSA powder, a 17 μg/ml VEGF solution in DI water with 5% BSA was obtained, and then mixed with HFIP in a 1:7 volumetric proportion. This mixture was used to dissolve PLGA to a final concentration of 17% (wt) and VEGF-embedded PLGA nanofiber nets were produced by solution electrospinning (hereinafter **PLGAsol_VEGF-BSA).**

Similarly, by dilution of the VEGF batch solution in DI water and addition of BSA powder, a 10 µg/ml VEGF solution in DIwater with 5% BSA was obtained, and then mixed with HFIP in a 1:7 volumetric proportion. This new mixture was used to dissolve PdlLA to a final concentration of 10% (wt) and VEGF-embedded PdlLA nanofiber nets were produced by solution electrospinning (hereinafter **PdlLAsol_VEGF-BSA).** In addition, PCL was dissolved in 75/25 CL/DMF at a concentration of 10% (wt).

| **Polymer** | **Samples Prepared** | **Solvent system** | **Polymer conc.** [% wt] | **Voltage** [kV] | **Work Distance** [cm] | **Feed rate** [ml/h] |
|---|---|---|---|---|---|---|
| **PLGA** | PLGAsol_AlbF | HFIP/water 7/1 vol. | 17 | 24 | 22 | 0.65 |
| | PLGAem_AlbF | CL-water-emulsifier* | 10 | 24 | 18 | 0.5 |
| | PLGAsol_VEGF-BSA | HFIP/water 7/1 vol. | 17 | 18 | 22 | 0.65 |
| | PLGAem_VEGF-BSA | CL-water-emulsifier* | 10 | 18 | 20 | 0.5 |
| **PdlLA** | PdlLAsol_AlbF | HFIP/water 7/1 vol. | 17 | 24 | 22 | 0.9 |
| | PdlLAem_AlbF | CL-water-emulsifier* | 10 | 24 | 18 | 0.8 |
| | PdlLAsol_VEGF-BSA | HFIP/water 7/1 vol. | 17 | 18 | 22 | 0.9 |
| | PdlLAem_VEGF-BSA PCL-PdlLA_VEGF-BSA | CL-water-emulsifier* | 10 | 18 | 18 | 0.2-0.8 |
| **PCL** | PCL-PdlLA_VEGF-BSA | CF/DMF 3/1 vol. | 10 | 26 | 24 | 0.3-1.1 |

*Table 5-1. Electrospinning parameters for the nanofiber mats prepared by solution and emulsion electrospinning (* Emulsion consisting of CL-water phase-emulsifier mixture with a 100-5-2 volumetric ratio)*

### 5.2.3 Preparation of the pre-spinning W/O emulsions and electrospinning

Protein-loaded electrospun PLGA and PdlLA nanofibers were also prepared by electrospinning of a water-in-oil (W/O) emulsions. Electrospinning parameters for electrospun nanofibers prepared by emulsion electrospinning are also listed in Table 5 – 1..

A combination of Span80 and Tween80 (9 to 1 in volume) was used as emulsifier to stabilize the emulsions. The volume of the aqueous phase and the volume of emulsifier were set to 1/20 and 1/50 of the volume of the organic solution, respectively. First, the organic phase and the emulsifier were homogenized in a glass vial with a magnetic stirrer, then the aqueous solution was added drop-by-drop under constant stirring. A magnetic stirring bar rotating at 1000 rpm was used for the emulsification process. A secondary stage of emulsification via ultrasonification was also considered.

Flourescently-labeled albumin, AlbF was encapsulated in PLGA and PdlLA nanofibers prepared by emulsion electrospinning for the visualization of the protein distribution. A 2 mg/ml solution of AlbF in DI water was emulsified with a 17% (wt) PLGA solution in CL. AlbF-loaded PLGA nanofibers prepared by emulsion electrospinning are hereinafter indicated as **PLGAem_AlbF**.

A 2 mg/ml solution of AlbF in DI water was also emulsified with a 11% (wt). AlbF-loaded PdlLA nanofibers prepared by emulsion electrospinning are hereinafter indicated as **PdlLAem_AlbF**.

W/O emulsions containing AlbF were examined with a confocal microscope to assess the distribution of the AlbF-marked dispersed phase (water phase) inside the continuous phase (polymeric organic solution).

In addition, a 17 μg/ml VEGF solution in DIwater with 5% BSA was emulsified with a 17% (wt) PLGA solutions in CL. Similarly, a 10 μg/ml VEGF solution in DIwater with 5% BSA was emulsified with a 11% (wt) PdlLA solutions in CL. VEGF-loaded PLGA and PdlLA nanofiber materials produced by emulsion electrospinning of the previously prepared emulsions are hereinafter indicated as **PLGAem_VEGF-BSA** and **PdlLAem_VEGF-BSA.**

### 5.2.4 PCL-PLGA and PCL-PdlLA graded scaffolds for spatially-confined release of VEGF

PCL-PLGA and PCL-PdlLA composite scaffolds with a compositional and biochemical gradient along their thickness were also prepared (hereinafter **PCL-PLGA_VEGF-BSA** and **PCL-PdlLA_VEGF-BSA**, respectively). VEGF-loaded PdlLA and VEGF-loaded PLGA nanofibers were electrospun by emulsion electrospinning of the corresponding emulsion prepared as indicated above.

A schematic representation of a composite scaffold is reported in Figure 5-1. The scaffold was obtained following the design of the basic drug-delivering element already described and tested in Chapter 3. Please, refer to Chapter 3 for a detailed description of the micropattern, scaffold composition, the drug distribution and preparation procedures.

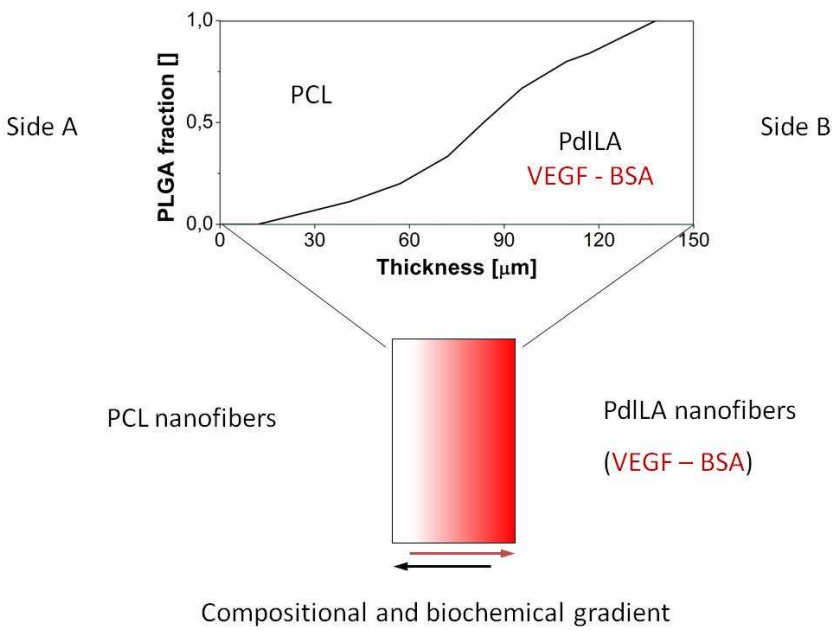


*Figure 5-1. Schematic illustration of the cross-section of PCL-PdlLA_VEGF-BSA electrospun scaffold with internal compositional and biochemical gradient.*

### 5.2.5 Nanofibers characterization

Nanofibers loaded with AlbF were examined as spun with a confocal microscope to assess the distribution of encapsulated molecules. The morphology of the electrospun fibers was observed using scanning electron Microscopy SEM.

### 5.2.6 In vitro release of VEGF

Phosphate buffer solution pH 7.4 used as release medium was prepared as indicated in Chapter 3, with the addition of 0.1% BSA.

VEGF-loaded PLGA and PdlLA nanofiber materials prepared by solution and emulsion electrospinning (PLGAsol_VEGF-BSA, PdlLAsol_VEGF-BSA, PLGAem_VEGF-BSA and

PdlLAem_VEGF-BSA) were immersed in the BSA-enriched release medium to assess in vitro release of VEGF. Three pre-cut specimens, approximately 20 mg in weight, were obtained from PLGA and PdlLA mats prepared either by solution or by emulsion electrospinning. Each specimen was placed in a separate test tube, covered with 2 ml of 0.1% BSA phosphate buffer solution and placed at 37°C for 7 days, under mild agitation. For the PCL-PdlLA composite scaffolds (PCL-PdlLA_VEGF-BSA) the in vitro release test was performed using the diffusion cell and methodologies for side-by-side release tests previously described in Chapter 3. Using this release system, it was possible to discriminate between VEGF delivered to Side A and VEGF delivered to side B.

Each day the supernatant was removed, the samples were briefly rinsed in DI water, and fresh release medium was added. Extracted samples were stored at -80°C, prior examination. VEGF content in the release medium was determined for elutions with the Quantikine® Human VEGF ELISA kit, following manufacturer's specifications. To reduce the number of analyzed samples, elutions extracted from the three repetitions of each data point were mixed together prior examination; for this reason, the reported values represent the average value of the release and no error bars are provided.

## 5.3 Results and Discussions

### 5.3.1 Preparation of stable W/O emulsions and electrospinning

A number of water solutions were mixed with either PLGA or PdlLA solutions in chloroform and stable emulsions was obtained under agitation. The aqueous solution was added into the oily phase drop-by-drop to ensure the atomization of the aqueous phase. A mixture of Span80 and Tween80 was added into the polymer solution prior to emulsification as a surfactant to lower the surface tension of the oily phase. Tween 80 belongs to a class of food additives also known as polysorbates, while Span 80 (Sorbitan monooleate) is a sorbitan ester widely used in food products and oral pharmaceuticals. Tween 80 and Span 80 are generally regarded as non-toxic and non-irritating. According to the hydrophile-lipophile balance system (HLB), surfactants with HLB values between 4 and 6 are suitable for making W/O emulsions. Therefore, a mixture of SPAN80 and Tween80 (9 parts of Span80 and 1 part of Tween80) with a resulting HLB value of 5 was used as emulsifier to prepare the W/O emulsions.

In the preliminary stage of the work, the concentration of the organic, polymeric solutions, the volume of aqueous phase and emulsifier and the emulsification conditions were considered. The organic phase and the emulsifier were homogenized in a glass vial with a magnetic stirrer, then the aqueous solution was added drop-by-drop under constant stirring. A magnetic stirring bar rotating at 1000 rpm was used for the emulsification process; a secondary stage of emulsification with ultrasonification was also considered. Preliminary electrospinning experiments were performed in order to evaluate the impact of the different parameters on

the electrospinning process. A optical microscopy was used to monitor the overall quality of the electrospun nets. Concentration and composition of the PLGA and PdlLA solutions resulted to be the particularly important for the formation of nanofibers during the electrospinning process. Stable emulsions were obtained by adding to the organic polymer solutions volumes of emulsifier ranging from 1/50 to 1/25 of the volume of the polymeric solutions. The volume of watery-phase with AlbF was successfully varied between 1/20 and 1/10 of the volume of the organic solutions. From the preliminary electrospinning experiments it was clear that larger amounts of water phase made the electrospinning process less effective and discontinuous. Generally, the presence of the emulsifier had a benign effect on the quality of the fibers and the overall process, but this effect was not related to the actual amount of emulsifier in the tested range. So, the volume of watery-phase and emulsifier were fixed at 1/20 and 1/50 of the oily-phase volume, respectively. PLGA and PdlLA were dissolved in CL at a concentration of 17% and 11%, respectively. Those values represented the best compromise between emulsion stability and quality of the electrospinning process for the present system of emulsifiers and solvents.

As far as the emulsification process itself, confocal micrographs were used to determine dimension and distribution of the dispersed phase after each stage of emulsification.

Figure 5-2a shows a confocal image of a W/O emulsion of a water solution of AlbF in a 17% PLGA in CL; the emulsion was obtained by stirring the two solutions at 1000 rpm for 10 min on a conventional magnetic stirrer.

Except in the short initial transient during the formation of the emulsion, the time of stirring was found not to be a significant factor in the emulsification process. As reported in the graph in Figure 5-2c, at front of a the time of stirring increased from 10 min to 1 hour, no

significative changes in the diameter and distribution of the water phase were found (from 5.6 ± 2.9 to 5.0 ± 2.9 μm). On the contrary, a similar emulsion was sonicated for 1 minute after 1 hour of stirring (see Figure 5-2b), resulting in a significative decrease of the water drops dimension to 2.4 ± 1.4 μm. However, all the emulsions remained stable for several hours after the emulsification, and we chose to avoid the sonication to preserve both the loaded biomolecules and the molecular weight of the polymers. A similar behavior was found when 11% PdlLA in CL was used as organic phase.

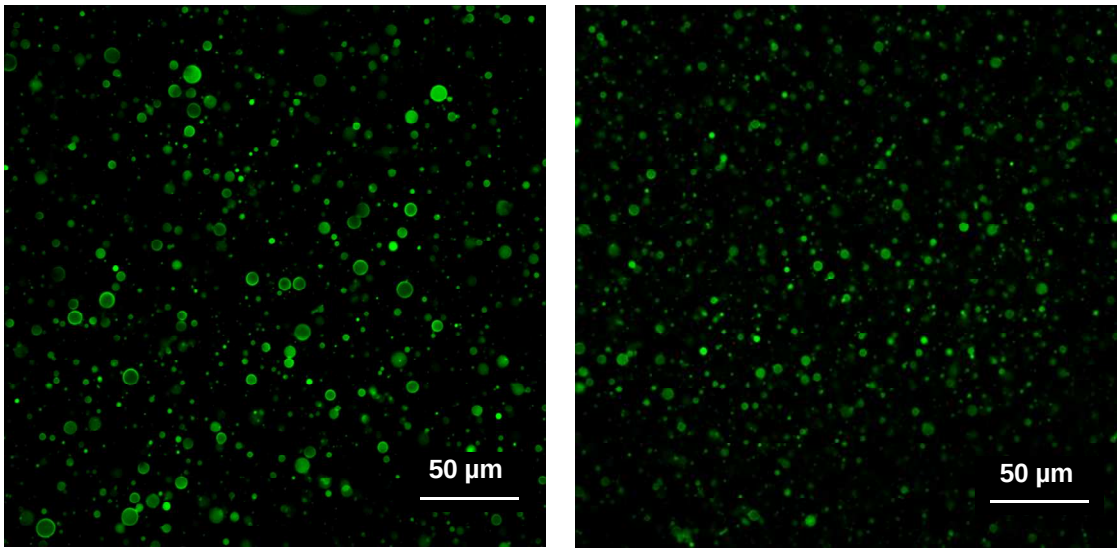


a. b.

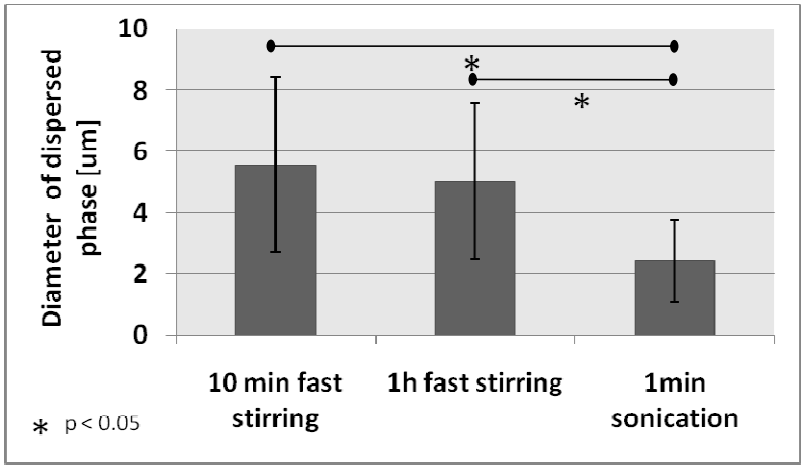


c.

*Figure 5-2. W/O emulsions consisting a 2 mg/ml water solution of ALbF dispersed in a 17% (wt) solution of PLGA in CL prepared with different emulsification methods. a.) W/O emulsion homogenized with a magnetic stirrer with magnetic bar rotating at 1000 rpm for 10 min; b.) W/O emulsion subjected to sonication for 1 min after stirring; c.) Diameter of the disperse phase as a result of different emulsification methods*

Figure 5-3 demonstrates the distribution of loaded molecules in electrospun nanofibers prepared from W/O emulsions.

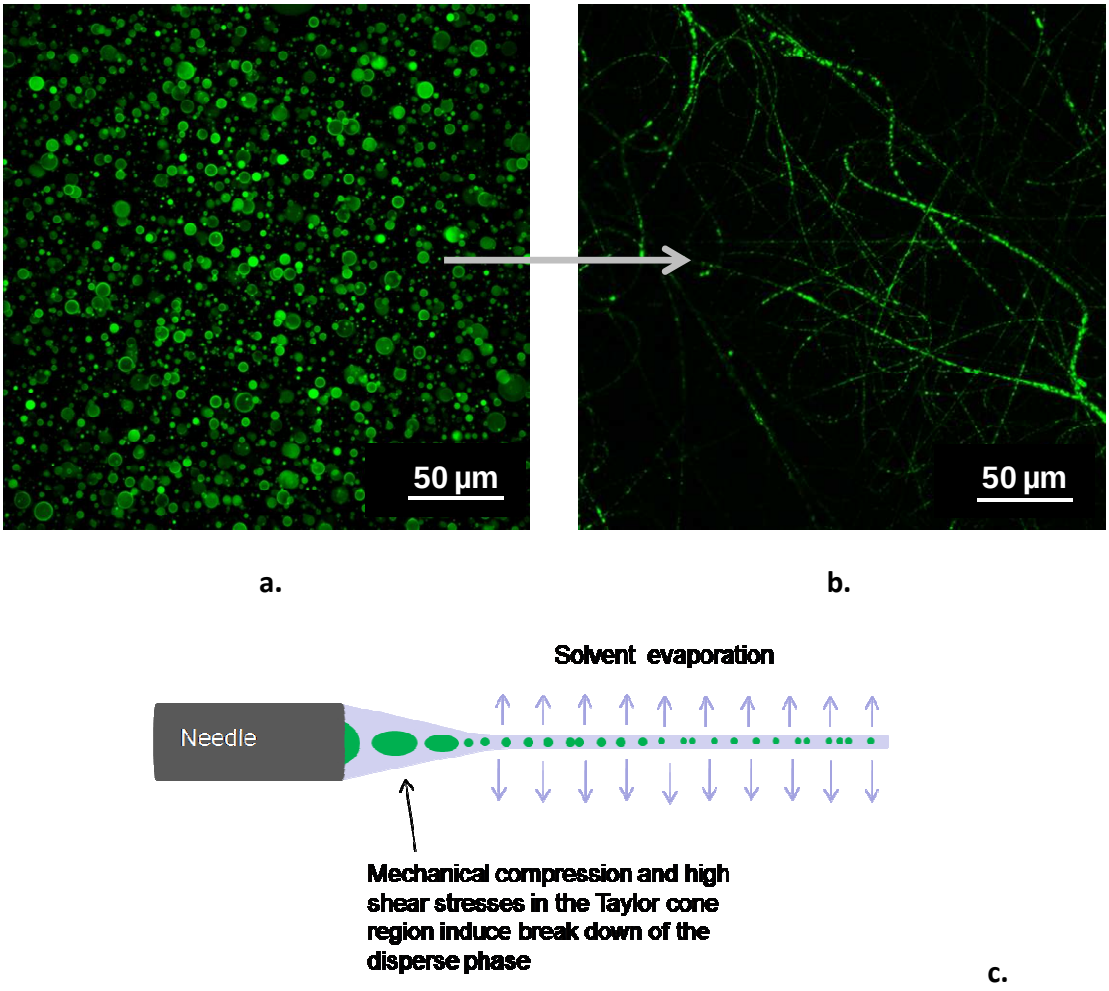


*Figure 5-3. Confocal images of a W/O emulsion of AlbF in and the corresponding electrospun nanofibers. a.) W/O emulsion consisting a 2mg/ml water solution of ALbF dispersed in a 17% (wt) solution of PLGA in CL (water phase/organic phase ratio equal to 1/20); b.) AlbF distribution in AlbF-loaded PLGA nanofibers obtained by electrospinning of the emulsion; c.) Schematic illustration of the microdroplets breakdown in the region of the Taylor cone and the formation of fluorescent nanoclusters along the nanofibers during electrospinning*

A W/O emulsion consisting a water solution of ALbF dispersed in a 17% (wt) solution of PLGA in CL was electrospun on a glass slide. The resulting nanofibers were imaged with the confocal microscopy.

AlbF was not homogeneously dispersed in the electrospun nanofibers; on the contrary, the entrapped biomolecules were confined in islands and rounded clusters along the nanofibers. It was not trivial to determine the dimension of those clusters, but we estimated that they ranged between 100 and 300 nm. It is interesting to recall that the dimension of the dispersed phase in the emulsion ranged between 1 and 8 μm. We think that large shear stresses and mechanical compression in the Taylor cone and in the linear region of the electrospinning induce an extended breakdown of the disperse phase, resulting in drastic reduction of the dimension of the drops. Evaporation of the solvent during the fiber formation may also contribute to the formation of the nanoclusters of the encapsulated molecules.

### 5.3.2 Preparation of AlbF-loaded nanofibers by solution and emulsion electrospinning

In Figure 5-4, AlbF-embedded nanofiber meshes prepared by solution electrospinning and emulsion electrospinning are compared. Nanofibers in Figure 5-4.a and Figure 5-4c were prepared by solution electrospinning of a one-phase, homogeneous pre-spinning solutions; nanofibers in Figure 5-4b and Figure 5-4d were prepared by emulsion electrospinning of a biphasic W/O emulsion.

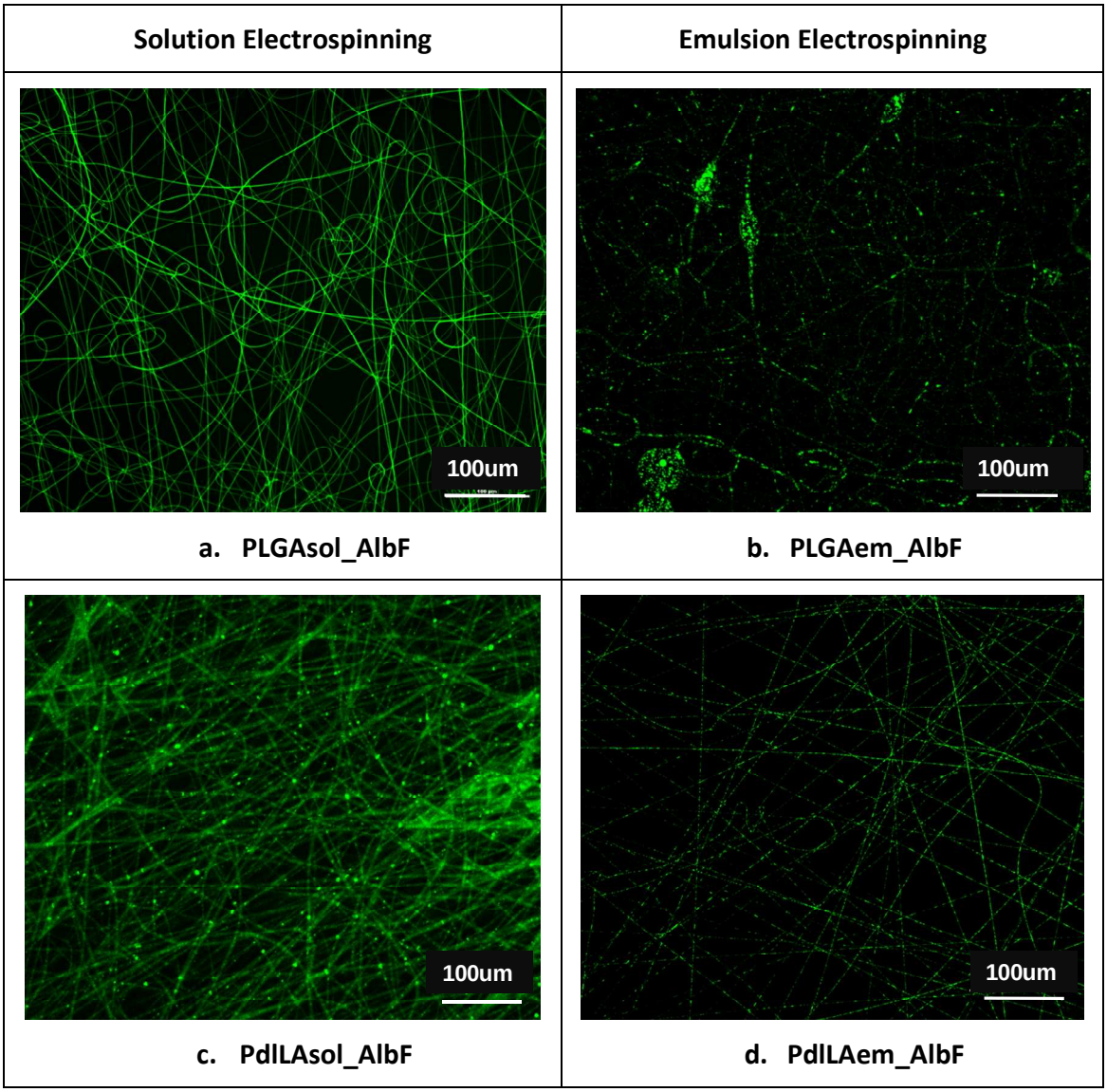


*Figure 5-4. Confocal images of PLGA and PdlLA nanofibers embedded with AlbF either prepared by one-phase, solution electrospinning (a.-c.) or by emulsion electrospinning (b.-d.).*

In the case of solution electrospinning the loaded AlbF was homogeneously dispersed into the nanofibers. On the contrary - as previously discussed - entrapped AlbF was confined in isolated nanoclusters along the fibers in the case of emulsion electrospinning. This is

particularly evident in the PdlLA nanofibers prepared by emulsion electrospinning (**PdlLAem_AlbF),** where AlbF clusters are aligned with great regularity along the fibers (Figure 5-4c). Emulsion electrospinning of PdlLA originated highly reproducible defect-free nanofibers and a high-quality electrospinning process.

Instead, as it is possible to see in Figure 5-4b, PLGA nanofibers prepared by emulsion electrospinning (**PLGAem_AlbF)** presented several microscopic defects. It is worth to emphasize here that, regardless all our efforts, it was not possible to prepare PLGA W/O emulsions with optimal electrospinning properties. Discontinuity in the electrospinning jet, instability of the Taylor cone, high viscosity of the emulsion and fast solvent evaporation resulted in the formation of polymeric agglomerates at the tip of the needle. The process was also highly discontinuous; excellent fibers were obtained at times, but macroscopic and microscopic droplets, large fibers and aggregates were also deposited onto the collector (see also Figure 5-5). At times, no electrospinning was obtained at all. We think that, due to its low molecular weight, PLGA in solution has a limited ability to withstand shear stresses during the formation of the fiber resulting in a instability of the polymer jet. In presence of a disperse phase, the polymer may not be able to overcome the increased viscosity of the emulsion. We also tried to use alternative solvents or mixtures of solvents (toluene and xylene between others) for the preparation of the PLGA organic solution. Regardless a large number of alternative formulations, no evident improvement of the process was found.

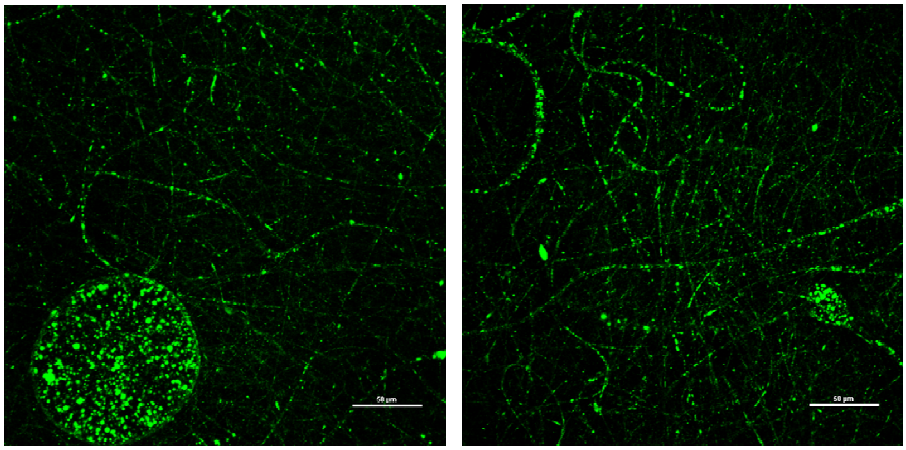

*Figure 5-5. PLGAem_AlbF nanofibers with macroscopic solidified polymer drops, large fibers and aggregates (Scale bar 50µm)*

SEM micrographs in Figure 5-6 display the morphology of the different Alb-loaded electrospun nets. Cylindrical, smooth nanofibers were observed in all cases. Spindle-like defects and irregular diameters were found for PLGA nanofibers. It is interesting to compare confocal images and SEM micrographs for samples prepared by emulsion electrospinning (for instance compare Figure 5-4d and Figure 5-6d). Although encapsulated AlbF had a non-homogenous distribution and it was confined in clusters, nanofibers did not present any evident bulges or irregularities on the exterior.

| Solution Electrospinning | Emulsion Electrospinning |
| --- | --- |
| 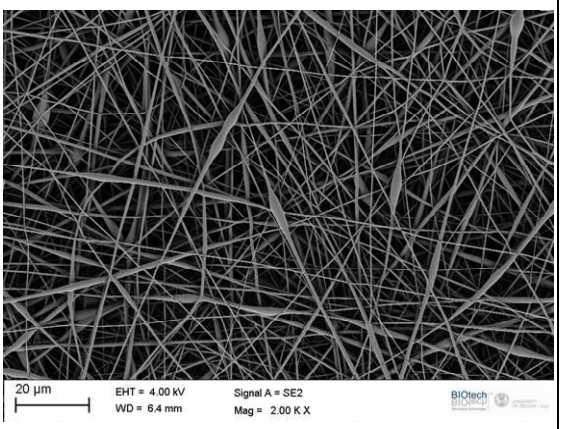  **a. PLGAsol_AlbF** | 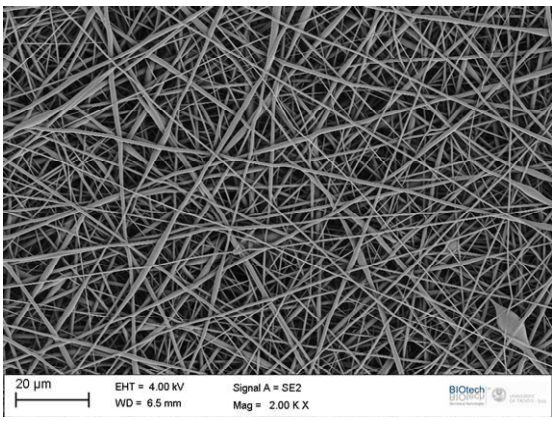  **b. PLGAem_AlbF** |
| 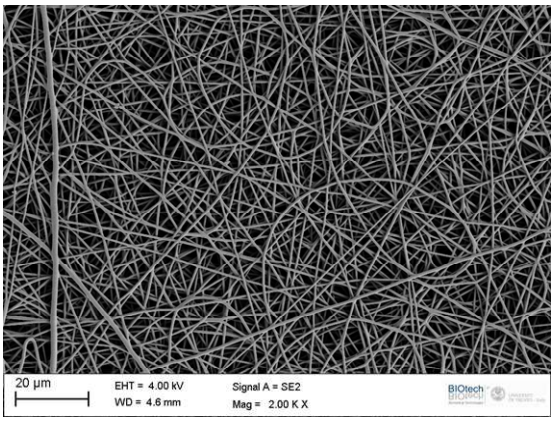  **c. PdlLAsol_AlbF** | 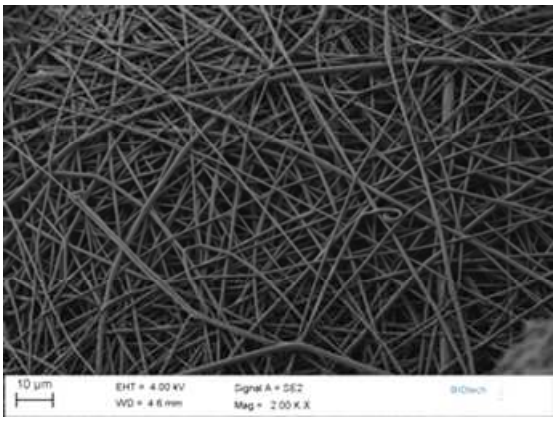  **d. PdlLAem_AlbF** |

*Figure 5-6. SEM micrographs of PLGA and PdlLA nanofibers loaded with AlbF. a.) PLGAsol_AlbF nanofibers were prepared by directly dissolving AlbF along with PLGA into a HFIP/water (7 to 1 vol.) solution; b.) PLGAem_AlbF nanofibers were obtained from a W/O emulsion of a AlbF aqueous solution into 17% (wt) PLGA in chloroform; c.) PdlLAsol_AlbF nanofibers were prepared by directly dissolving AlbF along with PdlLA into a HFIP/water (7 to 1 vol.) solution; d.) PdlLAem_AlbF nanofibers were obtained from a W/O emulsion of a AlbF aqueous solution into 11% (wt) PdlLA in chloroform*

### 5.3.3 VEGF-loaded nanofibers prepared by solution and emulsion electrospinning

In this study, electrospun nanofiber materials were prepared in which BSA was encapsulated along with VEGF. BSA is added as a protectant to the VEGF to prevent protein degradation and inactivation under extremely hostile environments, such a dissolution and dispersion in organic solvents during scaffold fabrication and protein encapsulation. In some manufacturing processes, the addition of albumin aided in protecting growth factors from denaturation in organic solvents [169],[170]. Other results suggested that BSA has the potential of stabilizing other protein or peptide drugs [171]. In addition, Valmikinathan et al. demonstrated that BSA helps in overcoming the most common drawbacks associated with hydrophobic polymers such as reduced loading efficiency, long degradation periods, and burst release [172].

All nanofibers loaded with VEGF and BSA exhibited a defect-free morphology (Figure 5-7) regardless the preparation method. Most likely, the presence of BSA increased the electrical conductivity of the solution, making the process of fiber drawing more efficient. However, very much like in the case of ALb, the electrospinning process of PLGA emulsions with VEGF and BSA presented several challenges. No large aggregates were observed, but the surface of the scaffold was interspersed with macroscopic and microscopic round defects originated by solvent-rich polymer droplets deposited over the time. Those defects are particularly harmful because of the residual solvent that could re-dissolve the nanofibers, and create discontinuities and even holes in the material.

| Solution Electrospinning | Emulsion Electrospinning |
| --- | --- |
| 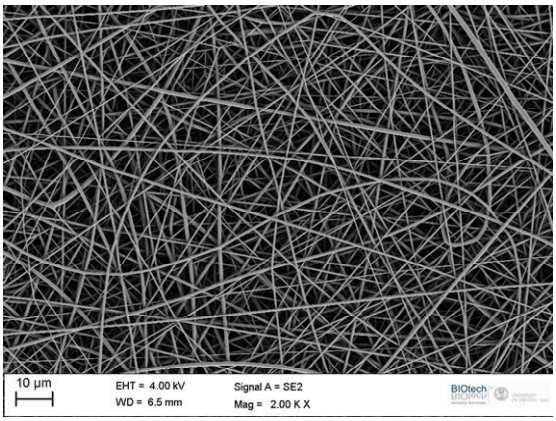 **a. PLGAsol_VEGF-BSA** | 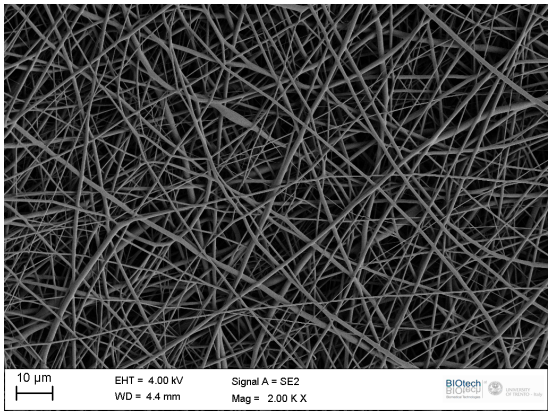 **b. PLGAem_VEGF-BSA** |
| 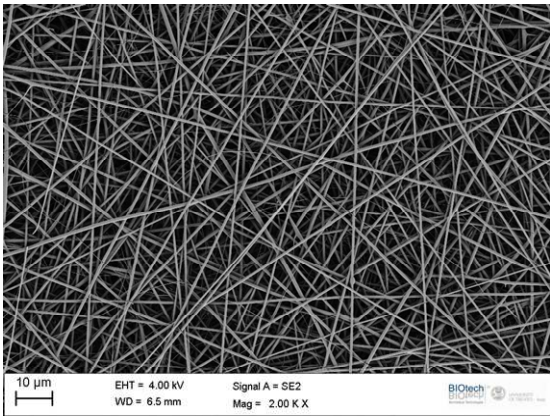 **c. PdlLAsol_VEGF-BSA** | 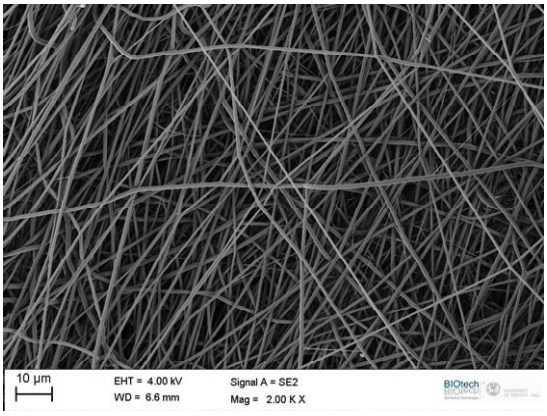 **d. PdlLAem_VEGF-BSA** |

*Figure 5-7. SEM micrographs of PLGA and PdlLA nanofibers loaded with VEGF and BSA. a.) PLGAsol_VEGF-BSA nanofibers were prepared by directly dissolving VEGF and BSA along with PLGA into a HFIP/water (7 to 1 vol.) solution; b.) PLGAem_VEGF-BSA nanofibers were obtained from a W/O emulsion of an aqueous solution of VEGF and BSA into 17% (wt) PLGA in chloroform; c.) PdlLAsol_VEGF-BSA nanofibers were prepared by directly dissolving VEGF and BSA along with PdlLA into a HFIP/water (7 to 1 vol.) solution; d.) PdlLAem_VEGF-BSA nanofibers were obtained from a W/O emulsion where an aqueous solution of VEGF and BSA was dispersed into 11% (wt) PdlLA in chloroform*

### 5.3.4 In vitro VEGF release from PLGA and PdlLA nanofiber mats prepared by solution and emulsion electrospinning

VEGF-loaded PLGA and PdlLA nanofiber materials prepared by solution and emulsion electrospinning were immersed in a phosphate buffer solution with 0.1% BSA to assess in vitro release of VEGF. Very dilute protein solutions more prone to inactivation and loss as a result of low-level binding to the storage vessel. Therefore, it is common practice to add proteins, such as bovine serum albumin (BSA) as carrier or filler to protect against such degradation and loss.

Buffer solution with released VEGF was completely removed every 24 hours and replace with fresh medium. Samples extracted at day 1, 2 and 4 were analyzed using Quantikine® VEGF ELISA kit to determine the amount of release VEGF. Results are summarized in Figure 5-8. For all the experiments, we found release profile with a strong burst at day 1, an intermediate amount of release at day 2 and very limited release at day 4.

The data suggest that, both in case PLGA and in case of PdlLA, samples prepared by emulsion electrospinning had a smaller amount of release at day 1 and a slightly more sustained release in the following days when compared with samples prepared by solution electrospinning. However, as no error bars are available, we cannot provide a conclusive result. In general term, the drug distribution along the fiber could explain a more gradual release in the case of samples prepared by emulsion electrospinning. As it results from confocal images, the clusters of encapsulated molecules in nanofibers prepared from emulsions appear to be located toward the center of the fibers (Figure 5-4b-d).

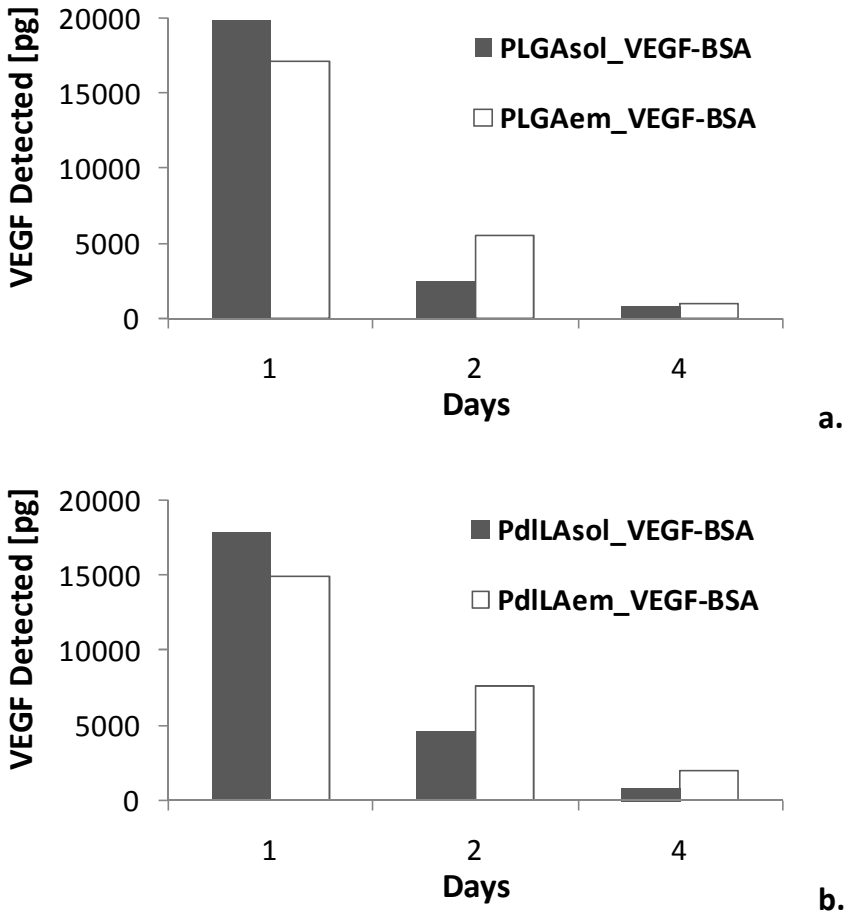


*Figure 5-8. VEGF released in days 1, 2, and 4 from PLGA (a.) and PdlLA (b.) nanofibrous scaffolds. VEGF-loaded nanofibers were prepared either by directly dissolving VEGF or by emulsifying an aqueous solution of VEGF the polymeric solution. The content of active-VEGF in the release medium was determined by enzyme-linked immunosorbent assay (ELISA). The reported values represent the average of three separate release samples. (Release area 3.14cm$^2$)*

As a consequence, a limited amount of drug is available on the surface or near the surface of the nanofibers for immediate release. On the other side, encapsulated molecules have a more uniform distribution in nanofibers obtained from solutions (Figure 5-4a-c). Thus, a larger share of molecules on the surface could result in a larger immediate (burst) release.

PCL-PLGA_VEGF-BSA and PCL-PdlLA_VEGF-BSA composite scaffolds with a compositional and biochemical gradient along their thickness for spatially-confined release of VEGF to a specific surface of the scaffold were prepared according to the scheme in Figure 5-1. We used side-by-side release chambers presented in Chapter 3 to separate VEGF delivered to the opposite sides of the composite scaffolds. Release data for the PCL-PdlLA composite scaffolds are presented in Figure 5-9.

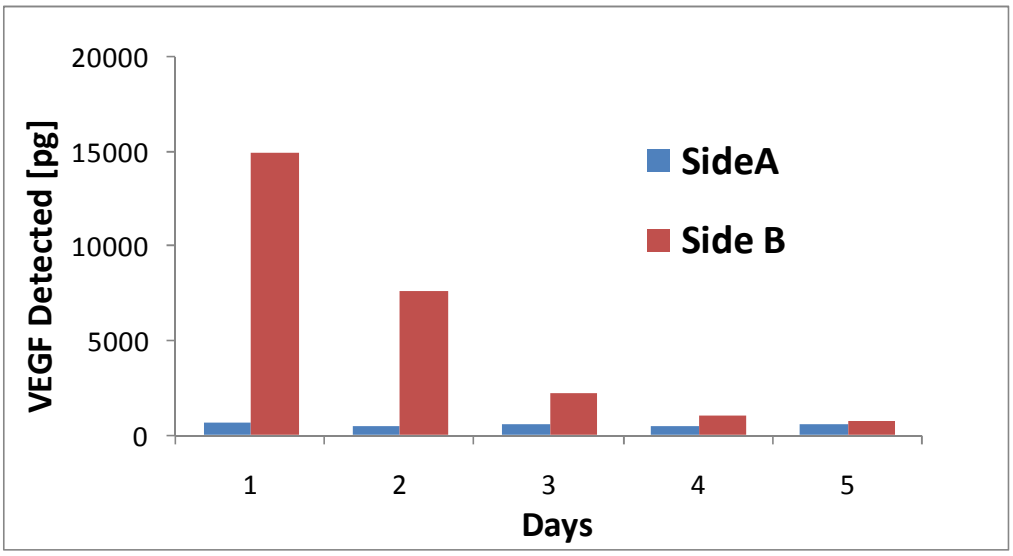


*Figure 5-9. Average amount of VEGF released daily from the opposite surfaces of a PCL-PdlLA composite scaffold. VEGF and BSA were encapsulated in the PdlLA nanofibers by emulsion electrospinning and released in 0.1% BSA release medium. Active-VEGF content in the release medium was determined by ELISA. The reported values represent the average of three separate release tests. (Release area 3.14 cm$^2$)*

The vast majority of the detected VEGF was release on side B, while very little amount of VEGF was found in the chamber on Side A. Again, as in the side-by-side experiments

presented in the previous chapters, composite scaffolds with internal gradients demonstrated the ability to confine with high efficiency the release of loaded molecules to a specific surface of the scaffold. In this case, the efficiency of separation was higher than 93%. Unfortunately, no results were obtained with PCL-PLGA_VEGF-BSA composite scaffolds. Macroscopic defects and poor overall quality of PLGA nanofibers obtained from emulsion spoiled the side-by-side release test.

In all the release experiments presented in this chapter, the amount of VEGF detected in the release media as soon as at day 4 was very limited. This result is in contrast with the findings that we presented in the previous chapters where an appreciable release of encapsulated molecules was demonstrated for 10 or more days. The reasons of this discrepancy are not clear. We think that the main reason is related to the detection technique itself. It is worth pointing out that ELISA kit can detect only active forms of the tested molecules. In fact, ELISA is designed to test protein activity based on the ligand (analyte)-protein interactions. The protein activity in the body is based on a ligand-specific recognition. If the binding site is denatured, the interaction does not occur, and unbound proteins are washed away. In principle, detected VEGF contents presented in Figure 5-8 and Figure 5-9 are different from the total amount of released VEGF (active and inactive). In fact, the fraction of inactive molecules is not taken into account. If one could quantify the total amount of VEGF in the release media, regardless its ligand-specific activity, it would be possible to provide more complete results. Bicinchoninic acid (BCA) assay, micro BCA assay and Bradford Reagent have been tentatively used in the effort to determine the total content of VEGF. Unfortunately, a

quantification of the total amount of VEGF in the release medium was not trivial. In fact, the extremely low levels of VEGF (tens of nanograms per ml), the preponderant and virtually unknown release of BSA from nanofibers, along with the presence of BSA in the release medium, made conventional protein quantification techniques ineffectual.

In relation to the release from PCL-PdlLA_VEGF-BSA composite scaffolds, we can estimate that the amount of VEGF detected in the release media accounted for about the 25% of the total VEGF encapsulated in the nanofibers. This means that about 75% of the loaded VEGF either was still in the fibers or was wasted cue to inactivation or denaturation. With data obtained here we cannot produce definitive results. For this reason, additional experimentation is necessary to determine the real efficiency of VEGF encapsulation, the complete release kinetics of VEGF and the VEGF/BSA ratio that maximize the release of functional proteins.

## 5.4 Conclusions

In this chapter we will show a preliminary study for the encapsulation and the controlled-release of medically relevant biomolecules. We successfully encapsulated vascular endothelial growth factor (VEGF) in poly(lactide-co-glycolide) acid and poly(d,l-lactide) acid nanofibers by using both conventional solution electrospinning and emulsion electrospinning process. In the first case, VEGF was directly mixed into the polymeric solution; in the second case, a aqueous VEGF solution was emulsified within the organic polymeric solution. Release experiments demonstrated the delivery of functional biomolecules for at least 4 days, although the efficiency of the process and overall release kinetics are still partially unknown. In the present chapter, we also confirmed that composite scaffolds with a compositional and biochemical gradient have the ability to confine the release of VEGF to a specific region of the scaffold. In addition, by using fluorescently-labeled molecules, we showed that encapsulated molecules are evenly distributed in nanofibers prepared by one-phase solution electrospinning, while they are arranged in discrete periodic domains along nanofibers prepared by emulsion electrospinning.

# 6 FINAL REMARKS

In this research work, a multicomponent scaffold for Vascular Tissue Engineering was designed, produced and characterized. The objective of this thesis was to prepare and characterize a tubular scaffold with adequate mechanical property, improved biocompatible surface for endothelial cell recognition and selective biomolecule release ability.

In the first part of this thesis, we have demonstrated a double-electrospinning technique to produce a robust tubular scaffold with well-integrated nanofibrous structure, anisotropic mechanical behaviour and endothelial-conducive surface. The advantage of this approach resides in the combination of superior biological properties of a natural polymer (silk fibroin) with higher mechanical stability and performance of a synthetic degradable polyester (PCL). A thick bulk PCL mesh of nanofibers, an intermediate intermixed fibrous layer, and a thin layer of silk-fibroin nanofibers have been combined to form a multilayered structure which is stable against mechanical delamination. Using a rotating cylindrical collector, anisotropic mechanical behavior of these electrospun structures was obtained and the anisotropy is found to be dependent on the rotation speed of the collector. It was previously known that a rotating collector allowed to produce a tubular structure with anisotropic mechanical properties; however, we recognized for the first time that the combination of the collector shape and the

collector rotation allows to obtain tunable mechanical properties. In particular, previous studies failed to recognize partial alignment of nanofibers along the longitudinal direction with slender collectors rotating at low speed, which in turn results in higher mechanical properties in the longitudinal direction with respect to circumferential direction. In fact, at lower rotation speeds the structure was stiffer in the longitudinal direction and more compliant in the circumferential direction, reaching up to 2.5 in the longitudinal-to-circumferential ratio in this study. In this context, fibroin fibers acted as an “active” cell-conductive component that could actively dialogue with endothelial cells, and PCL fibers acted as a “passive” component that control mechanical and deformational behaviour of the scaffold.

In the attempt to promote the “passive” PCL component of the scaffold to a more “active” role, we designed a graded electrospun structure able to sequester and deliver active biomolecules, while providing structural and mechanical integrity. In this view, we prepared a variety of tunable nanofiber micropatterns to control spatio-temporal release of one or multiple molecules. In fact, selective release of molecules that target specific cell types or tissue formation without influencing the activity of other cell populations or tissue functions is important to establish both *in vitro* physiological tissue models and *in vivo* tissue regeneration. Therefore, spatial and temporal control over release is critical to coordinate cell behaviors for healthy tissue formation. Herein, heterogeneous nanofibers scaffolds of PCL and PLGA with compositional and biochemical gradients along the scaffold thickness have been designed. Using PLGA nanofibers to encapsulate small molecules or proteins, we have characterized compositional and morphological changes as well as degradation behaviours of these composite scaffolds for up to 50 days *in vitro*. Using the precise graded composition and the

interplay between PCL and PLGA, we showed that the hierarchically-structured composite was capable of sustaining selective delivery of small molecules or larger proteins as well as multiple proteins to one specific side of the scaffold with efficiency of separation as high as 93%. We demonstrated that encapsulated molecules were released from one side of the scaffold with high efficiency of separation.

Moreover, various release profiles of combined biomolecules could be achieved by modulating the nanofibers micropattern. Thus, we obtained simultaneous and sequential release of two different model proteins on the two surfaces of a newly engineered graded scaffolds, and we showed that timing and the kinetics of molecule release can be influenced by changing the initial pattern of drug distribution and the composition of the scaffold.

We believed that scaffold preparation and release micropatterns presented in this work may represent the platform for the development of novel mechanically-competent scaffolds and multifunctional matrices able to actively control and direct the process of vascular tissue regeneration. However, the materials developed in this study can have also a broader impact in several fields of Tissue Engineering, where transitional components and active interfacial scaffolds with programmable and spatially controlled drug delivery ability are required.

## REFERENCES


1. Ratcliffe A. Tissue engineering of vascular grafts. Matrix Biology. 2000;19(4):353–7.

2. Martini FNJ. Fundamentals of Anatomy & Physiology. 8th ed. New York, NY: Benjamin-Cummings Pub Co; 2008.

3. Tu JV, Pashos CL, Naylor CD, Chen E, Normand SL, Newhouse JP, et al. Use of cardiac procedures and outcomes in elderly patients with myocardial infarction in the United States and Canada. The New England journal of medicine. 1997;336(21):1500–5.

4. World Health Organization. Cardiovascular Diseases Fact Sheet. 2009.

5. Tan, Wei; Bonani, Walter; Madhavan K. Nanofibrous Materials for Vascular Tissue Engineering and Regeneration. In: Popat K, editor. Nanotechnology in Tissue Engineering and Regenerative Medicine. CRC Press; 2011. p. 1–26.

6. Kannan RY, Salacinski HJ, Butler PE, Hamilton G, Seifalian AM. Current status of prosthetic bypass grafts: a review. J Biomed Mater Res. 2005;74B:570–81.

7. Kakisis JD, Liapis CD, Breuer C, Sumpio BE. Artificial blood vessel: the Holy Grail of peripheral vascular surgery. J Vasc Surg. 2005;41:349–54.

8. Zilla P, Bezuidenhout D, Human P. Prosthetic vascular grafts: Wrong models, wrong questions and no healing. Biomaterials. 2007;28(34):5009–27.

9. Herring M, Baughman S, Glover J, Kesler K, Jesseph J, Campbell J, et al. Endothelial seeding of Dacron and polytetrafluoroethylene grafts: the cellular events of healing. Surgery. 1984;96(4):745–55.

10. Zhang Z, Wang Z, Liu S, Kodama M. Pore size, tissue ingrowth, and endothelialization of small diameter microporous polyurethane vascular prostheses. Biomaterials. 2003;25:177–87.

11. Sauvage L, Berger K, Wood S, Nakagawa Y, Mansfield P. An external velour surface for porous arterial prostheses. Surgery. 1971;70(6):940–53.

12. Gupta BS, Kasyanov VA. Biomechanics of human common carotid artery and design of novel hybrid textile compliant vascular grafts. J Biomed Mater Res. 1997;34:341–9.

13. Taylor PR, Wolfe JH, Tyrrell MR, Mansfield AO, Nicolaides AN, Houston RE. Graft stenosis: justification for 1-year surveillance. Br J Surg. 1990;77(10):1125–8.

14. Stewart SF, Lyman DJ. Effects of a vascular graft/natural artery compliance mismatch on pulsatile flow. J Biomech. 1992;25:297–310.

15. Sarkar S, Schmitz-Rixen T, Hamilton G, Seifalian AM. Achieving the ideal properties for vascular bypass grafts using a tissue engineered approach: a review. Med Biol Eng Comput. 2007;45:327–36.

16. Mitchell SL, Niklason LE. Requirements for growing tissue-engineered vascular grafts. Cardiovascular Pathology. 2003;12:59–64.

17. Brewster LP, Bufallino D, Ucuzian A, Greisler HP. Growing a living blood vessel: Insights for the second hundred years. Biomaterials. 2007;28(34):5028–32.

18. Langer R, Vacanti JP. Tissue Engineering. Science. 1993;260(5110):920–6.

19. Lavik E, Langer R. Tissue engineering: current state and perspectives. Applied Microbiology and Biotechnology. 2004;65(1):1–8.

20. Lee KY, Peters MC, Anderson KW, Mooney DJ. Controlled growth factor release from synthetic extracellular matrices. Nature. 2000;408(6815):998–1000.

21. Sahoo S, Ang LT, Goh JCH, Toh SL. Growth factor delivery through electrospun nanofibers in scaffolds for tissue engineering applications. Journal of Biomedical Materials Research Part A. 2010;93A(4):1539–50.

22. Weinberg C, Bell E. A blood vessel model constructed from collagen and cultured vascular cells. Science. 1986;231(4736):397–400.

23. Xue L, Greisler HP. Biomaterials in the development and future of vascular grafts. Journal of Vascular Surgery. 2003;37(2):472–80.

24. Haruguchi H, Teraoka S. Intimal hyperplasia and hemodynamic factors in arterial bypass and arteriovenous grafts: a review. Journal of artificial organs : the official journal of the Japanese Society for Artificial Organs. 2003;6(4):227–35.

25. MacNeill BD, Pomerantseva I, Lowe HC, Oesterle SN, Vacanti JP. Toward a new blood vessel. Vascular Medicine. 2002;7(3):241–6.

26. Rayleigh J. On the equilibrium of liquid conducting masses charged with electricity. London Edinburgh Dublin Philos Mag. 1882;44:184–6.

27. Zeleny J. Instability of Electrified Liquid Surfaces. Physical Review. 1917;10(1):1–6.

28. Dole M, Hines RL, Mack LL, Mobley RC, Ferguson LD, Alice MB. Gas Phase Macroions. Macromolecules. 1968;1(1):96–7.

29. Formhals A. US Patent 1975504. 1934;

30. Formhals A. US Patent 2160962. 1939;

31. Simons HL. US patent 3280229. 1966;

32. Larrondo L, St. John Manley R. Electrostatic fiber spinning from polymer melts. III. Electrostatic deformation of a pendant drop of polymer melt. Journal of Polymer Science: Polymer Physics Edition. 1981;19(6):933–40.

33. Reneker DH, Yarin AL. Bending instability of electrically charged liquid jets of polymer solutions in electrospinning. Journal of Applied Physics. 2000;87(9).

34. Deitzel JM, Kleinmeyer J, Harris D, Tan NCB. The effect of processing variables on the morphology of electrospun nanofibers and textiles. Polymer. 2001;42:261–72.

35. Kowalewski TA, Barral S, Blonski S. Experiments and modelling of electrospinning process. Bull Pol Acad Sci Tech Sci. 2005;53(4):385.

36. Yarin a. L, Koombhongse S, Reneker DH. Bending instability in electrospinning of nanofibers. Journal of Applied Physics. 2001;89(5):3018.

37. Rutledge GC, Fridrikh SV. Formation of fibers by electrospinning. Advanced drug delivery reviews. 2007;59(14):1384–91.

38. Beachley V, Wen XJ. Effect of electrospinning parameters on the nanofiber diameter and length. Materials science & engineering. C, Materials for biological applications. 2009;29(3):663–8.

39. Sill TJ, von Recum HA. Electrospinning: applications in drug delivery and tissue engineering. Biomaterials. 2008;29(13):1989–2006.

40. Pham QP, Sharma U, Mikos AG. Electrospinning of polymeric nanofibers for tissue engineering applications: A review. Tissue Engineering. 2006;12(5):1197–211.

41. Zhang YZ, Su B, Venugopal J, Ramakrishna S, Lim CT. Biomimetic and bioactive nanofibrous scaffolds from electrospun composite nanofibers. Int J Nanomedicine. 2007;2:623–38.

42. Zhang Y, Lim CT, Ramakrishna S. Recent development of polymer nanofibers for biomedical and biotechnological applications. Business. 2005;6:933–46.

43. Bonani W, Maniglio D, Motta A, Tan W, Migliaresi C. Biohybrid nanofiber constructs with anisotropic biomechanical properties. Journal of Biomedical Materials Research Part B-Applied Biomaterials. 2011;96B(2):276–86.

44. Greiner A, Wendorff JH. Electrospinning: A fascinating method for the preparation of ultrathin fibres. Angewandte Chemie-International Edition. 2007;46(30):5670–703.

45. Li WJ, Laurencin CT, Caterson EJ, Tuan RS, Ko FK. Electrospun nanofibrous structure: a novel scaffold for tissue engineering. J. Biomed. Mater. Res. B. 2002;60:613.

46. Chakraborty S, Liao IC, Adler A, Leong KW. Electrohydrodynamics: A facile technique to fabricate drug delivery systems. Advanced Drug Delivery Reviews. 2009;61(12):1043–54.

47. Chew SY, Wen J, Yim EK, Leong KW. Sustained release of proteins from electrospun biodegradable fibers. Biomacromolecules. 2005;6(4):2017–24.

48. Goldberg M, Langer R, Jia XQ. Nanostructured materials for applications in drug delivery and tissue engineering. Journal of Biomaterials Science-Polymer Edition. 2007;18(3):241–68.

49. Cui W, Zhou Y, Chang J. Electrospun nanofibrous materials for tissue engineering and drug delivery. Science and Technology of Advanced Materials. 2010;11(1):014108.

50. Bhattarai SR, Bhattarai N, Yi HK, Hwang PH, Cha DI, Kim HY. Novel biodegradable electrospun membrane: scaffold for tissue engineering. Biomaterials. 2004;25(13):2595–602.

51. Bini T., Gao S, Wang S, Ramakrishna S. Poly(l-lactide-co-glycolide) biodegradable microfibers and electrospun nanofibers for nerve tissue engineering: an in vitro study. Journal of Materials Science. 2006;41(19):6453–9.

52. Puppi D, Piras AM, Detta N, Dinucci D, Chiellini F. Poly(lactic-co-glycolic acid) electrospun fibrous meshes for the controlled release of retinoic acid. Acta biomaterialia. 2010;6(4):1258–68.

53. Dong YX, Liao S, Ngiam M, Chan CK, Ramakrishna S. Degradation Behaviors of Electrospun Resorbable Polyester Nanofibers. Tissue Engineering Part B-Reviews. 2009;15(3):333–51.

54. Malafaya PB, Silva GA, Reis RL. Natural-origin polymers as carriers and scaffolds for biomolecules and cell delivery in tissue engineering applications. Advanced Drug Delivery Reviews. 2007;59(4-5):207–33.

55. Whatley BR, Kuo J, Shuai C, Damon BJ, Wen X. Fabrication of a biomimetic elastic intervertebral disk scaffold using additive manufacturing. Biofabrication. 2011;3(1):015004.

56. Baker BM, Mauck RL. The effect of nanofiber alignment on the maturation of engineered meniscus constructs. Biomaterials. 2007;28(11):1967–77.

57. Nerurkar NL, Elliott DM, Mauck RL. Mechanics of oriented electrospun nanofibrous scaffolds for annulus fibrosus tissue engineering. Journal of orthopaedic research : official publication of the Orthopaedic Research Society. 2007;25(8):1018–28.

58. Nerurkar NL, Baker BM, Sen S, Wible EE, Elliott DM, Mauck RL. Nanofibrous biologic laminates replicate the form and function of the annulus fibrosus. Nature materials. 2009;8(12):986–92.

59. Moffat KL, Wang I-NE, Rodeo SA, Lu HH. Orthopedic interface tissue engineering for the biological fixation of soft tissue grafts. Clinics in sports medicine. 2009;28(1):157–76.

60. Fujimoto KL, Tobita K, Merryman WD, Guan J, Momoi N, Stolz DB, et al. An elastic, biodegradable cardiac patch induces contractile smooth muscle and improves cardiac remodeling and function in subacute myocardial infarction. Journal of the American College of Cardiology. 2007;49(23):2292–300.

61. Li W-J, Jiang YJ, Tuan RS. Cell-nanofiber-based cartilage tissue engineering using improved cell seeding, growth factor, and bioreactor technologies. Tissue engineering. Part A. 2008;14(5):639–48.

62. Yang X, Shah JD, Wang H. Nanofiber enabled layer-by-layer approach toward three-dimensional tissue formation. Tissue engineering. Part A. 2009;15(4):945–56.

63. Griffin J, Delgado-Rivera R, Meiners S, Uhrich KE. Salicylic acid-derived poly(anhydride-ester) electrospun fibers designed for regenerating the peripheral nervous system. Journal of biomedical materials research. Part A. 2011;97(3):230–42.

64. Slater SC, Beachley V, Hayes T, Zhang D, Welsh GI, Saleem MA, et al. An in vitro model of the glomerular capillary wall using electrospun collagen nanofibres in a bioartificial composite basement membrane. PloS one. 2011;6(6):e20802.

65. Drilling S, Gaumer J, Lannutti J. Fabrication of burst pressure competent vascular grafts via electrospinning: effects of microstructure. Journal of biomedical materials research. Part A. 2009;88(4):923–34.

66. Karageorgiou V, Tomkins M, Fajardo R, Meinel L, Snyder B, Wade K, et al. Porous silk fibroin 3-D scaffolds for delivery of bone morphogenetic protein-2 in vitro and in vivo. Journal of biomedical materials research. Part A. 2006;78(2):324–34.

67. Mieszawska AJ, Kaplan DL. Smart biomaterials - regulating cell behavior through signaling molecules. BMC biology. 2010;8:59.

68. Hanjaya-Putra D, Bose V, Shen Y-I, Yee J, Khetan S, Fox-Talbot K, et al. Controlled activation of morphogenesis to generate a functional human microvasculature in a synthetic matrix. Blood. 2011;118(3):804–15.

69. Zhang X, Reagan MR, Kaplan DL. Electrospun silk biomaterial scaffolds for regenerative medicine. Advanced drug delivery reviews. 2009;61(12):988–1006.

70. Goldberg M, Langer R, Jia XQ. Nanostructured materials for applications in drug delivery and tissue engineering. Journal of Biomaterials Science-Polymer Edition. 2007;18(3):241–68.

71. Ionescu LC, Lee GC, Sennett BJ, Burdick JA, Mauck RL. An anisotropic nanofiber/microsphere composite with controlled release of biomolecules for fibrous tissue engineering. Biomaterials. 2010;31(14):4113–20.

72. Mironov V, Kasyanovand V, Markwald RR. Nanotechnology in vascular tissue engineering: from nanoscaffolding towards rapid vessel biofabrication. Trends in Biotechnology. 2008;26(6):338–44.

73. Vasita R, Katti DS. Nanofibers and their applications in tissue engineering. Int J Nanomedicine. 2006;1:15–30.

74. Smith LA, Ma PX. Nano-fibrous scaffolds for tissue engineering. Colloids Surf. B Biointerfaces. 2004;39:125.

75. Miller DC, Webster TJ, Hasirci V. Technological advances in nanoscale biomaterials: the future of synthetic vascular graft design. Expert Rev Med Devices. 2004;1:259–68.

76. Miller DC, Haberstroh KM, Webster TJ. PLGA nanometer surface features manipulate fibronectin interactions for improved vascular cell adhesion. Journal of Biomedical Materials Research Part A. 2007;81A(3):678–84.

77. Mo X. M, Xu C. Y, Kotaki M, Ramakrishna S. Electrospun P(LLA-CL) nanofiber: a biomimetic extracellular matrix for smooth muscle cell and endothelial cell proliferation. Biomaterials. 2004;25(10):1883–90.

78. Luong-Van E, Grondahl L, Chua KN, Leong KW, Nurcombe V, Cool SM, et al. Controlled release of heparin from poly(epsilon-caprolactone) electrospun fibers. Biomaterials. 2006;27(9):2042–50.

79. Matthews JA, Wnek GE, Simpson DG, Bowlin GL. Electrospinning of collagen nanofibers. Biomacromolecules. 2002;3:232.

80. Li M, Mondrinos MJ, Gandhi MR, Ko FK, Weiss AS, Lelkes PI. Electrospun protein fibers as matrices for tissue engineering. Biomaterials. 2005;26(30):5999–6008.

81. Boland ED, Matthews JA, Pawlowski KJ, Simpson DG, Wnek GE, Bowlin GL. Electrospinning collagen and elastin: preliminary vascular tissue engineering. Front. Biosci. 2004;9:1422.

82. Kidoaki S, Kwon IK, Matsuda T. Mesoscopic spatial designs of nano- and microfiber meshes for tissue-engineering matrix and scaffold based on newly devised multilayering and mixing electrospinning techniques. Biomaterials. 2005;26:37.

83. Ziegler J, Mayr-Wohlfart U, Kessler S, Breitig D, Günther K-P. Adsorption and release properties of growth factors from biodegradable implants. Journal of biomedical materials research. 2002;59(3):422–8.

84. Lefler A, Ghanem A. Development of bFGF-chitosan matrices and their interactions with human dermal fibroblast cells. Journal of biomaterials science. Polymer edition. 2009;20(10):1335–51.

85. Wei G, Jin Q, Giannobile WV, Ma PX. Nano-fibrous scaffold for controlled delivery of recombinant human PDGF-BB. Journal of Controlled Release. 2006;112(1):103–10.

86. Hile DD, Pishko MV. Solvent-free protein encapsulation within biodegradable polymer foams. Drug delivery. 2004;11(5):287–93.

87. Guan J, Stankus JJ, Wagner WR. Biodegradable elastomeric scaffolds with basic fibroblast growth factor release. Journal of Controlled Release. 2007;120(1-2):70–8.

88. Moore K, MacSween M, Shoichet M. Immobilized concentration gradients of neurotrophic factors guide neurite outgrowth of primary neurons in macroporous scaffolds. Tissue engineering. 2006;12(2):267–78.

89. Nie T, Baldwin A, Yamaguchi N, Kiick KL. Production of heparin-functionalized hydrogels for the development of responsive and controlled growth factor delivery systems. Journal of Controlled Release. 2007;122(3):287–96.

90. Al-Tahami K, Singh J. Smart polymer based delivery systems for peptides and proteins. Recent patents on drug delivery & formulation. 2007;1(1):65–71.

91. Sokolsky-Papkov M, Agashi K, Olaye A, Shakesheff K, Domb AJ. Polymer carriers for drug delivery in tissue engineering. Advanced drug delivery reviews. 2007;59(4-5):187–206.

92. Biondi M, Ungaro F, Quaglia F, Netti PA. Controlled drug delivery in tissue engineering. Advanced Drug Delivery Reviews. 2008;60(2):229–42.

93. Tayalia P, Mooney DJ. Controlled growth factor delivery for tissue engineering. Advanced materials (Deerfield Beach, Fla.). 2009;21(32-33):3269–85.

94. Discher DE, Mooney DJ, Zandstra PW. Growth Factors, Matrices, and Forces Combine and Control Stem Cells. Science. 2009;324(5935):1673–7.

95. Sy JC, Davis ME. Delivering regenerative cues to the heart: cardiac drug delivery by microspheres and peptide nanofibers. Journal of cardiovascular translational research. 2010;3(5):461–8.

96. Liu H, Fan H, Cui Y, Chen Y, Yao K, Goh JCH. Effects of the controlled-released basic fibroblast growth factor from chitosan-gelatin microspheres on human fibroblasts cultured on a chitosan-gelatin scaffold. Biomacromolecules. 2007;8(5):1446–55.

97. Deng T, Huang S, Zhou S, He L, Jin Y. Cartilage regeneration using a novel gelatin-chondroitin-hyaluronan hybrid scaffold containing bFGF-impregnated microspheres. Journal of microencapsulation. 2007;24(2):163–74.

98. Ghotbi Z, Haddadi A, Hamdy S, Hung RW, Samuel J, Lavasanifar A. Active targeting of dendritic cells with mannan-decorated PLGA nanoparticles. Journal of Drug Targeting. 2011;19(4):281–92.

99. Gandhi M, Srikar R, Yarin AL, Megaridis CM, Gemeinhart RA. Mechanistic examination of protein release from polymer nanofibers. Molecular pharmaceutics. 2009;6(2):641–7.

100. Ainslie KM, Kraning CM, Desai TA. Microfabrication of an asymmetric, multi-layered microdevice for controlled release of orally delivered therapeutics. Lab on a chip. 2008;8(7):1042–7.

101. Ainslie KM, Lowe RD, Beaudette TT, Petty L, Bachelder EM, Desai TA. Microfabricated devices for enhanced bioadhesive drug delivery: attachment to and small-molecule release through a cell monolayer under flow. Small (Weinheim an der Bergstrasse, Germany). 2009;5(24):2857–63.

102. Silva EA, Mooney DJ. Effects of VEGF temporal and spatial presentation on angiogenesis. Biomaterials. 2010;31(6):1235–41.

103. Hong Y, Guan J, Fujimoto KL, Hashizume R, Pelinescu AL, Wagner WR. Tailoring the degradation kinetics of poly(ester carbonate urethane)urea thermoplastic elastomers for tissue engineering scaffolds. Biomaterials. 2010;31(15):4249–58.

104. Nelson DM, Baraniak PR, Ma Z, Guan J, Mason NS, Wagner WR. Controlled Release of IGF-1 and HGF from a Biodegradable Polyurethane Scaffold. Pharmaceutical Research. 2011;28(6):1282–93.

105. Chen F-M, Zhang M, Wu Z-F. Toward delivery of multiple growth factors in tissue engineering. Biomaterials. 2010;31(24):6279–308.

106. Sohier J, Vlugt TJH, Cabrol N, Van Blitterswijk C, de Groot K, Bezemer JM. Dual release of proteins from porous polymeric scaffolds. Journal of Controlled Release. 2006;111(1-2):95–106.

107. Young S, Patel ZS, Kretlow JD, Murphy MB, Mountziaris PM, Baggett LS, et al. Dose effect of dual delivery of vascular endothelial growth factor and bone morphogenetic protein-2 on bone regeneration in a rat critical-size defect model. Tissue engineering. Part A. 2009;15(9):2347–62.

108. Huebsch N, Mooney DJ. Inspiration and application in the evolution of biomaterials. Nature. 2009;462(7272):426–32.

109. Sabella S, Brunetti V, Vecchio G, Torre AD, Rinaldi R, Cingolani R, et al. Micro/Nanoscale Parallel Patterning of Functional Biomolecules, Organic Fluorophores and Colloidal Nanocrystals. Nanoscale research letters. 2009;4(10):1222–9.

110. Martin TA, Herman CT, Limpoco FT, Michael MC, Potts GK, Bailey RC. Quantitative photochemical immobilization of biomolecules on planar and corrugated substrates: a versatile strategy for creating functional biointerfaces. ACS applied materials & interfaces. 2011;3(9):3762–71.

111. Davies N, Dobner S, Bezuidenhout D, Schmidt C, Beck M, Zisch AH, et al. The dosage dependence of VEGF stimulation on scaffold neovascularisation. Biomaterials. 2008;29(26):3531–8.

112. Sakano S, Hasegawa Y, Murata Y, Ito T, Genda E, Iwata H, et al. Inhibitory effect of bFGF on endochondral heterotopic ossification. Biochemical and Biophysical Research Communications. 2002;293(2):680–5.

113. Hutmacher DW. Scaffold design and fabrication technologies for engineering tissues - state of the art and future perspectives. Journal of Biomaterials Science-Polymer Edition. 2001;12(1):107–24.

114. Chen GP, Ushida T, Tateishi T. Scaffold design for tissue engineering. Macromolecular Bioscience. 2002;2(2):67–77.

115. Hutmacher DW. Scaffolds in tissue engineering bone and cartilage. Biomaterials. 2000;21(24):2529–43.

116. Conte MS. The ideal small arterial substitute: a search for the Holy Grail? Faseb Journal. 1998;12(1):43–5.

117. Yoshimoto H, Shin YM, Terai H, Vacanti JP. A biodegradable nanofiber scaffold by electrospinning and its potential for bone tissue engineering. Biomaterials. 2003;24(12):2077–82.

118. Mo XM, Weber HJ. Electrospinning P(LLA-CL) nanofiber: A tubular scaffold fabrication with circumferential alignment. Macromolecular Symposia. 2004;217:413–6.

119. Xu C, Inai R, Kotaki M, Ramakrishna S. Electrospun nanofiber fabrication as synthetic extracellular matrix and its potential for vascular tissue engineering. Tiss Eng. 2004;10:1160.

120. Burger C, Hsiao BS, Chu B. Nanofibrous materials and their applications. Annual Review of Materials Research. 2006;36:333–68.

121. Altman GH, Diaz F, Jakuba C, Calabro T, Horan RL, Chen JS, et al. Silk-based biomaterials. Biomaterials. 2003;24(3):401–16.

122. Unger RE, Sartoris A, Peters K, Motta A, Migliaresi C, Kunkel M, et al. Tissue-like self-assembly in cocultures of endothelial cells and osteoblasts and the formation of microcapillary-like structures on three-dimensional porous biomaterials. Biomaterials. 2007;28(27):3965–76.

123. Kim HJ, Kim U-J, Leisk GG, Bayan C, Georgakoudi I, Kaplan DL. Bone regeneration on macroporous aqueous-derived silk 3-D scaffolds. Macromolecular Bioscience. 2007;7(5):643–55.

124. Zhang X, Baughman CB, Kaplan DL. In vitro evaluation of electrospun silk fibroin scaffolds for vascular cell growth. Biomaterials. 2008;29(14):2217–27.

125. Bondar B, Fuchs S, Motta A, Migliaresi C, Kirkpatrick CJ. Functionality of endothelial cells on silk fibroin nets: Comparative study of micro- and nanometric fibre size. Biomaterials. 2008;29(5):561–72.

126. Hutmacher DW, Goh JCH, Teoh SH. An introduction to biodegradable materials for tissue engineering applications. Annals Academy of Medicine Singapore. 2001;30(2):183–91.

127. Li WJ, Danielson KG, Alexander PG, Tuan RS. Biological response of chondrocytes cultured in three-dimensional nanofibrous poly(epsilon-caprolactone) scaffolds. Journal of Biomedical Materials Research Part A. 2003;67A(4):1105–14.

128. Kweon H, Yoo MK, Park IK, Kim TH, Lee HC, Lee HS, et al. A novel degradable polycaprolactone networks for tissue engineering. Biomaterials. 2003;24(5):801–8.

129. Valluzzi R, He SJ, Gido SP, Kaplan D. Bombyx mori silk fibroin liquid crystallinity and crystallization at aqueous fibroin-organic solvent interfaces. International Journal of Biological Macromolecules. 1999;24(2-3):227–36.

130. Pham QP, Sharma U, Mikos AG. Electrospun poly(epsilon-caprolactone) microfiber and multilayer nanofiber/microfiber scaffolds: Characterization of scaffolds and measurement of cellular infiltration. Biomacromolecules. 2006;7(10):2796–805.

131. Sukigara S, Gandhi M, Ayutsede J, Micklus M, Ko F. Regeneration of Bombyx mori silk by electrospinning - part 1: processing parameters and geometric properties. Polymer. 2003;44(19):5721–7.

132. Sukigara S, Gandhi M, Ayutsede J, Micklus M, Ko F. Regeneration of Bombyx mori silk by electrospinning. Part 2. Process optimization and empirical modeling using response surface methodology. Polymer. 2004;45(11):3701–8.

133. Soffer L, Wang X, Mang X, Kluge J, Dorfmann L, Kaplan DL, et al. Silk-based electrospun tubular scaffolds for tissue-engineered vascular grafts. Journal of Biomaterials Science-Polymer Edition. 2008;19(5):653–64.

134. Thomas V, Jose MV, Chowdhury S, Sullivan JF, Dean DR, Vohra YK. Mechano-morphological studies of aligned nanofibrous scaffolds of polycaprolactone fabricated by electrospinning. Journal of Biomaterials Science-Polymer Edition. 2006;17(9):969–84.

135. Li W-J, Mauck RL, Cooper JA, Yuan X, Tuan RS. Engineering controllable anisotropy in electrospun biodegradable nanofibrous scaffolds for musculoskeletal tissue engineering. Journal of Biomechanics. 2007;40(8):1686–93.

136. Kenawy ER, Layman JM, Watkins JR, Bowlin GL, Matthews JA, Simpson DG, et al. Electrospinning of poly(ethylene-co-vinyl alcohol) fibers. Biomaterials. 2003;24(6):907–13.

137. Baker BM, Gee AO, Metter RB, Nathan AS, Marklein RA, Burdick JA, et al. The potential to improve cell infiltration in composite fiber-aligned electrospun scaffolds by the selective removal of sacrificial fibers. Biomaterials. 2008;29(15):2348–58.

138. Unger RE, Wolf M, Peters K, Motta A, Migliaresi C, Kirkpatrick CJ. Growth of human cells on a non-woven silk fibroin net: a potential for use in tissue engineering. Biomaterials. 2004;25(6):5137–46.

139. Crescenzi V, Manzini G, Calzolari G, Borri C. Thermodynamics of fusion of poly-β-propiolactone and poly-ϵ-caprolactone. comparative analysis of the melting of aliphatic polylactone and polyester chains. European Polymer Journal. 1972;8(3):449–63.

140. Zhang YZ, Wang X, Feng Y, Li J, Lim CT, Ramakrishna S. Coaxial electrospinning of (fluorescein isothiocyanate-conjugated bovine serum albumin)-encapsulated poly(epsilon-caprolactone) nanofibers for sustained release. Biomacromolecules. 2006;7(4):1049–57.

141. Huang ZM, He CL, Yang AZ, Zhang YZ, Hang XJ, Yin JL, et al. Encapsulating drugs in biodegradable ultrafine fibers through co-axial electrospinning. Journal of Biomedical Materials Research Part A. 2006;77A(1):169–79.

142. Xu XX, Yang L, Wang X, Chen X, Liang Q, Zeng J, et al. Ultrafine medicated fibers electrospun from W/O emulsions. Journal of Controlled Release. 2005;108(1):33–42.

143. Ritger PL, Peppas NA. A simple equation for description of solute release I. Fickian and non-fickian release from non-swellable devices in the form of slabs, spheres, cylinders or discs. Journal of Controlled Release. 1987;5(1):23–36.

144. Siepmann J, Siepmann F. Mathematical modeling of drug delivery. International journal of pharmaceutics. 2008;364(2):328–43.

145. Fu Y, Kao WJ. Drug release kinetics and transport mechanisms of non-degradable and degradable polymeric delivery systems. Expert opinion on drug delivery. 2010;7(4):429–44.

146. Chen RR, Silva EA, Yuen WW, Mooney DJ. Spatio-temporal VEGF and PDGF delivery patterns blood vessel formation and maturation. Pharmaceutical research. 2007;24(2):258–64.

147. Phillips JE, Burns KL, Le Doux JM, Guldberg RE, García AJ. Engineering graded tissue interfaces. Proceedings of the National Academy of Sciences of the United States of America. 2008;105(34):12170–5.

148. Ashammakhi N, Ndreu A, Nikkola L, Wimpenny I, Yang Y. Advancing tissue engineering by using electrospun nanofibers. Regenerative Medicine. 2008;3(4):547–74.

149. Liao S, Li B, Ma Z, Wei H, Chan C, Ramakrishna S. Biomimetic electrospun nanofibers for tissue regeneration. Biomedical Materials. 2006;1(3):R45–53.

150. Dahlin RL, Kasper FK, Mikos AG. Polymeric Nanofibers in Tissue Engineering. Tissue Engineering Part B-Reviews. 2011;17(5):349–64.

151. Saltzman WM, Olbricht WL. Building drug delivery into tissue engineering. Nature Reviews Drug Discovery. 2002;1(3):177–86.

152. Tessmar JK, Goepferich AM. Matrices and scaffolds for protein delivery in tissue engineering. Advanced Drug Delivery Reviews. 2007;59(4-5):274–91.

153. Sanchez A, Gupta RK, Alonso MJ, Siber GR, Langer R. Pulsed controlled-release system for potential use in vaccine delivery. Journal of Pharmaceutical Sciences. 1996;85(6):547–52.

154. Grayson ACR, Choi IS, Tyler BM, Wang PP, Brem H, Cima MJ, et al. Multi-pulse drug delivery from a resorbable polymeric microchip device. Nature Materials. 2003;2(11):767–72.

155. Liu X, Pettway GJ, McCauley LK, Ma PX. Pulsatile release of parathyroid hormone from an implantable delivery system. Biomaterials. 2007;28(28):4124–31.

156. Franssen O, Vandervennet L, Roders P, Hennink WE. Degradable dextran hydrogels: controlled release of a model protein from cylinders and microspheres. Journal of Controlled Release. 1999;60(2-3):211–21.

157. Chen RR, Mooney DJ. Polymeric growth factor delivery strategies for tissue engineering. Pharmaceutical Research. 2003;20(8):1103–12.

158. Suciati T, Howard D, Barry J, Everitt NM, Shakesheff KM, Rose FRAJ. Zonal release of proteins within tissue engineering scaffolds. Journal of Materials Science-Materials in Medicine. 2006;17(11):1049–56.

159. Burdick JA, Mason MN, Hinman AD, Thorne K, Anseth KS. Delivery of osteoinductive growth factors from degradable PEG hydrogels influences osteoblast differentiation and mineralization. Journal of Controlled Release. 2002;83(1):53–63.

160. Richardson TP, Peters MC, Ennett AB, Mooney DJ. Polymeric system for dual growth factor delivery. Nature Biotechnology. 2001;19(11):1029–34.

161. Jain RK. Molecular regulation of vessel maturation. Nature Medicine. 2003;9(6):685–93.

162. Peirce SM, Skalak TC. Microvascular remodeling: A complex continuum spanning angiogenesis to arteriogenesis. Microcirculation. 2003;10(1):99–111.

163. Gurdon JB, Harger P, Mitchell A, Lemaire P. Activin signalling and response to a morphogen gradient. Nature. 1994;371(6497):487–92.

164. Burgess BT, Myles JL, Dickinson RB. Quantitative analysis of adhesion-mediated cell migration in three-dimensional gels of RGD-grafted collagen. Annals of biomedical engineering. 2000;28(1):110–8.

165. Takeshita S, Zheng LP, Brogi E, Kearney M, Pu LQ, Bunting S, et al. Therapeutic angiogenesis. A single intraarterial bolus of vascular endothelial growth factor augments revascularization in a rabbit ischemic hind limb model. The Journal of clinical investigation. 1994;93(2):662–70.

166. Yang Y, Li X, Cui W, Zhou S, Tan R, Wang C. Structural stability and release profiles of proteins from core-shell poly (DL-lactide) ultrafine fibers prepared by emulsion electrospinning. Journal of biomedical materials research. Part A. 2008;86(2):374–85.

167. Li Y, Jiang H, Zhu K. Encapsulation and controlled release of lysozyme from electrospun poly(epsilon-caprolactone)/poly(ethylene glycol) non-woven membranes by formation of lysozyme-oleate complexes. Journal of materials science. Materials in medicine. 2008;19(2):827–32.

168. Li X, Su Y, Liu S, Tan L, Mo X, Ramakrishna S. Encapsulation of proteins in poly(L-lactide-co-caprolactone) fibers by emulsion electrospinning. Colloids and surfaces. B, Biointerfaces. 2010;75(2):418–24.

169. King TW, Patrick CW. Development and in vitro characterization of vascular endothelial growth factor (VEGF)-loaded poly(DL-lactic-co-glycolic acid)/poly(ethylene glycol) microspheres using a solid encapsulation/single emulsion/solvent extraction technique. Journal of biomedical materials research. 2000;51(3):383–90.

170. Cao X, Shoichet MS. Delivering neuroactive molecules from biodegradable microspheres for application in central nervous system disorders. Biomaterials. 1999;20(4):329–39.

171. Zhao H, Gagnon J, Häfeli UO. Process and formulation variables in the preparation of injectable and biodegradable magnetic microspheres. Biomagnetic research and technology. 2007;5:2.

172. Valmikinathan CM, Defroda S, Yu X. Polycaprolactone and Bovine Serum Albumin Based Nanofibers for Controlled Release of Nerve Growth Factor. Scanning. 2009;:1084–9.